DYNAMIC BEHAVIOR OF VEHICLES

DURING AN EARTHQUAKE

2016

Rishi Ram Parajuli

ABSTRACT

New method on seismic response analysis of vehicle is proposed. The 'circular path and linear momentum' (CPLM) method is suggested for the lateral and longitudinal stability analysis of vehicles under earthquake excitation. Momentum of the vehicles with its speed and force due to earthquake are taken to find the longitudinal and lateral positions of vehicle. Use of angular momentum on the toppling analysis of the vehicle during earthquake shaking are also presented. This method of vehicle response analysis can be used for both conditions of vehicles, as in motion or at rest. Validation of this method have done by comparing the results with the response of a vehicle at rest just before the shaking of the Gorkha 2015 earthquake.

The vehicle was modelled with six degrees of freedom system. The equation of motion was used as the basic equation for the analysis of the response of the tyres and the car body as well as the transformation of the acceleration from the road surface to the vehicle. The longitudinal and lateral responses were calculated using the CPLM method. We also considered the pitching, rolling and yawing motions of the vehicle as rotations in three directions. The forces acting on the tyres were calculated using the Magic Formula Model (MFM). The MFM coefficients were taken from previously published results using the trust region reflective (TRR) method algorithm. We analysed the responses of a car, bus and truck in the longitudinal and lateral directions for several conditions. The relationships between the vehicles' responses with speeds of up to 30.0 m/s from rest condition and peak ground acceleration (PGA) from 1.0 to 15.0 m/s^2 were also investigated. Toppling risk of vehicles during earthquake shaking are analyzed and presented using sine waves with different characteristics. Relationship of lateral peak ground acceleration (PGA) associated with toppling risk under several conditions are presented. Relationship of the amplitude of vertical component, dominant frequency of the input wave and phase delay of the vertical with amplitude of lateral input wave to topple are calculated. Moreover, different cases of weight and the dimension of vehicle and the speed of vehicle are also investigated and presented as dimensional and velocity scaling factors on toppling. Regression equations for all the relationships are shown to estimate the threshold value of PGA for the toppling risk of vehicle under several cases.

Case studies of two different earthquakes, related to vehicle responses are shown. The 2015 Gorkha earthquake struck in central Nepal, CCTV cameras on the roads and streets were recording the earthquake shaking and response of people and surroundings. Some videos those recorded the vehicle responses show that two wheelers are in higher risk during earthquake shaking. Vehicles follow the wave path when they are subjected to long period ground motion as response to earthquake. One of the video recorded in Sundhara, Kathmandu have used in the validation of CPLM method. Interviews with drivers who was driving during main shock of Gorkha earthquake were conducted. Recognition of earthquake by the drivers during driving is very uncertain in terms of time, but most of the drivers knew due to unusual behavior of vehicle. Moreover, the braking and stopping behavior are also ambiguous.

Kumamoto earthquake M7.3 hit southern Japan on April 16th, 2016. Extensive damages on structures were concentrated in the areas where the rupture exposed to the surface. We found many vehicles toppled on the site during damage survey in Tateno and Kurokawa area. Seismic response analyses of the car considering the circular path and linear momentum (CPLM) method for longitudinal and lateral responses and concept of angular momentum for rolling responses are executed in finding the toppling condition. Cars toppled during Kumamoto earthquake were examined using the seed ground motion recorded in KMMH16, NIED K-Net station in Mashiki town, data available nearby of the epicenter, having the highest PGA. Suzuki Every Wagon was chosen for the analysis whose threshold PGA using regression coefficients is 12.155 m/sec^2. Where lateral PGA corresponding to the toppling of the car is 14.172 m/sec^2 from the analysis using seed ground motion in Kurokawa and Tateno area, keeping the vertical component unchanged.

Car following mechanism is another major factor to be consider in responses of vehicles moving in the group. Autonomous decentralized mechanism, originally used for fish moving behavior are used in case of vehicles where effect of earthquake shaking reaction from drivers are added. Driving simulator experiment was conducted with thirty drivers under different conditions. Mainly two levels of earthquake shaking were set as lower and upper level where the trend of brake use and brake level were found. Priority factors with braking levels, distribution of brake use, brake levels and corresponding time of use are also found from the experiment. Brake model for vehicle following behavior under earthquake is proposed.

Elevated structures those mainly dominated in city expressways and highways in mountainous areas. Actual earthquake acceleration that excites the vehicle running on it, depends on the location where the response of structures subjected at that particular time. Local soil condition of the surrounding area play a role in vehicle excitation when they are running on the ground but that difference might be negligible in comparison with the structural response. Virtual symmetrical cable-stayed bridge of length 1330 meters is considered in the study with a central span of 580 meters between two central towers. Kobe and El Centro earthquake ground motions are selected for structural analysis. Nodal responses on deck level are calculated using finite element analysis of the model. Input earthquake motion for seismic response analysis of the vehicle is calculated through interpolation of nodal responses of the structure at deck level. Lagrange's three-point formula is used as the data follows simple parabolic function in between three points for interpolation. Frequency and the amplitude of interpolated earthquake motions are varying with the origin and speed. Speeds of the vehicle ranging from rest condition to the 30.0 m/sec are analysed for all three types of vehicles when the origin of the vehicle is starting of the bridge. Lateral displacements are increased with the ascending value of the speed in all types of vehicle when the earthquake motion was used from El Centro earthquake, in contrast with this trend, response of vehicles for Kobe earthquake is almost in descending order but very small in quantity. When the origin of the vehicle changed from start of the bridge to the last point of the bridge with the constant speed of 20 m/secs for all cases, lateral displacements of the vehicles follows the different trend. Vehicle response for the cases of vehicle position within bridge and exit from the bridge during shaking, affect on the result.

Lastly application of earthquake early warning system for vehicles in expressways are presented. Risk analysis of vehicle collision under different scenario found that vehicles running with same conditions are in different risk depending on location. When vehicles running with speed of 20 m/sec and brake level of 8.0 m/sec^2, there is no collision for surface road but one collision for bridge for Kobe earthquake. In contrast, using Elcentro earthquake result shows there was no collision on bridge but all cars were collided when running on surface road. Result shows that when the gap between vehicles is small and brake level of front vehicle is higher than rear, there is high chance of collision. Maintaining the safe gap between vehicles, use of hazard lights to transmit the information might reduce the risk of accidents along with the earthquake early warning.

ACKNOWLEDGEMENT

I am extremely grateful to my advisor Professor Dr. Junji Kiyono, who has been a tremendous mentor for me in every step of my research work. I would like to thank you for encouraging my research and idea. Your advice on both research as well as on my career have been priceless. Also, I am pleased to thank my co-supervisors associate professor Aiko Furukawa and Yoshikazu Takahasi for their incredible supports on my research. Further, I would like to express my appreciation to evaluation committee members for fruitful suggestions on research.

I would like to thank Associate Professor Nobuhiro Uno, Assistant professor Toshiyuki Nakamura and ITS laboratory in Kyoto University, Mr. Hitoshi Yatsumoto form Hanshin expressways company, assistant professor Yoshihiro Okamura for valuable support and suggestions during my research and study. I would like to thank Dr. Bhuddarak Charatpangoon for his unmeasurable help on my work. I equally admire the support of graduate student Mr. Ryoichi Murakami in the research project.

I am very grateful to Secretary Ms. Yoshida for all administrative supports along with all administrative staffs of graduate school of engineering, Kyoto University.

I am very thankful with colleagues Yuji Dohi, Shuanglan Wu, Sakai Yotsui and Angga Fajar. Further, I would like to thank all other members of earthquake and lifeline laboratory, Department of Urban management, Kyoto University.

I would like to express my sincere gratitude to president of Kyoto University, professors, associate professors and all other staffs as selecting me as a student from abroad. Also, I am extremely grateful with Ministry of Education, Culture, Sports, Science and Technology for providing full package of fund for my study in Japan.

Last but not the least I would like to thank my beloved wife Kusum Sharma for her incredible support in my research throughout the period of my study.

Table of contents

List of Figures

List of Tables

List of Photos

1 Introduction

1.1 Background

Risk of road users during the earthquake event not only associated with the direct vehicle response but there are several indirect risks of structural collapse, collapse of road side furniture, rock slide, land slide, unprecedented accidents etc.

Loma Prieta earthquake M7.0 caused severe damage to 13 bridges which were closed for reconstruction where other 78 bridges in state highway were also damaged [1]. In January, 1994, M6.8 earthquake struck in Los Angeles area which last for about one minute claimed life of 72 people. Major transportation network in California were devastated [2]. 1995 Kobe M6.9 earthquake in Japan hits badly to the highways including the settlements. Most damaged part of the highway was route 3 of the Hanshin expressway[1].

Photo 1.1 Damaged highway section due to Northridge earthquake 1994[2]

In 2014 March 28, moderate earthquake of M5.1 rocked southern California, epicenter near to the La Habra causes minor non-structural damages on the houses, few rock slides but there was

an accident with a car that hit the rock slide mass got overturn[3]. The photo of the overturned car taken by Kevin Warn for AP is shown in photo 1.2.

Photo 1.2 Overturned car on a highway in Carbon Canyon area of California due to hit by rock slide mass during earthquake shaking (Photo: Kevin Warn/AP)

Few studies regarding the seismic risk of transportation systems were conducted which mainly focused on the safety of road structures and other risk. Kiremidjian et al. in 2005 studied the seismic risk of transportation systems in California area. The work was focused on the safety of the bridge due to ground shaking, where structural and foundation safety are considered in terms of liquefaction susceptibility [4]. This study discusses on safety but only due to structural collapse, where risk of vehicle itself remained in shadow.

Human behaviour during the earthquake shaking is unpredictable. While one sits on the driving seat, it would be more dispersed. Perception of the people and their reaction on the steering, brake paddle and accelerator paddle are the main human factors on risk of moving vehicle under the earthquake shaking. Mechanical properties of the vehicle, size, weight and location of the centre of the gravity of vehicle also play the roles which responded the earthquake vibration.

Recently, studies about the resilient structures are getting advanced, new materials, technologies are now able to combat the structures against earthquakes. However, study on road user's response and risk are limited. Vehicle response and human behaviour to control the vehicle are yet to be studied further. Few studies had done in the field of vehicle response and drivers behaviour. When earthquake struck in any area, driver driving the vehicle could not recognize upon the initial phase of shaking, due to the vibration of vehicle itself. When the driver felt severe shaking, acceleration will be soared to higher level. Until that time, vehicle itself already has responded to earthquake, which might get derailed. If the shaking level shifts suddenly, vehicle might have experience accident prior to any reaction from the driver.

1.2 Literature Review

The effect of the earthquake on a driver of a moving vehicle during an earthquake may be negligible when the ground motion is small, as the vehicle itself is in motion. However, large shaking may tend to push the vehicle laterally or longitudinally, causing the driver to lose control of the vehicle. Drivers' responses and the characteristics of the ground motion during the 1983 Nihon-kai-chubu earthquake (M7.7) in Akita prefecture and the 1987 Chiba-ken-oki earthquake (M6.7) in Chiba prefecture, both of Japan Meteorological Agency (JMA) seismic intensity V [5] were studied using a questionnaire survey [6]. The survey revealed that about 50% of drivers felt the earthquake motion as the vehicle and their surroundings displayed unusual behaviour and movement. Most of the drivers stopped their vehicles (65.7% and 43.3% in 1983 and 1987 events, respectively) because they felt they were in danger. The survey also found that steering instability was felt in directions both longitudinal and lateral to the car (73.8% and 52.4%, respectively) while driving the vehicles. A similar study after the 2003 Miyagiken-Oki earthquake (M7.0) found a relationship between the JMA intensity of the earthquake and the drivers' recognition of the event and their driving response to it [7]. Only 40% of the drivers recognized earthquakes of JMA intensity less than 4.0 but more than 80% noticed and most of them reacted when the intensity was larger than 4.0. For JMA intensities larger than 4.5, 20% of the drivers stopped on the shoulders of the roads.

Maruyama and Yamazaki studied the response of a moving vehicle to earthquake motion with various JMA intensities in 2002[8], where the vehicle was modelled with six degrees of freedom. That model used the equation of motion with a constant longitudinal speed. The vehicle drift for four earthquakes (Kobe, El Centro, Tottori and Chiba-ken-oki) was mostly

unidirectional and linear. However, this model could not accommodate the behaviour of the vehicle at rest.

Drivers' reaction during the strong shaking of earthquake had been studied using driving simulator experiments. Maruyama and Yamazaki in 2004 studied the drivers' response characteristics based on driving simulator experiment with 33 drivers [9]. They found that drivers' reaction during earthquake depends on the shaking level of earthquake, when JMA seismic intensity nearly the value of 6.0. The time lag of the driver in recognizing the shaking cause large lateral deviation of vehicle. Accidents can be reduced by controlling the steering, however over reaction on it is risky.

Vehicle risk during the earthquake should consider the mechanism of their "Following Behaviour" which had been studied since fifties. Now, there are several models using different perspectives. Chandler, Herman and Montroll [10] proposed the first car following model in 1958 based on the hypothesis of acceleration applied by the driver is proportional to the speed of the vehicle or following distance. Another concept on avoidance of collision for safety, keeping the safe distance between cars, collision avoidance model was formulated by Kometani and Sasaki in 1959 [11]. Linear model on car following was attributed by Helly in 1959 [12]. Michaels in 1963 [13] put forward the idea of psychological factors in vehicle following model. Several studies following this concept and did their best to improve the formula and getting finer results [14] [15] [16][17][18].

Recently earthquake early warning (EEW) systems are using in many countries. Mexico started first EEW system with network of seismometers in 1991 [19]. Japan have started EEW system since 2007, which is supposed to be more advanced system around the globe [20]. Istanbul, Taiwan and Bucharest are also using EEW system in some extent [21]. USGS has started to develop EEW system in west coast of USA since 2006 and starting to send messages among test users from 2012, January [22]. Chinese government also initiated in constructing the EEW system from 2015 with target in operation from 2020. Israel is also trying to implement Earthquake Alarms System algorithm in cooperation with American scientists [20].

Great east Japan earthquake 2011 was a deadly disaster, where earthquake early warning system of Japan sent the message to millions of public near the epicentre, just before 15 – 20 seconds of the main shaking [23]. Jibiki et al. (2015) studied about drivers' behaviours on highways in Tohoku Earthquake, in comparison with relevant previous researches [24]. They had conducted a questionnaire survey with the drivers who had been driving on highways.

Study found that as expected there were no major accidents, neither there were more slips of vehicles nor the accidents. They found that time gap of receiving EEW message was common problem that should consider in improvement of safety.

Japan Meteorological Agency (JMA) has issued the leaflet as education to the public, mentioning what to do and what not to do during shaking or after receiving the early warning [25]. Leaflet issued by JMA is attached in annex IV, Regarding the condition of driving, JMA has issued the message as follows:

When driving:

> "Do not slow down suddenly
>
> Turn your hazard lights to alert other drivers, slow down smoothly
>
> If you are still moving when you feel the earthquake, pull safely to the left and stop"

1.3 Objectives

Seismic response analysis of vehicles is the goal of this study along with effectiveness of earthquake early warning system in highways. Vehicle responses during recent earthquakes, redefining the car following model to use under the earthquake shaking are also equally important in this study. This research has another goal of having new approach on analysis of vehicle running over the elevated structures.

1.4 Outline of work

Here, new approach on analysis of vehicle response during earthquake is proposed and discussed elaborately. The method considering momentum of the vehicle in earthquake response, Circular Path and Linear Momentum (CPLM) is validated form the response of vehicle during Gorkha earthquake. And the vehicle responses during several major earthquakes around the world have presented. Toppling risk of vehicles under several conditions of ground motion and vehicle parameters are proposed in chapter two as theoretical aspects. Vehicle responses during recent earthquakes are analyzed in chapter three where we mainly discussed on Gorkha earthquake of 2015 and Kumamoto earthquake of 2016. Video analysis of vehicle responses during Gorkha earthquake and questionnaire survey with drivers, who were driving

during shaking have been presented. Vehicle toppled during the Kumamoto earthquake are also studied and suggested the peak ground acceleration on corresponding area form the analysis. Chapter four discussed on car following models where we extend the autonomous decentralized mechanism (ADM) model, originally used in fish behavior to sue in vehicle following. Driving simulator experiment to analyze the drivers' reaction during earthquake was performed. Vehicle following behavior and trend of using brakes are studied. We propose the priority factor and brake level for different conditions of shaking. Brake model related to the earthquake shaking levels are proposed to use in the ADM model of vehicle follow. Elevated structures and vehicle responses are discussed in chapter five where we use a cable stayed bridge with length of 1330 meters used to analyze the vehicle response for different state. Interpolation of bridge response are used as input of vehicle analysis which tend to real condition of vehicle excitation during earthquake. Risk of vehicles with different speeds and origin are also discussed in this chapter. Earthquake early warning system and its effectiveness are discussed in chapter six, where several scenarios of vehicles in group are studied to find the corresponding risk. Finally, Chapter seven is all about wrapping up of the study with summary and conclusions.

2 Seismic response analysis of vehicle

2.1 Introduction

Risk associated with earthquake are mainly studied for structures and lifeline systems that ultimately calculated in terms of human and economic losses. Road structures such as bridges, tunnels and retaining walls for slope stability are well designed and constructed to combat with such disasters. Road users' risk are not only relying on the safety of the road structures but also depending on the vehicle response and reaction of driver during shaking. Mechanical and human responses during the shaking are under the consideration, this chapter discusses on the approach to analyse the mechanical response without the driver's responses on consideration.

Considering the three axes, the major responses of the vehicles are translations and rotations along three axes. Rotations along longitudinal, lateral and vertical axes are defined as rolling, pitching and yawing as shown in figure 2.1.

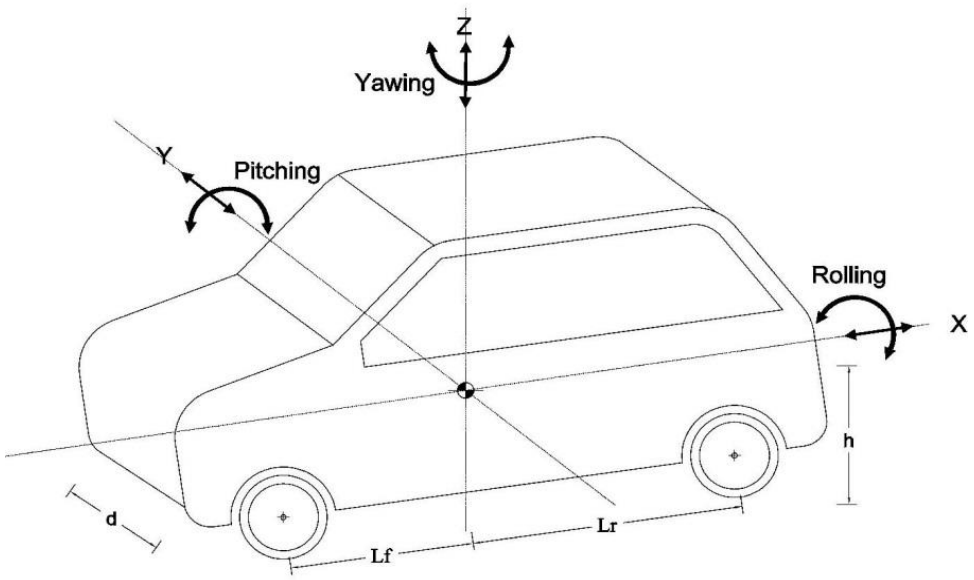

Figure 2.1 Basic motions of the vehicle in three axes

Study on vehicle responses are limited, Maruyama and Yamazaki (2002) studied the response of a moving vehicle to earthquake motion with various JMA intensities, where the vehicle was modelled with six degrees of freedom. That model used the equation of motion with a constant longitudinal speed. The vehicle drift for four earthquakes (Kobe, El Centro, Tottori and Chiba-

ken-oki) was mostly unidirectional and linear. However, this model could not define the behaviour of the vehicle at rest. Hence, we propose a new method of seismic response analysis the 'circular path and linear momentum' (CPLM) method for the lateral and longitudinal stability analysis of vehicles both in motion and at rest. We compare the result with the response of a vehicle which was at rest just before the shaking of the Gorkha 2015 earthquake.

The vehicle was modelled with six degrees of freedom to analyst the vehicle's response to seismic motion. The equation of motion was used as the basic equation for the analysis of the response of the tyres and the car body as well as the transformation of the acceleration from the road surface to the vehicle. The longitudinal and lateral responses were calculated using the CPLM method. We also considered the pitching, rolling and yawing motions of the vehicle as rotations in three directions. The forces acting on the tyres were calculated using the Magic Formula Model (MFM) (Pacejka 2006). The MFM coefficients were taken from previously published results (Alagappan et al. 2014) using the trust region reflective (TRR) method algorithm. We analysed the responses of a car, bus and truck in the longitudinal and lateral directions for several conditions. The relationships between the vehicles' responses with speeds of up to 30.0 m/s from rest condition and peak ground acceleration (PGA) from 1.0 to 15.0 m/s^2 were also investigated.

2.2 Circular path and linear momentum (CPLM) method

The seismic response of a vehicle is different from the response of a structure that is fixed to the ground; in the case of a vehicle, the tyres roll on the ground as forces act on them. As a force is applied to a vehicle, friction produces resistance to the lateral movement, which differs from the resistance in the direction in which the vehicle is moving. Rolling friction is the force required to overcome the resistance between the tyre and the road surface while at rest to initiate the rolling movement of the wheel; this is a relatively small quantity compared with the friction between the rubber tyre and the road surface. When a vehicle is at rest, without applying the hand brake and in neutral gear, the longitudinal force needed to move the car forward is equal to a force that is slightly more than the rolling frictional force that acts in the opposite direction to the applied force. When a vehicle wheel starts to roll, it will acquire linear momentum from the speed that the vehicle develops.

When a lateral force acts on a vehicle at rest, the vehicle may remain at rest or move sideways. If the frictional force is sufficiently high, the vehicle will not move; however, if the lateral force

exceeds the frictional force the vehicle will shift laterally. The lateral movement will depend on the amplitude of the resultant force. In the case of a moving vehicle the lateral force acts for a very short time, pushing the vehicle from the side. As a result, the vehicle's path will bend, forming a curve during that time interval.

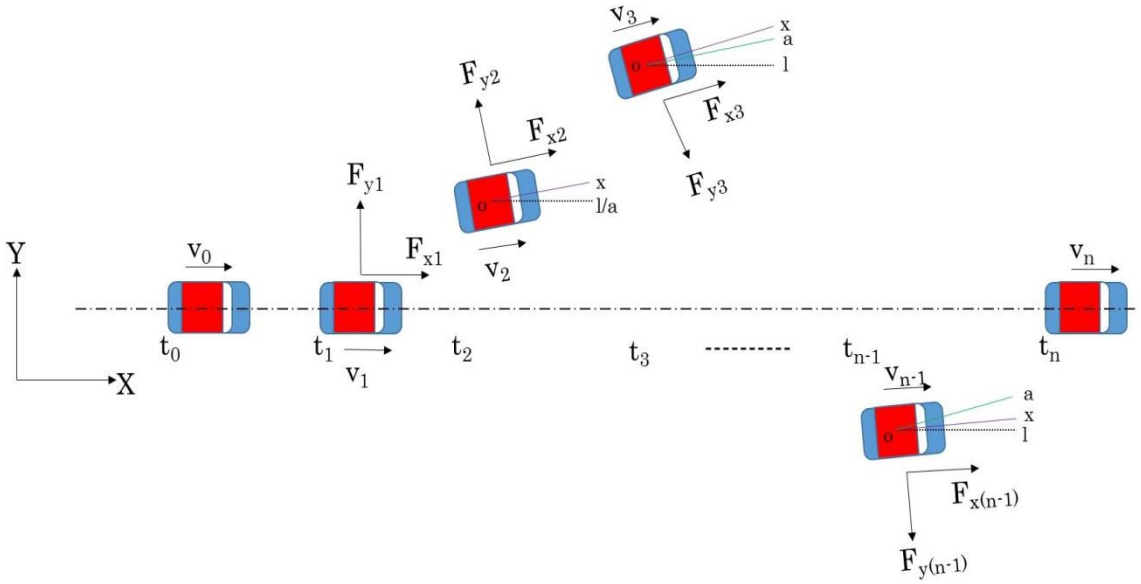

Figure 2.2 Schematic diagram on the concept of CPLM method

To simulate lateral forces on a moving vehicle, the CPLM method assumes that the earthquake forces in each time interval push the vehicle body in a lateral direction, acting as a centripetal force exerted on the vehicle as it moves in a circular path. The lateral force varies with time as the earthquake force changes not only in direction but also in magnitude. The variation of the lateral force in each time step determines the radius of the arc that defines the vehicle path in each time interval. Changes in the radius and centre of rotation of a moving vehicle under earthquake loading can be described by the kinematics of a turning vehicle considering moving centrodes (Guiggiani 2014). Hence, the direction in which the vehicle moves during each step is determined by the relation between the length and the radius of the arc. The length of the arc can be calculated from the speed of the vehicle at that time step. The absolute direction of the vehicle can be determined from the accumulation of angular deviation in each time step for that arc. The position of the vehicle in each time step is derived using the principle of conservation of linear momentum. The force acting in the longitudinal direction is the external force applied at a particular time, changing the momentum and producing the vehicle velocity that is used in the next step of the modelling. Hence, by integrating the concept of the centripetal

force acting on a vehicle moving along a circular arc and the principle of linear momentum we obtain the position of the vehicle during an earthquake. Figure 2.2 shows a schematic diagram of the vehicle movements considered in each time step of the calculation. We set the absolute coordinate system X and Y in the longitudinal and lateral directions; t_0, t_1, t_2, t_3… where t_{n-1} and t_n are the time intervals for the calculation, **v** is the velocity vector, and F_x and F_y are longitudinal and lateral forces that act on the vehicle, respectively. The line 'o–l' is parallel to the absolute longitudinal axis, where 'o–x' represents the local longitudinal axis and 'o–a' represents the line parallel to the local longitudinal axis of the vehicle in the previous step.

2.2.1 Vehicle Model

Each vehicle model is defined by a system with six degrees of freedom consisting of three translational and three rotational motions. The longitudinal, lateral, and vertical translational motions, as well as the corresponding rotational motions – roll, pitch, and yaw – along the X, Y and Z axes, along with dimensional parameters are shown in Figure 2.3. The vehicle model parameters were obtained for a HONDA CIVIC car, a HINO SELEGA_R GD bus and a HINO PROFIA CARGO FR truck. All of these double-axle vehicles are assumed to be running in dry road conditions for this study. The mass of the vehicle bodies and tyres, vehicle dimensions and other parameters for the three vehicle types are shown in **Table 2.1**.

Table 2.1 Parameters of the vehicle models

Parameters	Symbols	Vehicle			Unit
		Car	Bus	Truck	
Each tyre mass	m_1	25.00	41.25	41.25	kg
Vehicle body mass	m_2	1100.00	19490.00	24705.00	kg
Length between front wheel and CG[1]	l_f	1000.00	3375.00	4585.00	mm
Length between rear wheel and CG	l_r	1635.00	2825.00	2595.00	mm
Height of CG	h_0	350.00	863.00	1000.00	mm
Length between right and left axel	d	1505.00	2065.00	2055.00	mm
Stiffness for rolling motion	K_φ	117.60	117.60	117.60	kN m
Elastic constant of steering	K_{st}	48.50	48.50	48.50	kN m/rad

[1] Center of gravity of the car mass

Spring constant between tyre and ground	k_1	800.00	784.00	784.00	kN/m
Suspension spring constant between tyre and mass	k_2	70.00	68.60	68.60	kN/m
Tyre damping	c_1	0.098	0.098	0.098	kN s/m
Suspension damping	c_2	4.90	4.90	4.90	kN s/m

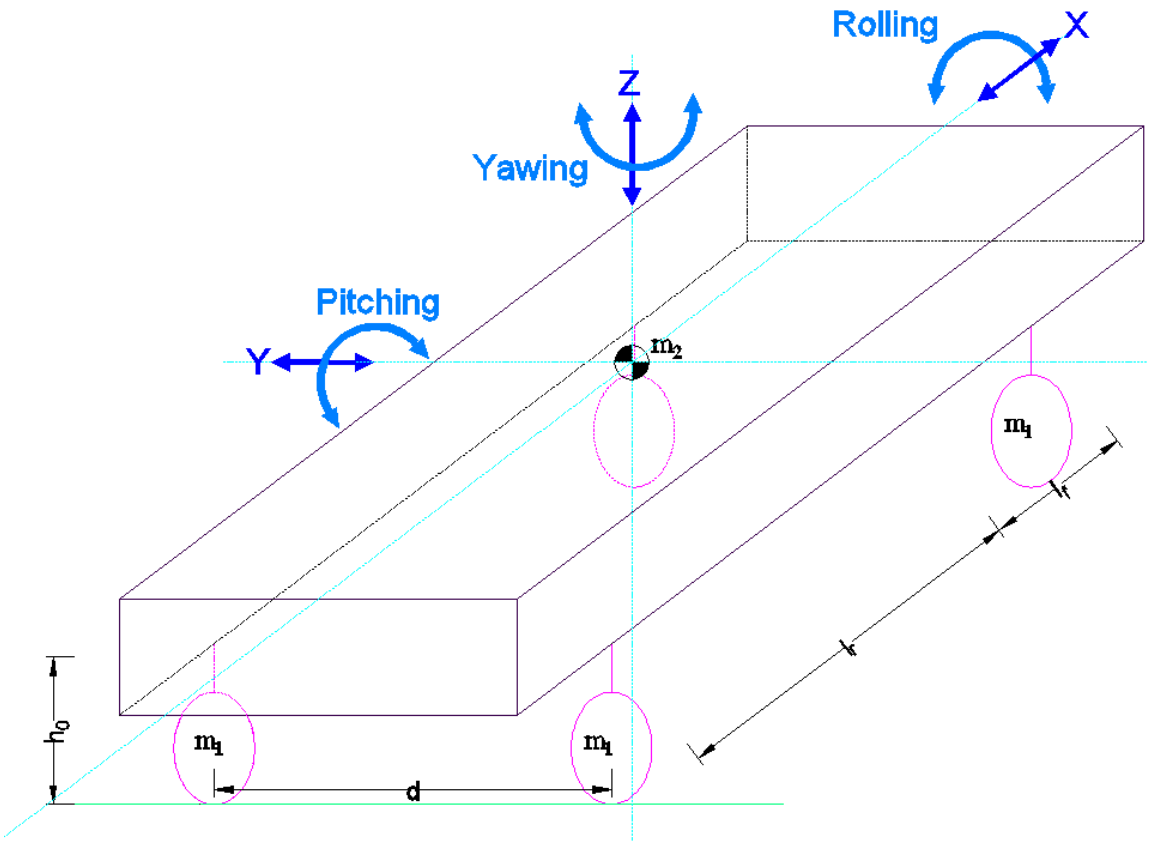

Figure 2.3 Vehicle model with degrees of freedom and dimensional parameters

2.2.2 Analysis

Translational and rotational motions of the vehicle are analyzed using the concepts of inertial forces acted upon it. Mostly used equations of motion considering the spring and dashpot in the joint between two elements are not enough to define all cases in vehicle. Vehicles having rollingtyres with guides could have different response hence for the lateral and longitudinal analysis we used CPLM method. When we calculate the vertical response, we can assume the

tyres as the base and connected to the ground as fixed for instant of time, hence we could use the spring and dashpot system. Rotational motions are calculated considering the moments acted on the vehicle in its state along with effect of speed and accelerations that is subjected to vehicle.

2.2.2.1 Translational motions

Longitudinal, lateral and vertical translational motions are discussed and analyzed in this section. The initial direction of vehicle movement or heading direction of the parked vehicle is taken as longitudinal and the orthogonal axis to the longitudinal is lateral direction. Vertical motion is in up down direction like bumping in undulated surface where lateral is position deviation from the longitudinal axis. For the lateral response of moving vehicle, we look at superfluous or sort of actual distance associated with defined velocity. First of all, let us discuss on the vertical response of the vehicle followed by longitudinal and lateral responses.

Vertical response

The vertical response of the vehicle to earthquake excitation is defined using a two-degrees-of-freedom system. The representation of the road, tyre and vehicle body using springs and dashpots as a quarter vehicle model (Figure 2.4) is used in this study. Each tyre is represented by an element with mass m_1 where vehicle body is represented by mass m_2 in the system. Springs and dashpots are introduced for the connection of ground and tyre and similar for tyre and the vehicle body where vehicle suspension works. Spring and damping constants k_1 and c_1 represents the joint between tyre and ground and k_2 and c_2 are constants of joint between tyre and the vehicle body respectively. Equations (2.1) and (2.2) are the equations of motion for the given model, where z_g is the vertical displacement of the ground and z_1 and z_2 are the relative vertical displacements of the tyre and the vehicle body, respectively.

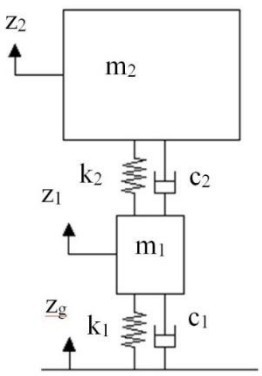

Figure 2.4 Quarter vehicle model to analyse vertical response of the

$$m_1\left(\ddot{z_1} + \ddot{z_g}\right) + c_1\dot{z_1} + c_2(\dot{z_1} - \dot{z_2}) + k_1 z_1 + k_2(z_1 - z_2) = 0 \quad (2.1)$$

$$m_2\left(\ddot{z_2} + \ddot{z_g}\right) + c_2(\dot{z_2} - \dot{z_1}) + k_2(z_2 - z_1) = 0 \quad (2.2)$$

Longitudinal and lateral response

Longitudinal and lateral responses of the vehicle are determined with the CPLM method as mentioned earlier. Acceleration that act on the vehicle in longitudinal and lateral directions are not identical with the ground motion as the joint between road surface and tyre will change the characteristics. Here similar concept of vertical response on tyre to transfer accelerations is used for lateral and longitudinal respectively. Single degree of freedom system model of vehicle is used to transfer the ground motion to the vehicle as shown in the figure 2.5. The stiffness and damping constants used for the tyre properties in the vertical response analysis were used for the lateral and longitudinal acceleration calculation (Eqs. (2.3) and (2.4)). Notations $\ddot{x}_g$ and $\ddot{y}_g$ are the ground accelerations where $\ddot{X}$ and $\ddot{Y}$ are the accelerations in longitudinal and lateral directions respectively, transferred to the vehicle.

$$m\ddot{X} + c_1\dot{X} + k_1 X = -m\ddot{x}_g \quad (2.3)$$

$$m\ddot{Y} + c_1\dot{Y} + k_1 Y = -m\ddot{y}_g \quad (2.4)$$

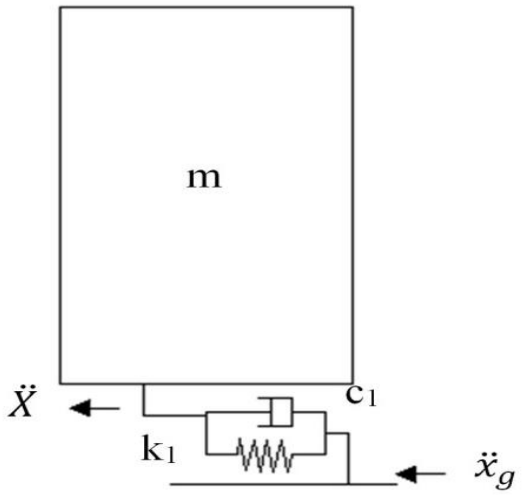

Figure 2.5 Single degree of vehicle model to transfer longitudinal and lateral ground motion to the vehicle

Coordinate system are also transferred to local coordinate as the vehicle deviation for the forces calculations along the longitudinal and lateral directions (global axes). The external forces acting on the vehicle body are now determined by using the vehicle accelerations after

transferring the parameters from a global coordinate system to the local coordinate system. First, obtain the absolute acceleration vector acting on the vehicle using Eqs. (2.5) – (2.9), where 'a' and 'θ_a' are the magnitude and direction of the acceleration vector, and '$\ddot{x}$' and '$\ddot{y}$' are the acceleration vectors along the longitudinal and lateral axes of the vehicle in the local coordinate system. 'θ_l' is the angle of the longitudinal axis relative to the global axis (∠lox in Figure 2.2), and 'θ_f' defines the position of the acceleration vector relative to the local axis.

$$a = \sqrt{\ddot{X}^2 + \ddot{Y}^2} \tag{2.5}$$

$$\theta_a = \tan^{-1}\frac{\ddot{Y}}{\ddot{X}} \tag{2.6}$$

$$\theta_f = \theta_a - \theta_l \tag{2.7}$$

$$\ddot{x} = a\cos\theta_f \tag{2.8}$$

$$\ddot{y} = a\sin\theta_f \tag{2.9}$$

Consider a vehicle moving in a circular trajectory with lateral force acting on it. This force is the sum of all the external forces in terms of the acceleration and the rotational movement of the vehicle body. The rolling of the vehicle body also exerts some lateral force, which depends on the deviation angle during each step. Let's assume that there is no rolling motion in the first step of the analysis. In the next step, as the lateral force is activated, the vehicle begins to roll. The orientation of vehicle will begin to change as the vehicle starts to move longitudinally while the lateral force is acting on it.

The longitudinal forces acting on the vehicle are:

- The rolling resistance of the tyres
- The force generated by the slip of the tyres on the ground
- The external force exerted by the earthquake acceleration

Rolling resistance force

When a vehicle is in rest condition, without any brake applying on it, without any gear, i.e. in neutral on the plain ground it needs external force to start on moving. The force needed to start moving of vehicle on the road surface against bearings and frictions is known as the rolling resistance force (F_{roll}). It represents the resistance that should be overcome by the applied force to initiate the vehicle motion. When the vehicle is running with constant speed, we can neglect

the rolling resistance as there must be a constant acceleration that nullify the rolling resistance effect. In cases where the vehicle decelerates and stops or where the vehicle is at rest, the rolling resistance should include in the analysis. Rolling resistance force can be calculated using the equation (2.10).

$$F_{roll} = C_{roll} mg \tag{2.10}$$

Table 2.2 Rolling resistance coefficients for various vehicles (Wong 2001)

Road surface	Vehicle type	
	Car	Bus/Truck
Concrete, Asphalt	0.013	0.006 – 0.01
Rolled gravel	0.02	-
Tarmacadam	0.025	-
Unpaved road	0.05	-
Field	0.1 – 0.35	-

where 'g' is the gravitational acceleration, Coefficient of rolling resistance is denoted by 'C_{roll}' and 'm' is total mass of the vehicle. The coefficients of rolling resistance (C_{roll}) for various vehicles moving on concrete and asphalt road surfaces are shown in **Table 2.2** (Wong 2001).

Force induced by slip of tyre

When the speed of the vehicle is either faster or slower than the speed of the rolling tyre, there will be slipping of tyre on the ground. In order to find the condition of slip effect we should know the maximum value of acceleration or retardation of the vehicle. When the applied acceleration or retardation exceeds the threshold value of acceleration for non-slip condition we can calculate the slip force exerted on tyres. The threshold values of maximum acceleration that can be applied to the vehicle for the non-slip condition can be found from the rolling dynamics of the tyre. Figure 2.6 shows the forces act on the tyre.

R: Radius of the tyre

m_t: Mass of the tyre

F_{rt}: Frictional force between tyre and road surface

I: Angular moment of inertia about centre of the tyre

α: Angular acceleration of the tyre

V: Linear velocity of the tyre

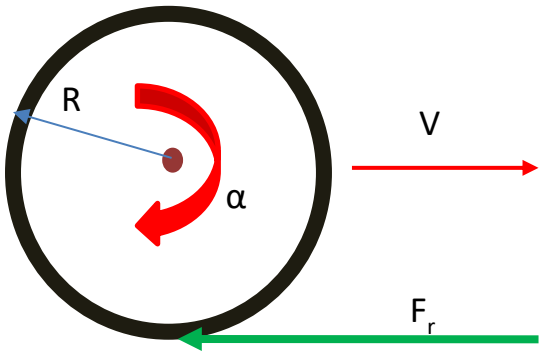

Figure 2.6 System of forces acting on rolling tyre

Moment due to the friction force about the centre of the tyre is given by equation (2.11) where the momentum due to the angular acceleration of tyre to the centre is given by equation (2.12).

$$M_{cl} = F_{rt}R \tag{2.11}$$

$$M_{ca} = I\alpha \tag{2.12}$$

When there will be the equilibrium of moment about the centre there will not be any slip condition. Hence, equating these both moment about the centre of the wheel,

$$F_{rt}R = I\alpha \tag{2.13}$$

Where,

$$I = \frac{1}{2}m_t R^2 \tag{2.14}$$

$$\alpha = \frac{a}{R} \tag{2.15}$$

$$F_{rt} = \mu m_t g \tag{2.16}$$

Linear acceleration is denoted by 'a' and 'μ' is the frictional coefficient. Using the Eqs. (2.14) – (2.16) on equation (2.13) we can get the maximum value of acceleration as threshold for slip effect to start. Maximum linear acceleration of tyre (vehicle acceleration) for non-slip condition is given by equation (2.17).

$$a_{max} = 2\mu g \tag{2.17}$$

The frictional coefficient between the tyres and dry asphalt concrete are taken as 0.8 [30] for further calculation in this study. When the applied acceleration or deceleration is larger than a_{max} the slip can be calculated, and represented as the slip ratio as given in equation (2.18),

$$Slip\ ratio = \frac{v_2 - v_a}{v_2} \tag{2.18}$$

Where 'v_2' is, the resultant velocity considering the input acceleration and 'v_a' is the velocity considering the maximum acceleration.

Longitudinal force (F_{xs}) acting on the tyres due to the slip can be calculated using the MFM for slip ratio. Detailed on MFM are explained in Appendix I.

The lateral movement of the vehicle depends on the lateral force applied on the vehicle body. The slip angle 'θ' determines the trajectory of the vehicle subjected to a lateral load. To calculate the slip angle, we can use the centripetal force that moves the vehicle in a circular path, as described previously.

The centripetal force that acts on a vehicle body moving in a circular path is given by equation (2.19).

$$F_c = \frac{mv^2}{R_p} \tag{2.19}$$

Where 'R_p' is the radius of the circular path, and *'v'* is the velocity of the vehicle.

Again, the lateral force acting on the vehicle is the sum of the external forces caused by lateral acceleration and the force generated by the rotational motion about the longitudinal axis (rolling) is given by equation (2.20).

$$F_c = m\ddot{y}_{tg} + mgsin(\emptyset) \tag{2.20}$$

Now, radius of the circular path for each time interval (R_p) can be derived from Eqs. (2.19) and (2.20). The subtended angle 'θ' for that arc can be calculated using Eq. (2.21), where '*D'* is the distance travelled by the vehicle during the time interval 'dt' as shown in Eq. (2.22).

$$\theta = \tan^{-1}\frac{D}{R_p} \tag{2.21}$$

$$D = v\mathrm{dt} \tag{2.22}$$

The slip angle calculated in equation (2.22) considers the radius value from the CG of the vehicle to the centre of the circular path. Considering the variation of the radius for the left and right tyres, the slip angles for the left and right front tyres 'θ_{lt}' and 'θ_{rt}' can be derived from Eqs. (2.23) and (2.24), respectively. The rear tyres are aligned with the vehicle body; therefore, we can assume zero slip angles for the rear tyres.

$$\theta_{lt} = \tan^{-1}\frac{D}{R_p - \frac{d}{2}} \tag{2.23}$$

$$\theta_{rt} = \tan^{-1}\frac{D}{R_p + \frac{d}{2}} \tag{2.24}$$

When there is large lateral force on the vehicle with the slower speed, consideration all the lateral forces play the role to deviate the vehicle, it results higher value of the deviation angle. There are limitations on the tyre rotation where tyres do not allow the vehicle to turn in a full circle in fraction of time. The maximum value of the turning angle or the slip angle is assumed to be the same as that used in the geometric design of highways and roads by the American Association of State Highways and Transportation Officials [31]. Maximum turning angle of the vehicles are listed in table 2.3.

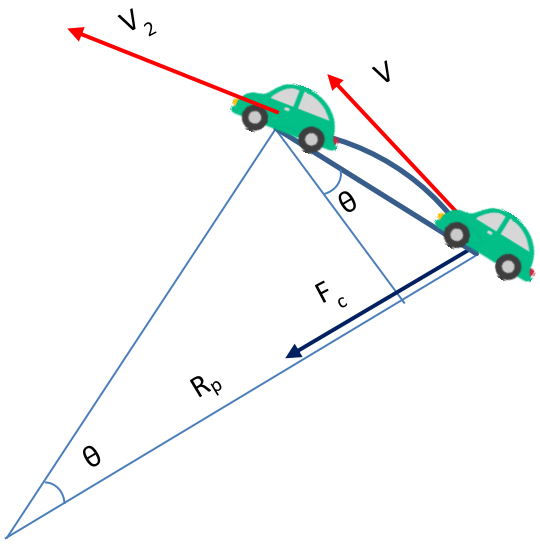

Figure 2.7 Schematic diagram of the vehicle movement with deviation angle

Schematic diagram of vehicle movement with the deviation angle is shown in figure 2.7, where 'v' is the velocity of vehicle at point of time under consideration and 'v_2' represents the velocity of the vehicle after the time step. Especially for the slower speed vehicle, to overcome the

problem of getting higher deviation angle, we can set the minimum radius of turn for the vehicle. Minimum radius of turn sets the deviation of the vehicle, where excess force will act as the lateral force on vehicle.

Table 2.3 Maximum steering angle of vehicles

Vehicle type	Maximum steering angle (degree)
Car	31.6
Bus	38.7
Truck	31.7

The longitudinal and lateral forces acting on each tyre are calculated using the MFM, considering pure slip conditions. Slip ratio for the longitudinal force and slip angle for the lateral force are used to find the coefficients which are later multiplied with the vertical load of vehicle to get corresponding forces on tyres. Calculation details on the MFM and final coefficients to calculate the force are provided in appendix I.

The total longitudinal force acting on the tyre can be calculated using Eq. (2.25). F_{roll} will always act against the moving direction. F_{xg} is the external force from the earthquake acceleration in the longitudinal direction.

$$F_x = F_{xg} + F_{xs} \pm F_{roll} \tag{2.25}$$

$$F_{xg} = m\ddot{X} \tag{2.26}$$

Lateral sliding of the tyres will occur when the net force acting in the lateral direction is higher than the resistive force in opposite. This value depends on the frictional force (F_r) that acts against the applied force; it is a factor of the frictional coefficient and the normal load. If the lateral force F_{yg} exerted on the tyres due to the earthquake is larger than the frictional resistance, the vehicle will slide laterally. Forces those acts on the tyre and the road surface are shown in Eq. (2.27).

$$F_y = \left|F_{yg}\right| - F_r \tag{2.27}$$

$$F_{yg} = m\ddot{Y} \tag{2.28}$$

When there is the condition of calculated radius less than the minimum then we should set the minimum radius, residual forces those cannot turn the vehicle are now additionally applied in equation (2.27) even in cases of total force is less than the frictional force.

Considering the principle of conservation of momentum along the vehicle axis, we can obtain a new velocity vector v_2 along that axis from Eq. (2.29). F_x is the total external force applied during the time interval (*dt*) in this system.

$$mv + F_x dt = mv_2 \tag{2.29}$$

$$v_x = v_2 \cos\theta_1 \tag{2.30}$$

$$v_y = \left[v_2 + \frac{F_y dt}{m}\right] \sin\theta_1 \tag{2.31}$$

$$\theta_1 = \theta_1 + \theta \tag{2.32}$$

$$D_{x_i} = D_{x_{i-1}} + v_{x_i} dt \tag{2.33}$$

$$D_{y_i} = D_{y_{i-1}} + v_{y_i} dt \tag{2.34}$$

The velocity and displacement of the vehicle are now calculated from Eqs. (2.30) – (2.34) in global coordinates. The path of the vehicle in each step is determined by summing the slip angles using Eq. (2.35).

$$\theta_{1_{i+1}} = \theta_{1_i} + \theta_i \tag{2.35}$$

2.2.2.2 Rotational motions

Rotational motions of the vehicle along three axes, rolling, pitching and yawing are discussed in this section. Changes in the position of vehicle in different axes, represented in angular form are rotational motions of the vehicle. Rolling motion of the vehicle is angular motion in longitudinal axes of the vehicle, it rolls the vehicle in lateral direction, if the rotational angle reached 90° then vehicle will get topple. Pitching is the rotational motion along lateral axis, vehicle has rotated on back and forth. The direction of pitching motion is almost like the tyre rotation while rolling is like pushing from the side. Whereas yawing motion is the rotational motion of vehicle along vertical axis.

On calculation of moments due to the forces acted on vehicle in different axes separately; provides the rotational motions as a result. Considering only the moments might not well define the system when the vehicle get supported only in one side (either right or left during high rolling motion or back or forth during high pitching motion). When the vehicle subjected to high pitching motion, it pushed the vehicle back or forth, as tyres get roll it has not more effect than the rolling motion where tyre cannot roll in lateral direction hence we use the concept of angular momentum for case of toppling.

Pitching motion

The pitching motion of the vehicle is the rotational motion about the lateral axis. Taking the moments of the forces acting on lateral axis, the relationship of the forces is shown in equation (2.36).

$$\left\{2K\left(l_f^2 + l_r^2\right)\right\}\theta_p = m(\dot{u} - vr)h \tag{2.36}$$

where m is the mass of the vehicle, K is the stiffness of the tyre, θ_p is the pitching angle, h is the height of the centre of gravity (CG) of the vehicle mass, and $\dot{u}$ and v are the longitudinal acceleration and lateral velocity of the vehicle, respectively. The yaw angular velocity is denoted by r, and l_f and l_r are the distances of the front and rear axle from the CG of the vehicle mass, respectively.

Rolling motion

The rolling motion of the vehicle is the rotational motion about the longitudinal axis. When the vehicle stands on all tyres, Toppling mechanism of vehicle do not start then taking the moments of the forces acting on longitudinal axis, the relationship of the forces is as shown in equation (2.37).

$$(K_{\emptyset} - mgh)\emptyset = m(\dot{v} + ur)h \tag{2.37}$$

Here $K_{\emptyset}$ is the rolling stiffness and '$\emptyset$' is the rolling angle.

When a vehicle starts to topple, only the single side tyres take vertical loads then it starts toppling. A simple model for rolling analysis is shown in figure 2.8 where 'd' is the trade length, 'h' is the height of the CG, 'θ_g' is the angle from lower corner to CG.

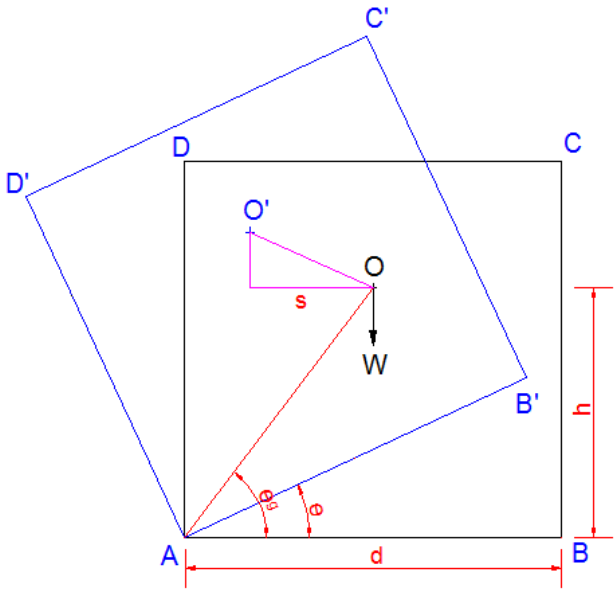

Figure 2.8 Vehicle model to analyse the rolling motion in toppling condition

Vehicle toppling mechanism starts when the vehicle load initiates to transfer to ground through the tires in one side. Considering the up-down component of the ground motion, threshold value of the lateral acceleration (a_t) to start the toppling mechanism of vehicle is given by equation (2.38).

$$a_t = \frac{d(g - \ddot{z})}{2h} \tag{2.38}$$

Where 'g' is the gravitational acceleration and '$\ddot{z}$' is vertical acceleration. Total angle 'θ_a' including the rolling angle and 'θ_g' is calculated for location of CG in each step as shown in equation (2.39). Changes in angular momentum due to the vertical and lateral acceleration are calculated by using the equation (2.40).

$$\theta_a = (\theta_g + \emptyset_i) \tag{2.39}$$

$$\Delta L = mR_g[\ddot{y}\sin(\theta_a) + \dot{y} \mp \{(g - \ddot{z})\cos(\theta_a)\}] \tag{2.40}$$

Where 'ΔL' is change in angular momentum, 'R_g' is the distance from bottom corner to the locus of CG (AO in figure 2.8). Lateral acceleration and velocity of the vehicle are denoted by

"ÿ" and "ẏ". Sign of vertical component of momentum in equation (2.40) is depends on support condition of vehicle. When we consider the left bottom corner as the support and the lateral acceleration is anticlockwise, negative sign is used and vice versa. Summation of angular momentum in each step of calculation is now used to find out the linear velocity of body in lateral direction centred on lower corner by equation (2.41). Equation (2.42) shows the calculation of change in rolling angle.

$$\mathrm{V_i} = \frac{\mathrm{L_i}}{\mathrm{R}_g \mathrm{m}} \tag{2.41}$$

$$\Delta\emptyset = \frac{\mathrm{v_i} * \mathrm{dt}}{\mathrm{R}_g} \tag{2.42}$$

$$\emptyset_{\mathrm{i+1}} = \emptyset_{\mathrm{i}} + \Delta\emptyset \tag{2.43}$$

Toppling mechanism of vehicle continues up to when the rolling angle reaches 90°, the vehicle toppled on the side. Total rolling angle of the vehicle in each step of time can be calculated using equation (2.43). Whenever the lateral acceleration could bring back the vehicle on its original position, even though the CG crossed the support point hence we should calculate until the rolling angle reached π/2.

Yawing motion

The yawing motion of the vehicle is the rotational motion about the vertical axis, and can be described by Eq. (2.44),

$$I_z \frac{dr}{dt} = \left(F'_{y11} + F'_{y12}\right) l_f - \left(F'_{y21} + F'_{y22}\right) l_r + \left(-F'_{x11} + F'_{x12}\right) \frac{d}{2} + \left(-F'_{x21} + F'_{x22}\right) \frac{d}{2} \tag{2.44}$$

Where 'I_z' is the moment of inertia of the vehicle, '*d'* is the distance between the right and left wheels, and F'_y and F'_x are the lateral and longitudinal forces acting on each tyre, respectively, (indices 1 and 2 refer to the front and rear and left and right, respectively).

2.2.3 Validation of CPLM method

The Gorkha earthquake in Nepal was one of the largest earthquakes of 2015 and is noted for the unique nature of its ground motion. The ground motion recorded in Kathmandu had a long period and shook central Nepal severely even though the PGA was relatively low (Parajuli and Kiyono, 2015). The Nepal police released several closed-circuit television (CCTV) videos[2] after the earthquake that recorded the shaking in the streets of Kathmandu. For our study, we used one of these videos that captured the vehicle response during the earthquake in Sundhara, one of the major public transport hubs in Kathmandu.

Figure 2.9 Microvan in dotted circle with road orientation shown in dotted line with respect to North

The video shows a microvan that stopped just before the earthquake struck, with passengers getting out of the vehicle while others are trying to get in (circled in yellow, Figure 2.9). When the shaking started, people got panic, the doors moved and some people got out of the vehicle during the shaking. To track the position of the minibus we picked its' location in the photo frame of every 0.2 s. We also established a baseline about a stiff object nearby to correct for the effect of shaking. Comparison of the vehicle motion during the earthquake tracked from the video to the seismic response of the modelled vehicle using the CPLM method has done.

[2] Video shared on YouTube https://www.youtube.com/watch?v=I20dIt88-u4

The orientation of the vehicle is N14°30′E, calculated using two points along with the reference to the road side which has a bearing of N3°30′E (Figure 2.9). The vehicle is a Toyota HiAce, the dimensions and weight parameters are taken from the Toyota specification sheet (Toyota 2015). The wheelbase of the vehicle is 2.57 m; the distance between the right and left wheels is 1.47 m and the kerb weight is 1825 kg. We assumed that the CG of the vehicle is in the centre of the wheelbase; the other parameters are used as listed in **Table 2.1**.

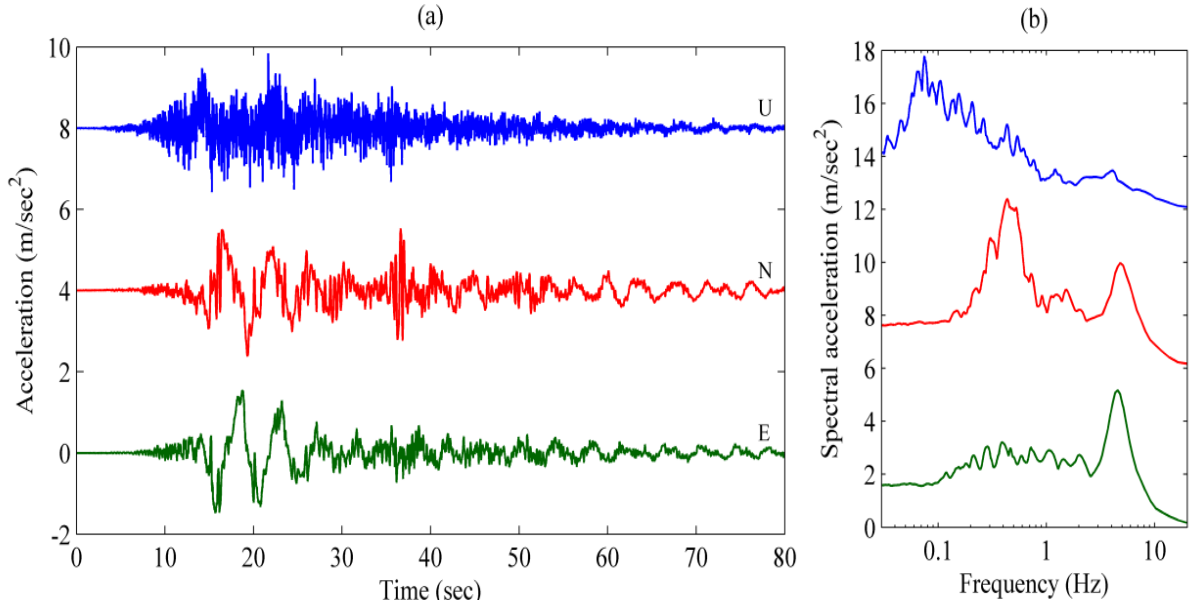

Figure 2.10 Ground motion acceleration and spectral accelerations of Gorkha earthquake recorded in KATNP station Kathmandu

As the vehicle was oriented towards the northeast, we used the N–S component of the ground motion as the longitudinal axis and the E–W component as the lateral direction of the vehicle. We used the Gorkha earthquake data recorded at the US Geological Survey's KATNP station (USGS 2015), 1.2 km from the location of the video camera. The ground motion records and corresponding response spectra, considering 5% damping, are shown in Figure 2.10. The orientation of the vehicle is also used in the analysis. The results showing the longitudinal and lateral displacements of the vehicle in response to the earthquake motion are shown in Figure 2.11 for the CPLM method and the video analysis. Tendency of response curves from analytical method and video are well matched. Note that the video shows that people were getting on and off the bus, and the driver initially may have used the brakes; these are factors that are not accounted in the numerical simulation.

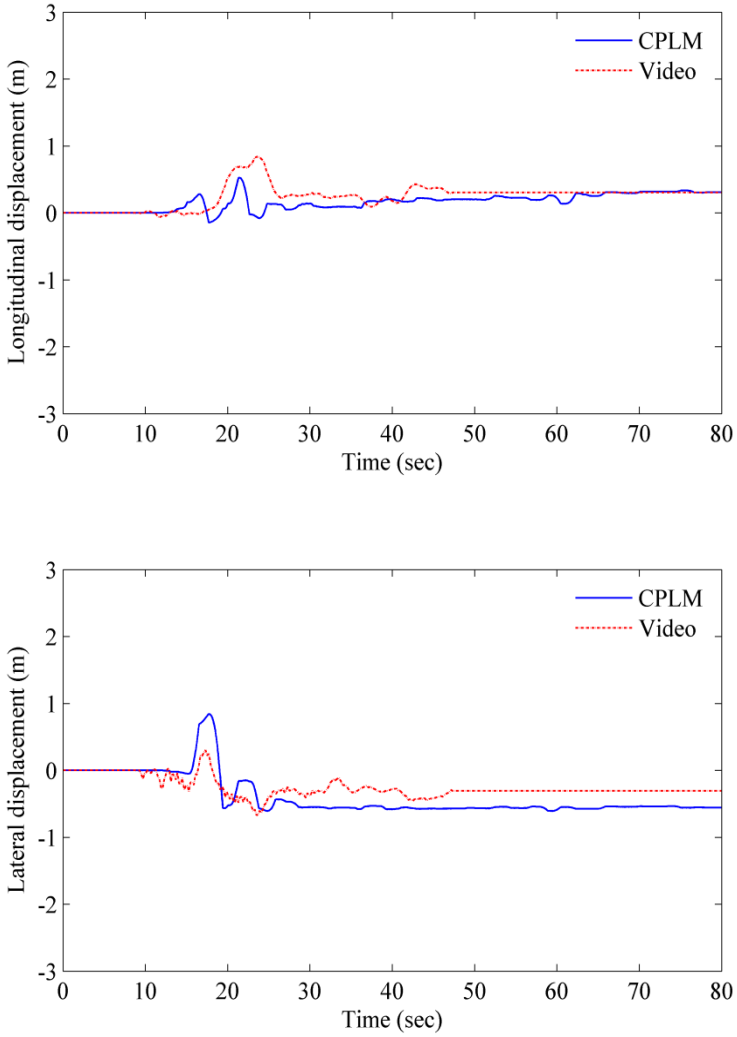

Figure 2.11 Comparison of CPLM result and vehicle response during Gorkha earthquake

2.3 Lateral and longitudinal responses of vehicles

Positions of vehicle during the earthquake shaking are important to analyze the risk associated with it. Lateral response corresponds to the deviation of vehicle from its lane where longitudinal response could affect the distance between vehicles which might lead to collision with vehicles. Drivers' response with steering control could be enough for lateral response but reaction time will surely affect on this phenomenon. The longitudinal response of vehicle is like accelerating or braking the vehicle, which is hard to control by drivers' action.

Table 2.4 List of earthquake datasets used in the analysis

Earthquake	Date	Magnitude	Station	Epicentral Distance (km)
Northridge	17-01-1994	6.4 Ml	Tarzana	5.5
El Centro	18-05-1940	6.9 Mw	El Centro	16.9
Kobe	17-01-1995	6.9 Mw	KJMA	1.0
Loma Prieta	17-10-1989	7.0 Ml	Watsonville	18.1
New Zealand	03-09-2010	7.0 Mw	Greendale	6.9
Miyagi Ken-Oki	26-05-2003	7.0 Mw	Oshika	59.0
Chi-Chi	20-09-1999	7.6 Mw	Taichung	8.3
Gorkha	25-04-2015	7.8 Mw	KATNP	76.9
Chile Coquimbo offshore	16-09-2015	8.3 Mw	El Pedregal	92.3
Great East Japan	11-03-2011	9.0 Mw	Tsukidate	125.9

Table 2.5 Earthquakes and ground motion parameters

Earthquake	Peak acceleration (m/sec^2)		Dominant Frequency (Hz)	
	EW	NS	EW	NS
EQ01 Northridge – 1994[§]	17.40	9.71	2.91	2.22
EQ02 El Centro – 1940[§]	2.14	3.49	2.37	1.47
EQ03 Kobe – 1995	8.21	5.99	1.47	1.42
EQ04 Loma Prieta – 1989[§]	3.52	2.67	1.37	1.47
EQ05 Christchurch – 2010[§]	7.38	6.64	0.76	0.71
EQ06 Miyagi Ken-Oki – 2003[¡]	8.25	11.10	7.89	6.96
EQ07 Chi-Chi – 1999[§]	2.92	4.34	3.66	1.61
EQ08 Gorkha – 2015[§]	1.54	1.60	0.22	0.22
EQ09 Chile Coquimbo – 2015[§]	6.77	5.45	5.70	8.73
EQ10 Great East Japan – 2011[¡]	12.20	25.90	5.08	6.01

[§] Strongmotioncenter.org [34]

[¡] K-NET, KiK-net [35]

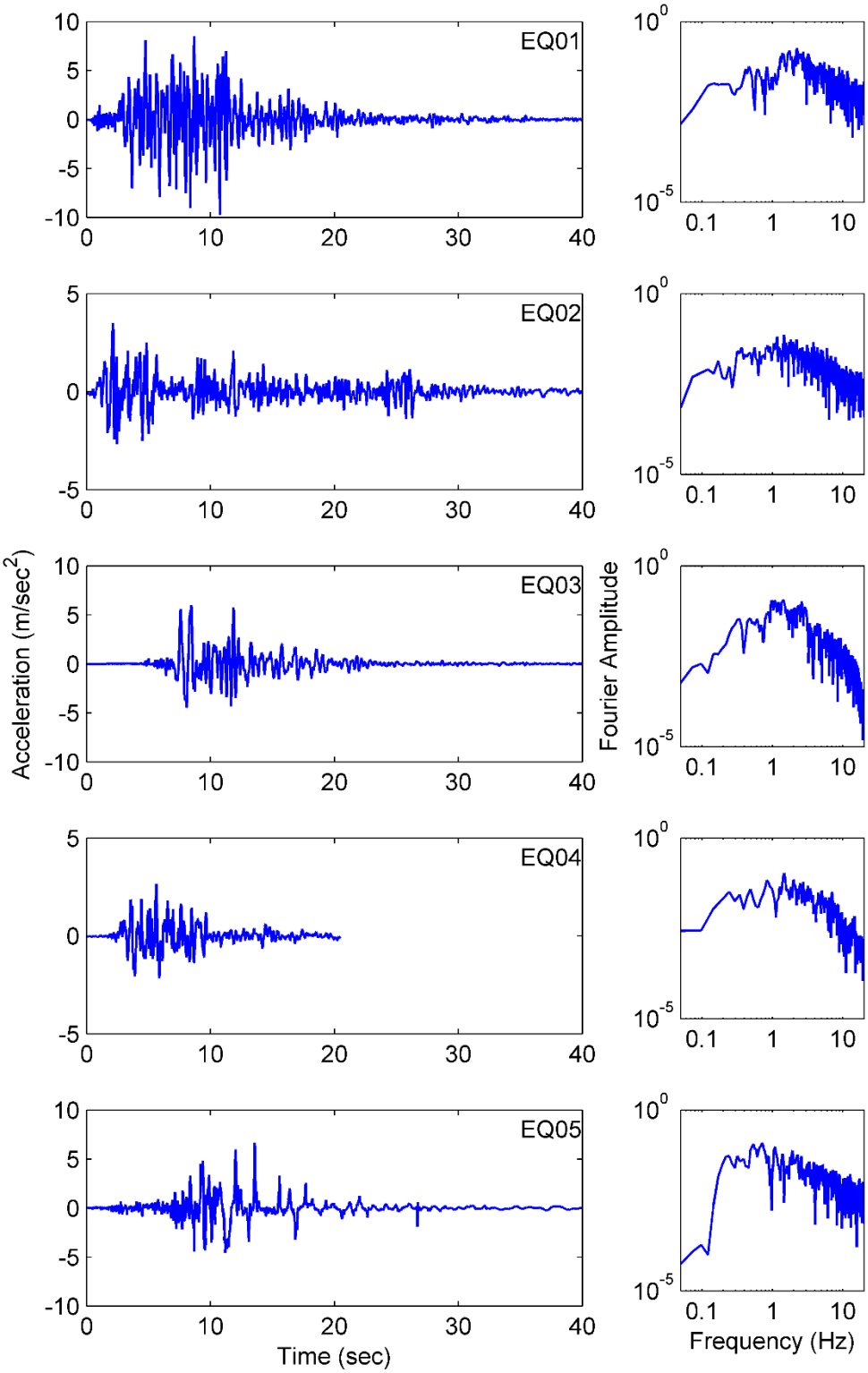

(a) N-S component of earthquake records used in the analysis (1-5)

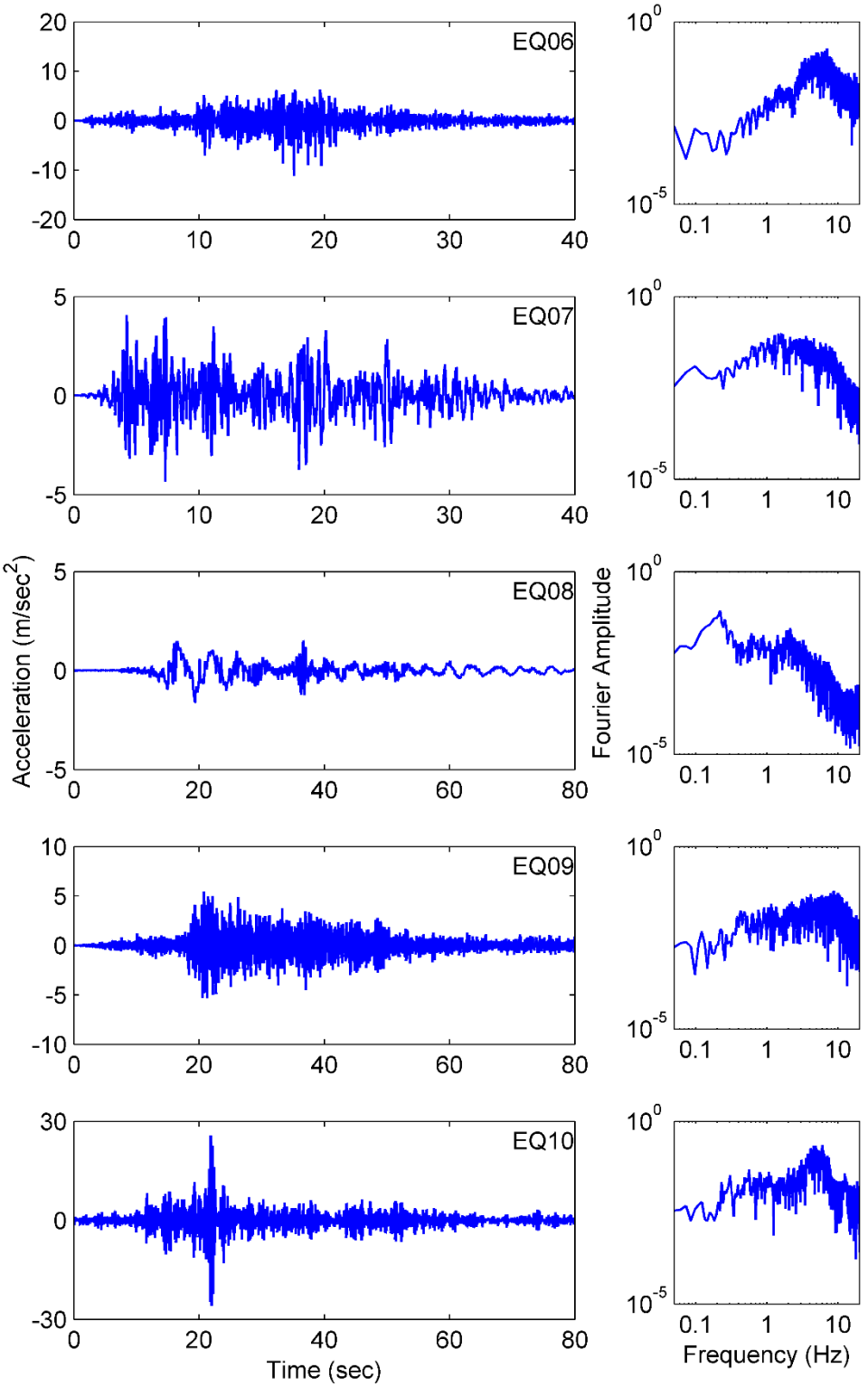

(b) N-S component of earthquake records used in the analysis (6-10)

Figure 2.12 N-S component of earthquake records used in the analysis (a: 1-5, b: 6-10)

Seismic responses of the vehicles are now analysed for different situations in longitudinal and transverse direction. The vehicle seismic response analyses were performed in ideal situations that considered the movement of the vehicle without any responsive actions from the driver.

We have chosen 10 earthquake datasets from around the globe (**Tables 2.4 and 2.5**) with moment magnitudes of 6.7 to 9.0. The selected earthquakes occurred between 1940 and 2015. The minimum and maximum PGA in the E–W direction vary between 1.54 m/s^2 for the Gorkha earthquake and 17.40 m/s^2 for the Northridge earthquake. In the N–S direction, the minimum and maximum PGA are 1.60 and 25.9 m/s^2 for the Gorkha and Great East Japan earthquakes, respectively.

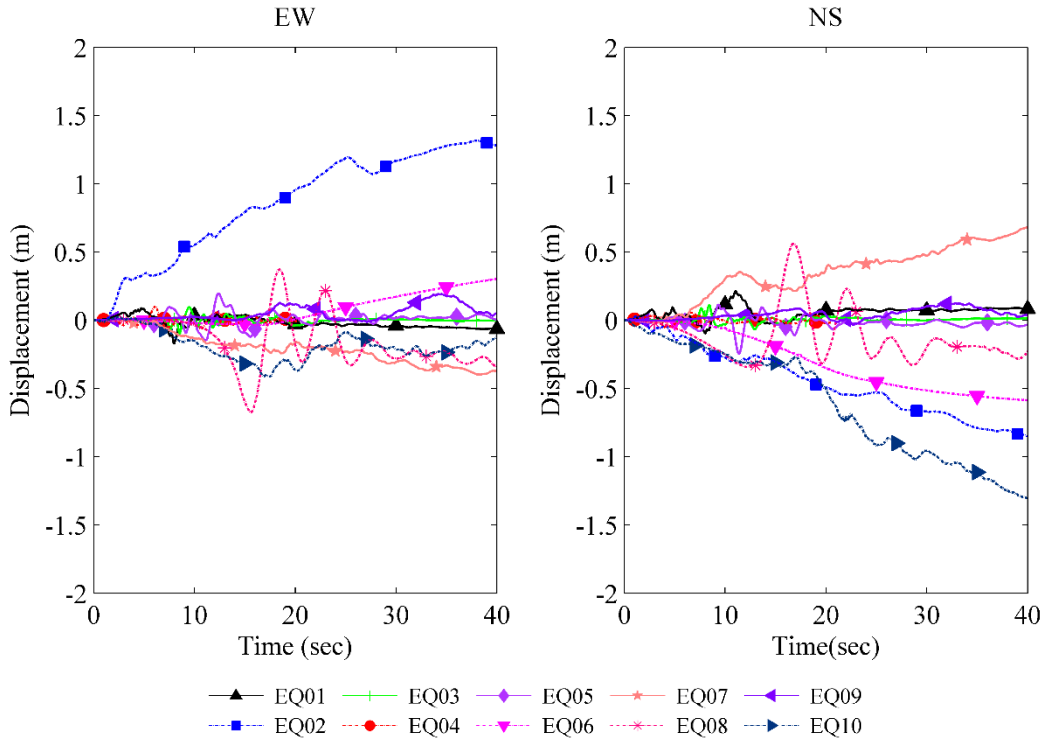

Figure 2.13 Displacement time series of given earthquakes

The N–S components for all the earthquake records are shown in Figure 2.12 along with corresponding Fourier spectra. The ground acceleration data-sampling rate varied from 50 to 200 Hz; for consistency, select all the data sampled at 50 Hz for analysis. The displacement time series of all the earthquakes (Figure 2.13) were calculated using Newmark's integration method.

The seismic responses of the vehicles for the selected earthquakes were calculated for various conditions; we assumed that when a vehicle is moving at a speed of more than 5.0 m/s, there

will be the driving force with constant acceleration to keep on driving that will nullify the rolling resistance. Hence, the effect of the rolling resistance will be significant only when the vehicle is moving at speeds below 5.0 m/s. We modelled the three vehicle types (i.e., car, bus and truck) in each of the analysis cases. Figure 2.14 shows the response of the vehicles at rest in the longitudinal direction (top panels) and in the lateral direction (lower panels). The first, second and third columns show the response of the car, bus and truck, respectively. The bus has the largest response even though the mass of the truck is larger than that of the bus, potentially because the maximum turning angle of front tyre plays a role.

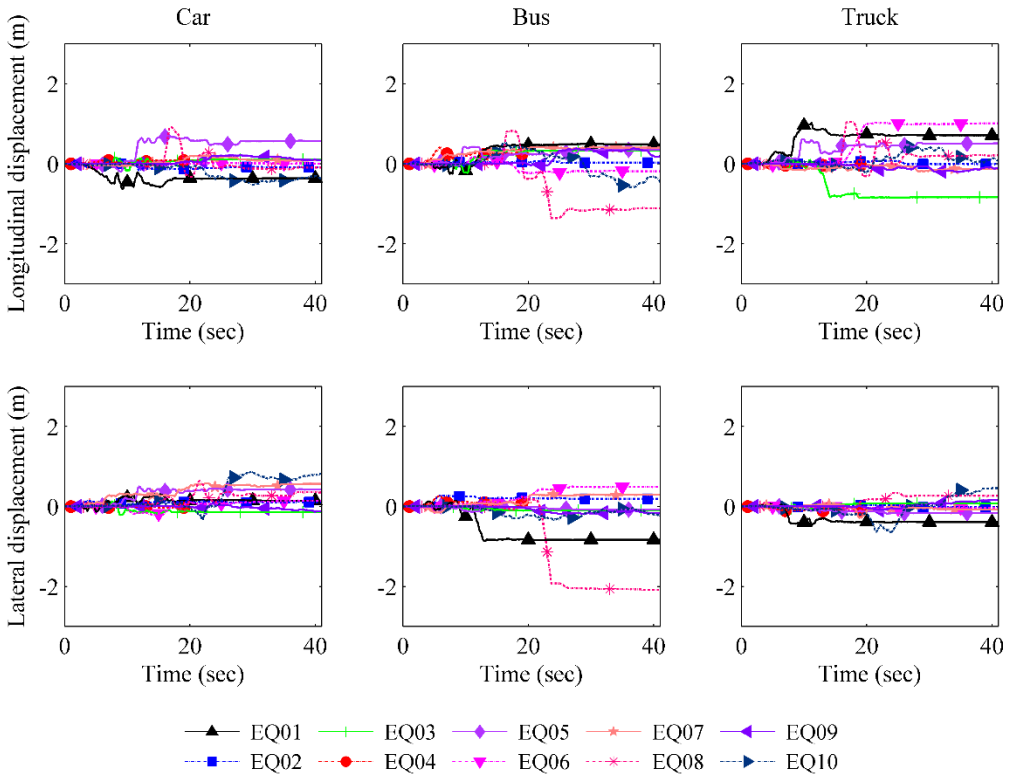

Figure 2.14 Parked vehicle response during specified earthquakes

We assumed an ideal scenario of a vehicle moving at a certain speed where the driver does not react to the effects of the earthquake and the vehicle is moving freely at a constant speed. The responses of the moving vehicles with a constant speed of 20.0 m/s are shown in Figure 2.15. The longitudinal displacements are the seismic displacements of the vehicle, where the displacement due to the initial constant speed of the vehicle is unknown. It is worth noting that the longitudinal response of the El Centro earthquake (California, USA) deviates from the general trend of the other earthquakes, which is attributed to the effect of the residual displacement (Figure 2.13). The accumulated acceleration in the longitudinal direction sustains a higher momentum on the vehicle, pushing it further in the longitudinal direction. The lateral

responses of the vehicles vary for the different cases mainly because of deviations in the moving trajectory of the vehicle.

In many cases, the deviation of a vehicle's path due to ground motion effects leads to unreal values for the maximum response. Therefore, we fixed the time window to check the maximum response. We selected a time window for tracing of the maximum response as the time of PGA plus an extra 5 seconds for each case. The maximum response of the vehicle in the given time frame is then identified. **Table 2.5** shows the time of PGA and the corresponding time window used for each earthquake.

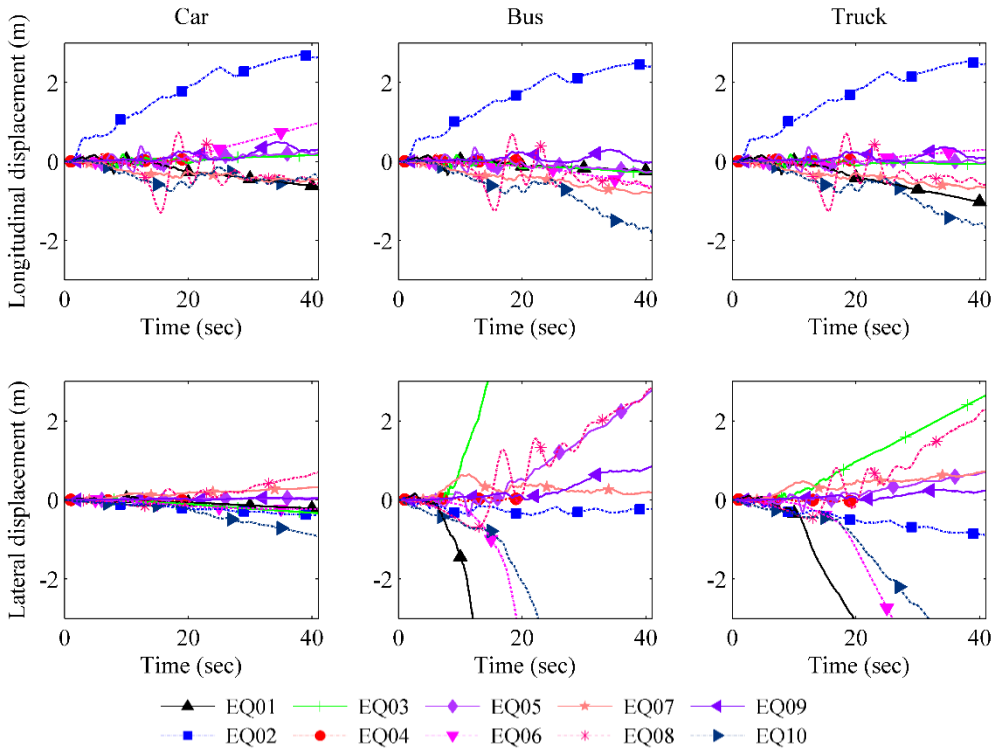

Figure 2.15 Response of vehicles with speed 20 m/sec under specified earthquakes

We performed the simulation for the 10 selected earthquake records with different vehicle speeds; the modelled PGA remains the same as that which was recorded during those events. The relationship between the maximum longitudinal and lateral responses of the vehicles and the velocity are shown in Figure 2.16. The maximum response of the vehicles occurred at speeds of about 2.0 m/s; the response then decreased gradually as the velocity increased to about 10.0 m/s and then slightly increased. The car showed the smallest displacements whereas the truck and bus were more affected by misalignment. There were sudden changes in the maximum response over a range of velocities up to 5 m/s, which are mainly due to the use of linear equations in this method. The linear momentum of a vehicle moving at a lower velocity

is less than that of a vehicle with a higher velocity; at the same time, the force exerted due to earthquake shaking remains unchanged as replicated in Figure 2.16.

Table 2.6 Time of PGA occurrence and the time window selected for picking the maximum vehicle response

Earthquake	Time of PGA		Time window (sec)
	EW	NS	
EQ01	8.38	10.76	0 - 15.76
EQ02	11.46	2.14	0 - 16.46
EQ03	8.54	8.46	0 - 13.54
EQ04	5.76	5.64	0 - 10.76
EQ05	9.60	13.56	0 - 18.56
EQ06	17.54	17.58	0 - 22.58
EQ07	18.08	7.30	0 - 23.08
EQ08	18.70	19.30	0 - 24.30
EQ09	21.86	20.76	0 - 26.86
EQ010	24.08	21.98	0 - 29.08

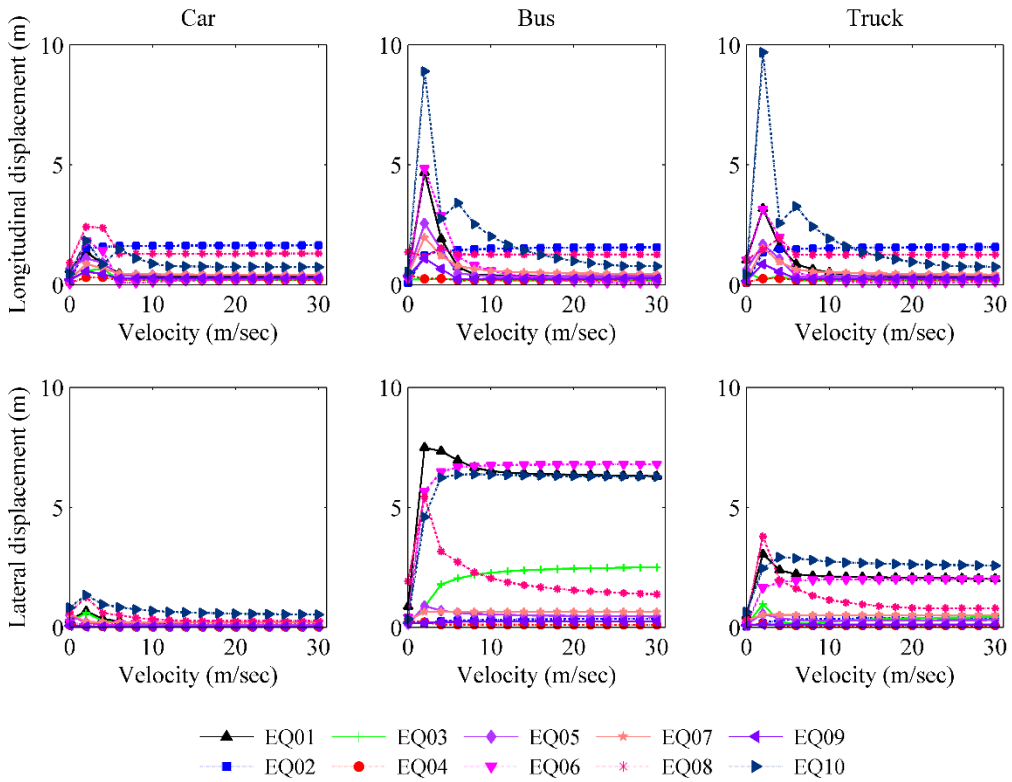

Figure 2.16 Vehicle responses during specified earthquakes for range of speeds

Figure 2.17 shows the changes in the maximum longitudinal and lateral displacements with PGA of 1–15 m/s^2 and at a constant vehicle speed of 20.0 m/s. The earthquake ground motions were scaled to the same amplitude before the analysis.

The longitudinal response of the vehicle plays a vital role in the vehicle control during the earthquake and may lead to a collision, depending on the vehicle speed. The responses of the vehicles during the simulated earthquakes varied. The longitudinal response of each vehicle increased linearly as the velocity increased for speeds higher than 10.0 m/s. The results also show that vehicles moving at just 2.0 m/s are at higher risk of losing control. As the velocity of the vehicle increases from a resting state, the vehicle response increases as the vehicle gains speed up to 2.0 m/s and then the response trends downward as the speed rises to 10.0 m/s. The effect of rolling resistance is felt at speeds up to 5.0 m/s and the response fluctuates in this range. The CPLM method considers the momentum of the vehicle, which is linearly dependent on the velocity of the vehicle. Hence, the longitudinal responses change linearly with the velocity for speeds higher than 10.0 m/s.

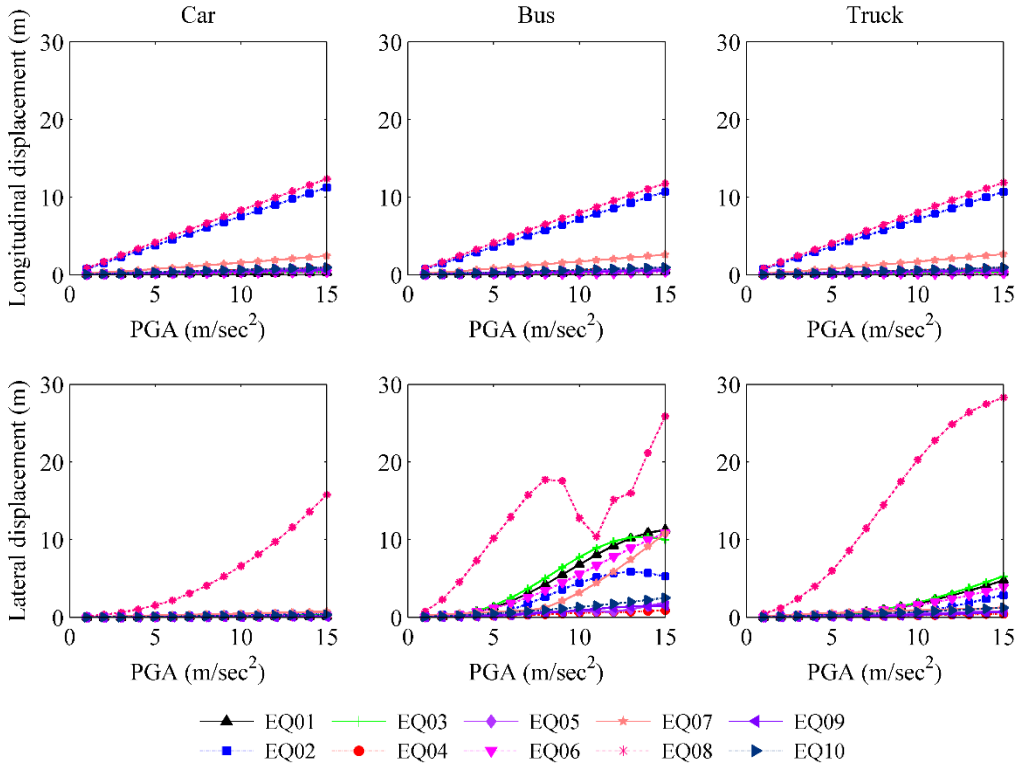

Figure 2.17 Vehicle responses during specified earthquakes for ranges of PGA

The lateral response of the vehicle is another risk factor. Lateral movement may result in vehicles moving into another lane or onto the shoulder of the road, causing an accident. The

lateral movement of the bus was found to be higher than that of the truck or car for similar cases. When the vehicle velocity increases, the lateral response curve is similar to the longitudinal response curve. The maximum turning angle is another major factor in calculating the response; the bus has a maximum turning angle of 38.7° whereas the car and truck have turning angles of 31.7° and 31.6°, respectively.

When the PGA data of all the earthquakes are scaled to the same values, the longitudinal responses of the vehicles seem to vary linearly relative to the ground motion, whereas the lateral responses do not follow the trend seen in the cases of velocity changes for real earthquakes. The ground motion characteristics of the earthquakes have a strong effect on the vehicle response. For example, the Gorkha earthquake resulted in the strongest response with much diversity of motion in both longitudinal and lateral directions. The El Centro earthquake also resulted in a strong longitudinal response, similar to that of the Gorkha earthquake for all vehicle cases.

2.4 Toppling analysis of vehicle

Vehicle model analysed for the toppling risk under several conditions with varying vertical PGA, frequency dominance, phase difference, physical parameters and the speed of vehicle. We proposed the relationships of those parameters along with the coefficients for the calculation. We supposed that the vehicle response can be taken as a reference to estimate the PGA values in that area. Relationships of lateral PGA and other parameters are studied using the sinusoidal waves as input. Moreover, the vehicle toppling mechanism during Kumamoto earthquake is discussed and finds the PGA on that area with dominant frequency in Kurokawa and Tateno area.

2.4.1 Relationship of lateral PGA with ground motion characteristics

Toppling mechanism of the vehicle mainly dominated by the lateral acceleration where similar effect of vertical component is also existed. Sine waves of varying frequencies in ranges of 0.4 to 12 Hz in increment of each 0.4 Hz are used in the analysis. We used the similar sinusoidal waves in vertical direction of same frequency in all cases of lateral input where the amplitude is constant. Total thirty lateral input wave samples are used for the analysis of single case with varying frequency. Amplitude of the lateral input wave started from 1.0 m/sec^2 and constant

for 5 seconds and then increased by 0.5 m/sec^2 for next 5 seconds and so on, until the vehicle toppled on side. There are eleven cases with increasing values of vertical amplitudes from 4 to 14 m/sec^2, analyzed for all 30 cases of lateral acceleration. Phase difference of the lateral and vertical acceleration is also a key parameter in toppling mechanism. Hence, we analyze the model for sixteen cases with same phase and increasing phase delay of $\pi/8$ up to $15\pi/8$ radians.

Sample input waves in lateral and vertical directions for four cases with varying phase delay (same phase, $\pi/2$, π and $3\pi/2$) are shown in figure 2.18 (1-A, 2-A, 3-A and 4-A) with corresponding rolling angles (1-B, 2-B, 3-B and 4-B). All cases are of frequency 4 Hz with the constant amplitude of vertical acceleration as 5.0 m/sec^2. Time span in the figure shows only last six seconds where vehicle got toppled. Lateral accelerations are denoted by blue lines where green one shows the vertical wave in all cases. Duration is different in all cases as amplitude varies with phase delay.

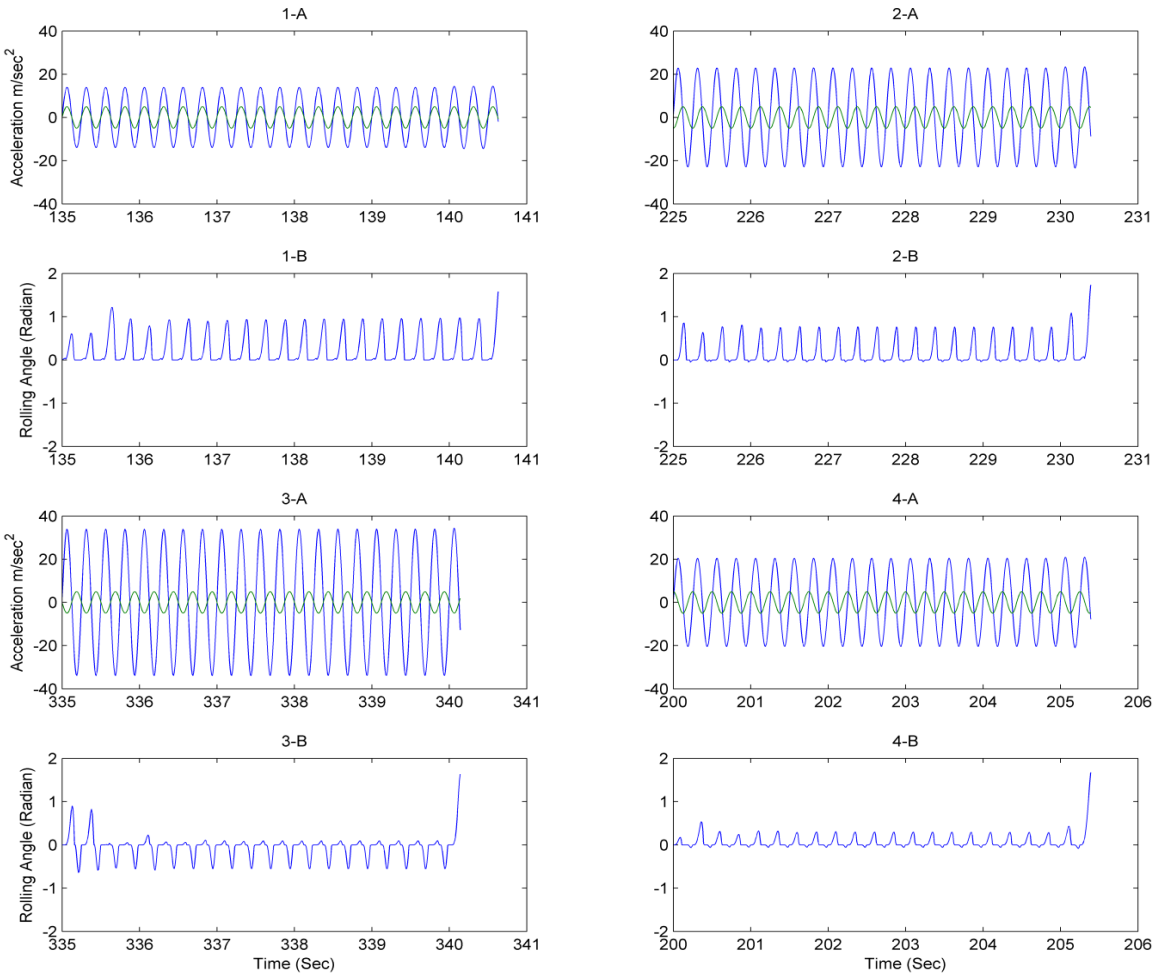

Figure 2.18 Input waves (lateral in blue and vertical in green) and rolling angles for different four cases of phase delay

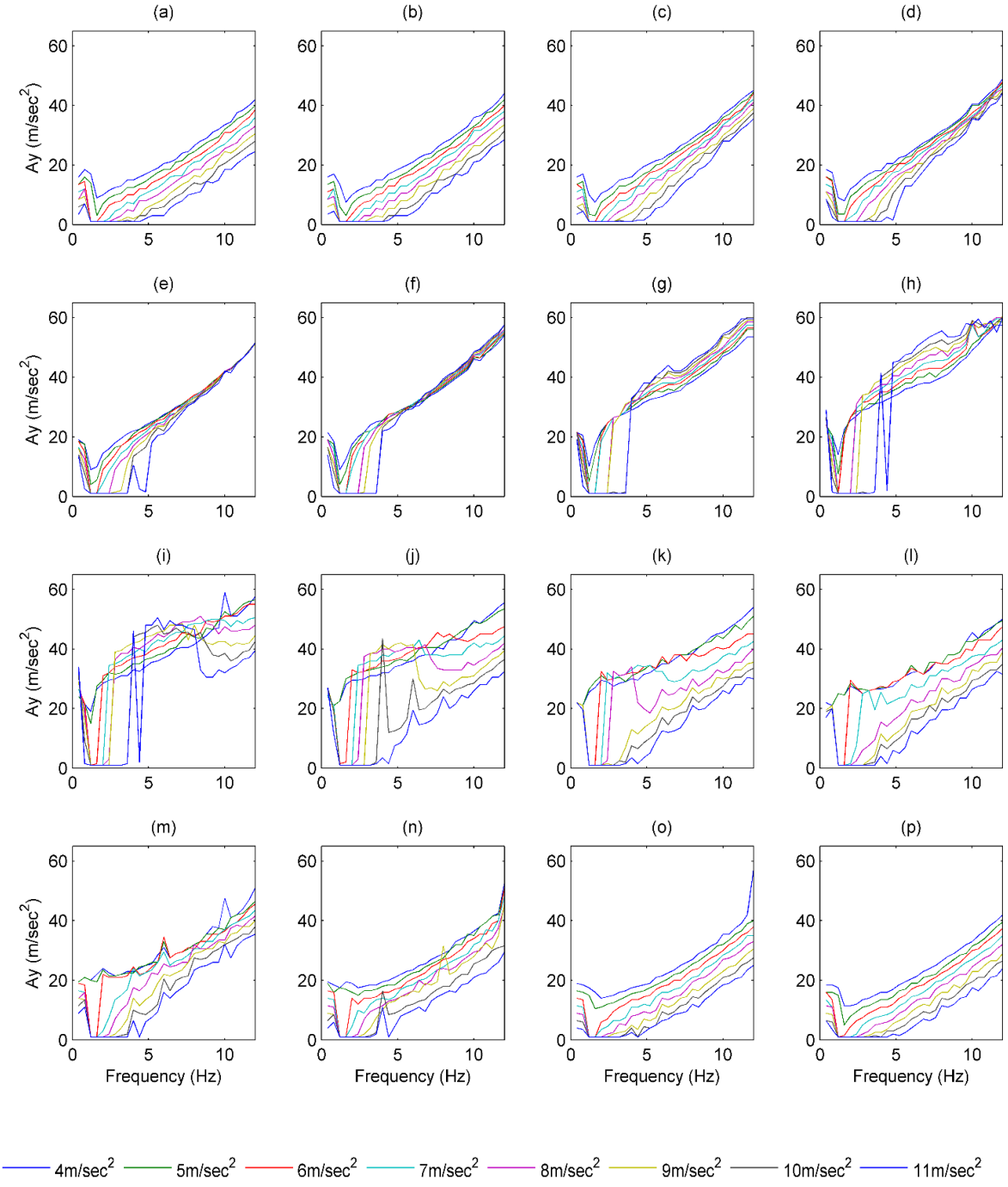

Figure 2.19 Relationship of lateral amplitude with vertical amplitude under different frequency dominance for different cases of phase delay

Figure 2.19 shows the relationship of lateral amplitude with vertical amplitude for the toppling of vehicle under different cases in given range of dominant frequencies. Figure 2.19 (a) – (p) shows the case of no phase delay and phase delay of $\pi/8$, $\pi/4$, $3\pi/8$, $\pi/2$, $5\pi/8$, $3\pi/2$, $7\pi/8$, π, $9\pi/8$, $5\pi/4$, $11\pi/8$, $3\pi/2$, $13\pi/8$, $7\pi/4$ and $15\pi/8$ respectively. Each line in the figures represents

the relationship of lateral amplitude with constant vertical amplitude. Amplitudes of the vertical accelerations are shown as the legend in m/sec^2.

When there is no phase delay, as the vertical amplitude increases, peak value for the lateral input wave decreases. Similar trend can see up to the case with phase delay of $\pi/2$ but the variation is getting smaller and converging to a point in higher frequency range.

When the phase delay is getting increase then shifting trend keeping constant as the lines crosses in higher frequency ranges that shows higher value of lateral amplitude required for the cases of higher amplitude in vertical. The trend of line shifting move in reverse direction as the phase delay approaches to π and back to the similar when the phase delay is 15 $\pi/16$ which is almost same as the no phase delay.

Relationship of the lateral amplitude to the frequency under several amplitudes of vertical component and phase delay is shown in equation (2.45). We analyzed the data for range of 0.4 – 12 Hz in frequency 0 – 2π in phase delay. Values of regression coefficients used in the equation are shown in table 2.6.

$$Ay_{max} = \alpha_1 f^2 + \alpha_2 f + \alpha_3 \emptyset f\ddot{z} + \alpha_4 \ddot{z} + \alpha_5 \sin\left(\frac{\emptyset}{2}\right) + C \qquad (2.45)$$

Table 2.7 Regression coefficient in calculation of maximum lateral amplitude to topple the vehicle

Variable	Coefficient	Std. Err.	Lower 95%	Upper 95%
$\boldsymbol{\alpha_1}$	0.160	0.010	0.139	0.180
α_2	1.274	0.140	1.000	1.547
$\boldsymbol{\alpha_3}$	-0.023	0.000865	-0.025	-0.021
$\boldsymbol{\alpha_4}$	-1.239	0.043	-1.323	-1.156
$\boldsymbol{\alpha_5}$	25.967	0.375	25.231	26.703
C	5.679	0.570	4.562	6.797

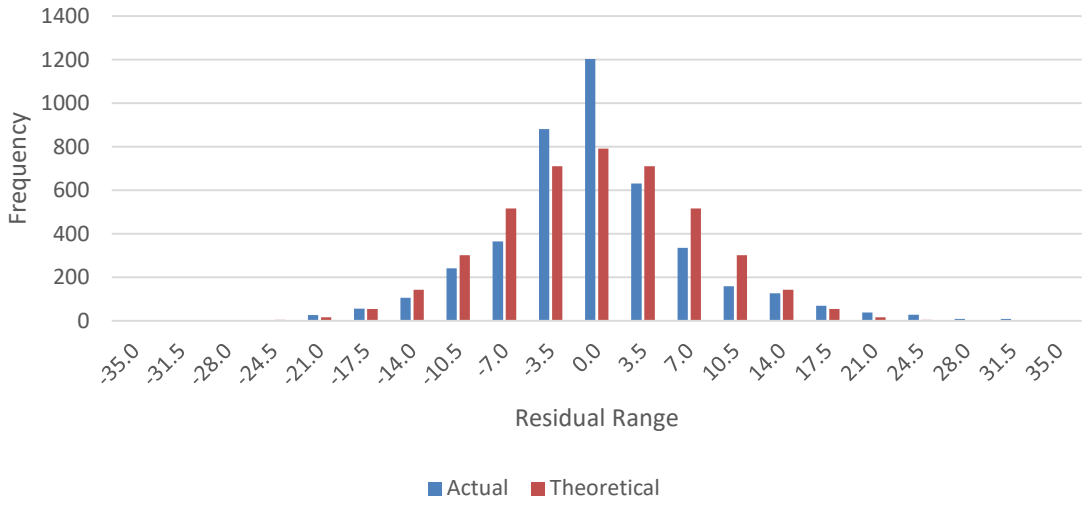

Figure 2.20 Histogram of the residuals of lateral amplitude using the relation of frequency, vertical amplitude and phase delay

Regression equation for the relationship of the parameters is formed from the data set of 4292 sampling results. Total size of the data is 5280 form the result of each vertical amplitude for all ranges of frequencies and phase delay but we omit the data that lies in line of 1.0 m/sec^2. Maximum amplitude of lateral acceleration starts from 1.0 m/sec^2 hence we take out these data from the bin, results total sample size reduced to 4292. R^2 value of the proposed equation is 0.733. Standard errors and the values of lower and upper range for confidence level of 95% are shown in table 2.6. Histogram of the theoretical and actual residuals is shown in figure 2.20.

2.4.2 Relationship of lateral PGA with vehicle parameters

Vehicle parameters are other major factors in toppling of the vehicle. Specifically, dimension and load are crucial parameters in toppling analysis. We focused on the dimensions' *d* and *h* of the vehicle along with the mass *M* in this study. Lateral amplitude is calculated as a function of *d/h* ratio (2.84 – 6.02) for several cases of loading condition (800.0 – 3200.0 kg). Frequency of the input waves and the amplitude of vertical component are also taken in consideration. Figure 2.21 shows the relationship of lateral amplitude for d/h ratios with different loading conditions under different cases of frequency and amplitude of vertical component. Figure 2.21 (a) shows the case with frequency of 0.8 Hz where (b) and (c) have frequency of 5.8 Hz and 9.8 Hz respectively with constant amplitude of 5.0 m/sec^2 in vertical direction. Figure 2.21 (d) (e) and (f) are the results for the vertical amplitude of 9.0 m/sec^2 with frequencies of 0.8 Hz,

5.8 Hz and 9.8 Hz respectively. Green zone in the figures denotes the safe range for all loading conditions considered in this study, where red zone represents the toppled condition for all. The yellow zone in the figures denotes the variation of amplitude under different loading condition. Lower boundary of the yellow region corresponds to the highest load and upper to the lowest load used in this study. Effect of loading condition depleted in higher frequency ranges where it has significant variation in lower frequency ranges. Ratio of d/h has main role on the toppling of vehicle as it increases, PGA demand is also increases in all cases. For the cases of lower frequency dominance, effect of loading condition and the dimensional effects vary accordingly.

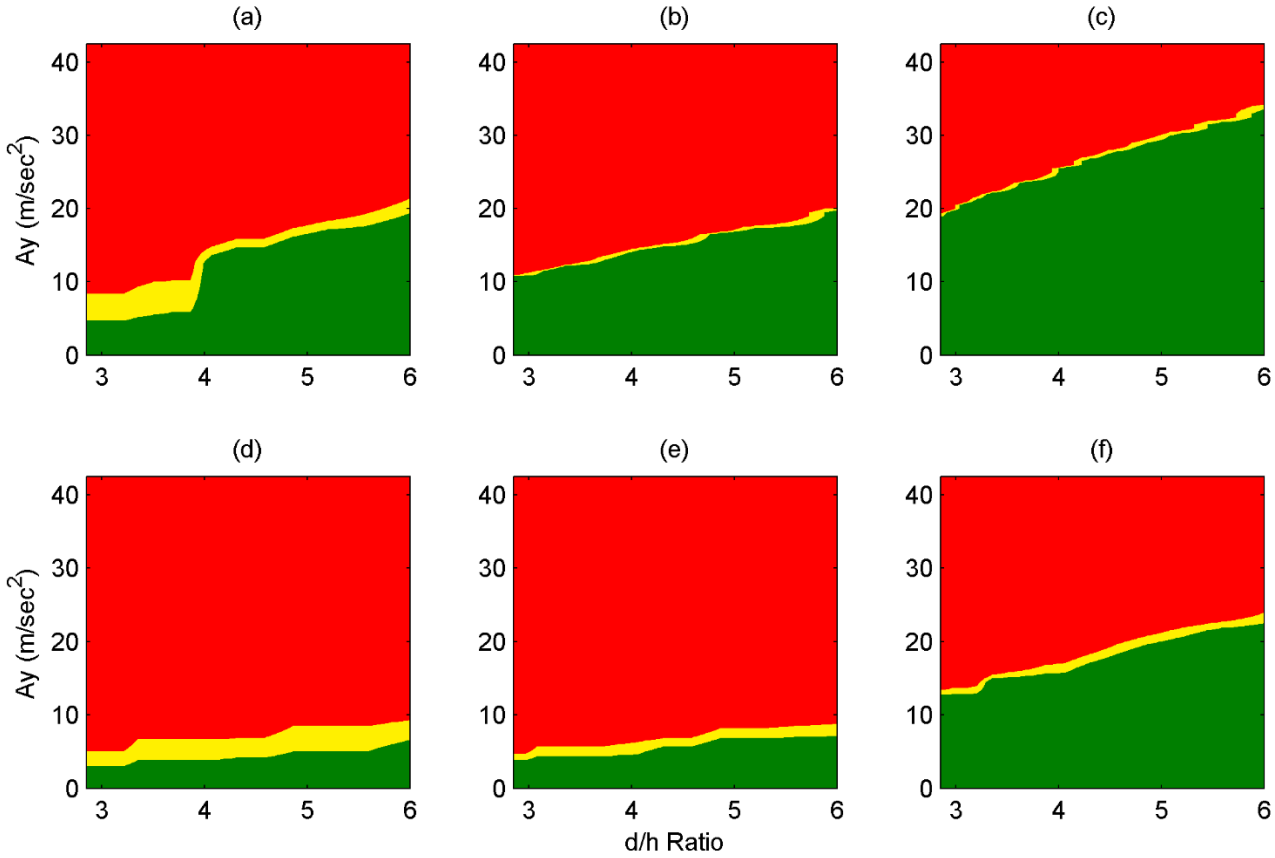

Figure 2.21 Relationship of lateral PGA with d/h ratio for several cases of loading

Effects of the vehicle load and *d/h* ratio are now presented in terms of scaling factor to use in the equation (2.44). PGA demand on toppling of vehicle are calculated for different frequency ranges of input values with ratios of *d/h* and variable loading and scaled with the sample car having *d/h* ratio of 4.3. Dimensional scaling factor (ρ_d) is now calculated as a function of *d/h*

ratio, mass and dominant frequency as shown in equation (2.46). Where D is the coefficient as function of *M* (in kg) and *f* (in Hz). Regression coefficients are shown in tables 2.7.

$$\rho_d = \beta_1 \mathrm{f} + \beta_2 \mathrm{f}\ddot{\mathrm{z}} + \beta_3 \ddot{\mathrm{z}} + \beta_4 \left(\frac{\mathrm{d}}{h}\right) + \beta_5 \left(\frac{\mathrm{M}}{\mathrm{f}}\right) + \beta_6 \left(M \frac{\mathrm{d}}{\mathrm{h}}\right) + \mathrm{D} \qquad (2.46)$$

Table 2.8 Regression coefficients for the calculation of dimensional scaling factor

Variable	Coefficient	Std. Err.	Lower 95%	Upper 95%
$\boldsymbol{\beta_1}$	0.072	0.005054	0.062	0.082
$\boldsymbol{\beta_2}$	-0.008810	0.000595	-0.009977	-0.007642
$\boldsymbol{\beta_3}$	0.083	0.004219	0.075	0.091
$\boldsymbol{\beta_4}$	0.222	0.005064	0.212	0.232
$\boldsymbol{\beta_5}$	0.000903	0.000055	0.000795	0.001011
$\boldsymbol{\beta_6}$	-0.000013	2.207E-06	-0.000017	-8.399E-06
D	-0.724	0.048	-0.818	-0.630

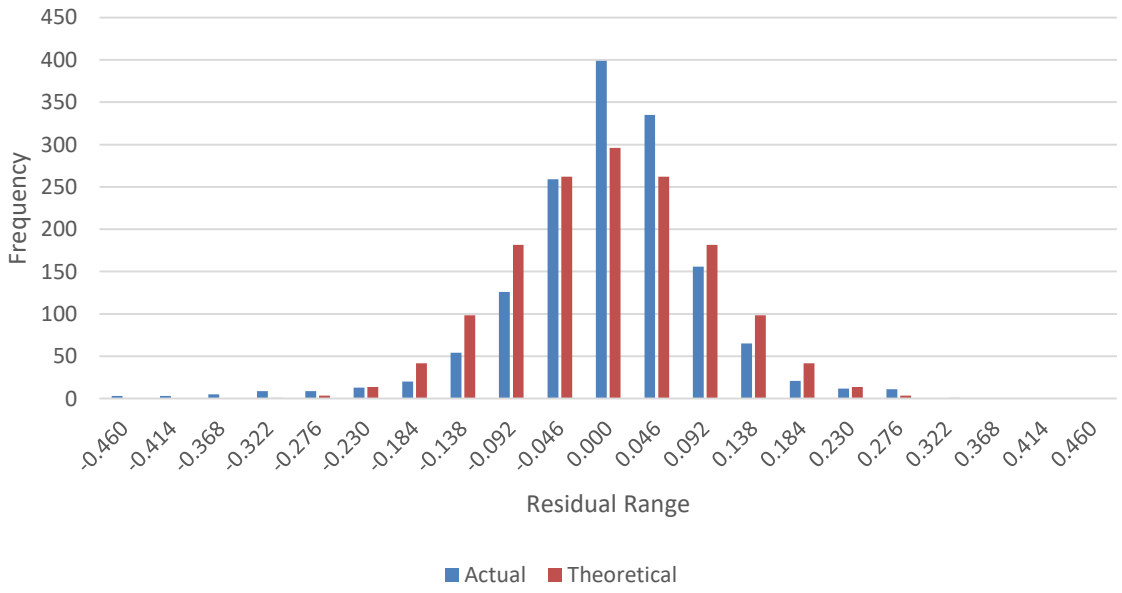

Figure 2.22 Histogram of the actual and theoretical residuals of the relationship of the dimensional scaling factor

Sample size for the regression equation of dimensional scaling factor is 1500, where the scaling values ranges from 0.545 to 1.909. Regression coefficients with 95% confidence level are shown in table 2.7 with standard error and lower and upper range of coefficients. R^2 value of the relationship is 0.852 and the residual values are shown in Figure 2.22 as histogram.

2.4.3 Relationship of lateral PGA with speed of vehicle

Speed of the vehicle can play a role in the toppling behavior as the lateral speed of the vehicle supplement the angular momentum on the side. Speed in the range of 30 to 100 kmph are considered and compared with the result of vehicle at rest condition. The scaling factor the speed is getting merely fluctuated in about 1% which we can neglect in this study. Figure 11 shows the relationship of lateral amplitude to the frequency and vertical amplitude for several cases of speed. Figure 2.23 (a) shows the case with speed 30 kmph where (b), (c) and (d) shows the cases of speeds 40 kmph, 50 kmph and 60 kmph respectively. Cases with speeds 70 kmph, 80 kmph, 90 kmph and 100 kmph are shown in figure 11 (e), (f), (g) and (h) respectively.

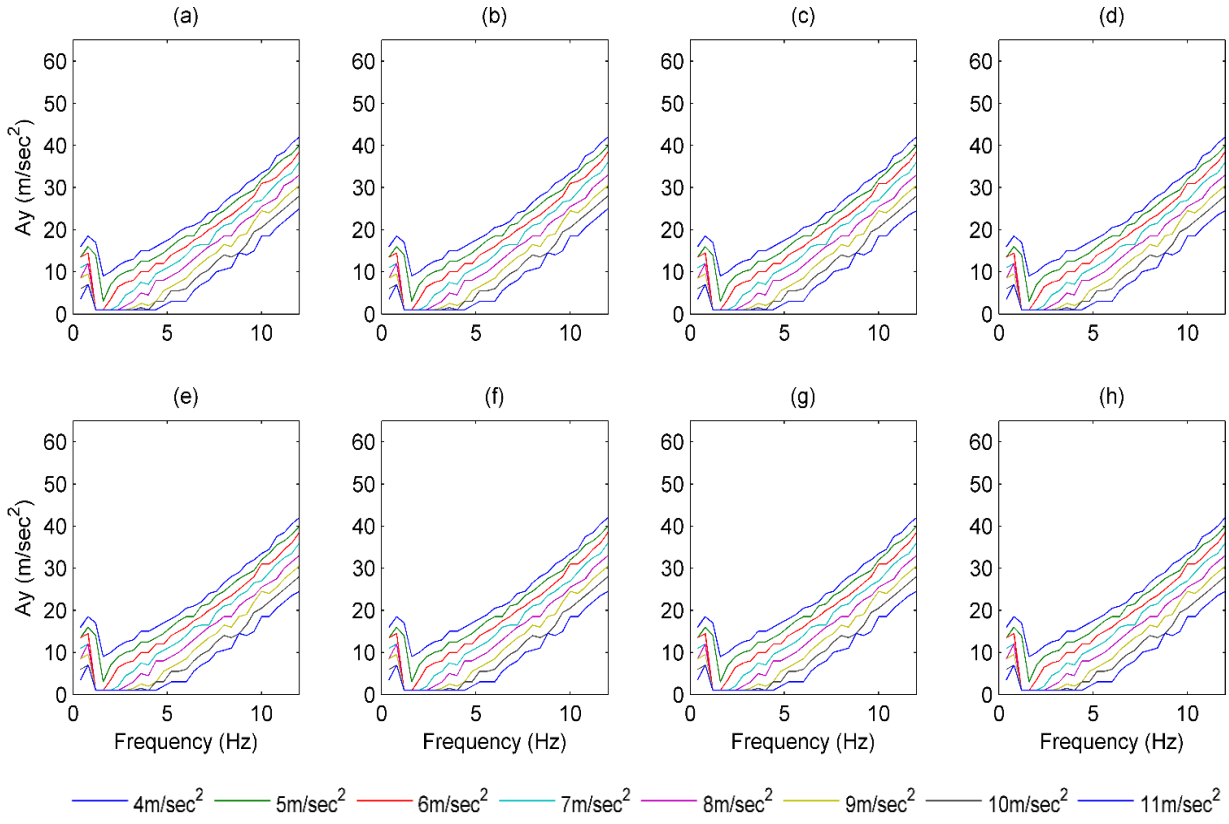

Figure 2.23 Relationship of lateral PGA with frequency and vertical amplitude for several cases of speed ((a) 30 kmph, (b) 40 kmph, (c) 50 kmph, (d) 60 kmph, (e) 70 kmph, (f) 80 kmph, (g) 90 kmph and (h) 100 kmph)

Finally considering the effect of weight and dimensions and neglecting the effect of speed of the vehicle we can find the threshold PGA in toppling risk analysis from equation (2.47).

$$\ddot{y}_{max} = \rho_d \times \mathrm{Ay}_{max} \qquad (2.47)$$

2.5 Orientation of vehicle effect on response

Vehicle response during the earthquake shaking also depends on the direction in which the vehicle is moving with respect to the components of earthquake acceleration. The left side of Figure 2.24 shows a polar plot of the maximum longitudinal (X) and lateral (Y) responses for the car example during the Gorkha earthquake within a given time window. The right side of the same figure shows a plot of the longitudinal (X) and lateral (Y) components of the Gorkha earthquake acceleration in a 24.3 s time window with a sampling frequency of 50 Hz. The longitudinal response is more varied than the lateral response in the case of Gorkha earthquake. The shape of the loop of the maximum longitudinal response compares closely with the outer envelop of the acceleration plot. The initial orientation of the vehicle (150°), or its opposite with the longitudinal axis, will be at highest risk whereas the lowest risk associated with the vehicle will be when it is oriented perpendicular to those angles.

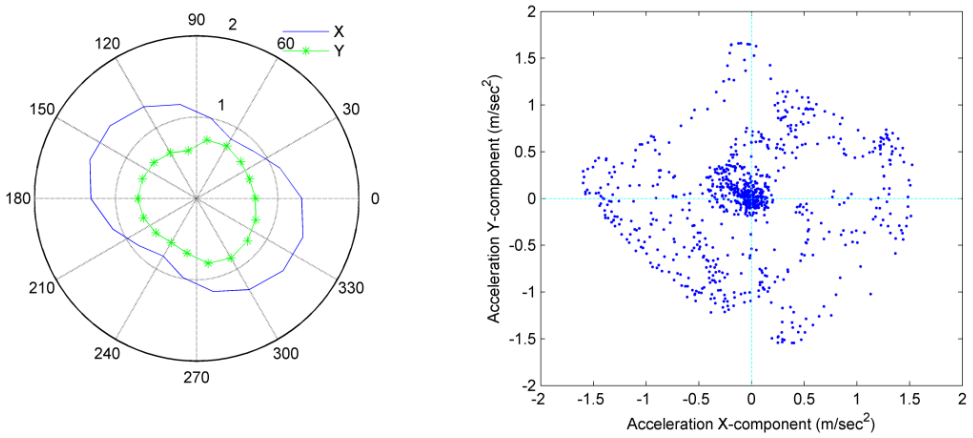

Figure 2.24 Variation of the maximum longitudinal (X) and lateral (Y) response of the vehicle with different orientation of the vehicle (left) and plot X-component and Y-component of acceleration vector of Gorkha earthquake for time window of 24.30 s (right).

2.6 Chapter overview

In this study, we have proposed a model that simulates vehicle responses to the maximum ground acceleration of earthquakes within a fixed time window for each event, assuming ideal vehicle conditions. Analysis of video footage of vehicle motion during the Gorkha earthquake supported the results of the simulation undertaken with the CPLM method. The CPLM method can be used effectively in scenarios with a range of vehicle speeds, including being at a full stop. In a real earthquake scenario, vehicle conditions will be different from the ideal situation, and the driver's behaviour will be a major factor. We have discussed the maximum response of the vehicles within the fixed time window; however, this requires further research. The time it takes for the driver to recognise that an earthquake is occurring is important for simulating the driver's behaviour and actions in the model. Additionally, issues concerning the provision of information to drivers about the earthquake e.g., an early warning system that may enable drivers to react and prevent accidents should be investigated further. Unlike the smooth driving conditions used in the simulation, moving vehicles will shake because of irregular road conditions or mechanical issues, making it difficult for drivers to identify shaking caused by ground motion.

Our results show that the response of the vehicles depends mainly on the ground motion characteristics and orientation of the vehicle, rather than on the PGA excitation alone. Slow moving vehicles have a higher risk of being affected than faster ones; hence, vehicles in the city are more at risk. However, slow vehicles are easier to control than faster ones; therefore, vehicle drivers in an urban setting have better steering control and can react more quickly. Thus, their level of risk is lower compared with vehicles in an ideal situation (i.e., with no driver reaction).

The authors are working further on research to incorporate the driver's reaction and response during earthquake shaking. The CPLM method will be used for the response mechanisms of various vehicle models whereas the driver's control over the steering system while following other vehicles will be analysed using a driving simulator experiment.

Vehicle analysis using the angular momentum along with CPLM method (Extended CPLM Method) defines the toppling condition of vehicle. PGA required to topple the vehicle depends on the dominating frequency along with the amplitude of vertical

acceleration and phase delay. When the amplitude of UD component decreases, the lateral PGA value need to topple the vehicle getting down but for increasing dominant frequency condition PGA demand also increases. Dimensional parameters of vehicle play vital role in PGA estimation. When b/h ratio increases, PGA demand also increases. Speed of the vehicle could also effect on the toppling scenario. Hence, we introduced DSF and VSF along with regression coefficients. We can estimate the PGA when some vehicle got toppled or we could introduce the toppling risk of any vehicle under different circumstances using these results.

3 Case studies on vehicle behavior during earthquakes

3.1 Introduction

Vehicle behavior during earthquake is the main risk associated to the vehicle and the user during earthquake shaking. Seismic response of the vehicle mainly depends on the ground shaking as discussed in the chapter two, state of the vehicle (speed, condition, location etc.) and the handling behavior of the driver. We have discussed about the vehicle behavior without the drivers' reaction in chapter two and three. The driver's reaction and car following behavior will be discussed in chapter four. In this chapter vehicle behaviors during the real earthquake shaking are discussed mainly focusing on the vehicle response and drivers' behavior.

Recent earthquakes, the 2015 Gorkha earthquake (M7.8) of Nepal and the 2016 Kumamoto earthquake (M 7.3) of Japan are taking as the case studies. Several closed-circuit television cameras recorded videos in Kathmandu and other parts of Nepal during earthquake shaking. Thirty drivers, who drove vehicles during shaking of Gorkha earthquake, were interviewed. Discussions based on the interview follow the video analyses in first part. During the 2016 Kumamoto earthquake six cars and a truck were spotted toppled on Kurokawa and Tateno area, JR train and bullet train (Shinkasen) got derailed near Akamizu and Kumamoto stations respectively. Toppling analysis of the car and corresponding PGA estimation of Kurokawa and Tateno area are presented in this chapter.

3.2 Gorkha earthquake 2015

The Gorkha earthquake that struck on April 25 at 11:56 am (NST) had an epicenter in Barpak, Gorkha. It ruptured to the east of the epicenter for a length of about 100 km at a strike angle of 295° [36]. The size of this earthquake is 7.8 in moment magnitude and is 7.6 in local magnitude, as measured by Nepal's seismological center (NSC). The recent Gorkha earthquake claimed a total of 8,857 lives (as of August 8, 2015) [32]. The greatest death toll was in the Sindhupalchok district, in the eastern part of Nepal, near to the estimated end point of the rupture. In this region, a total of 3,532 people lost their lives, whereas just 1,573 were seriously injured due to the quake. The district with the next highest death toll was the capital, Kathmandu, where 1,226

deaths were recorded, along with 7,952 injuries. Considering the three districts in the Kathmandu valley, the total death toll soared to 1,739, significantly more than in Gorkha, the district where the epicenter was located with the death toll of 449. The death toll was affected by the timing of event, as it happened at noon when most of people in the hardest hit areas were out of their houses at work in the fields. Another factor that lowered the death toll and damage was the low-frequency dominant component of ground motion. Figure 3.1 shows the Modified Mercalli Intensity (MMI) map of the affected districts due to The Gorkha earthquake 2015 prepared by National Society for Earthquake Technology (NSET) Nepal. MMI in Kathmandu seems highest as it nearly reached to intensity level of IX.

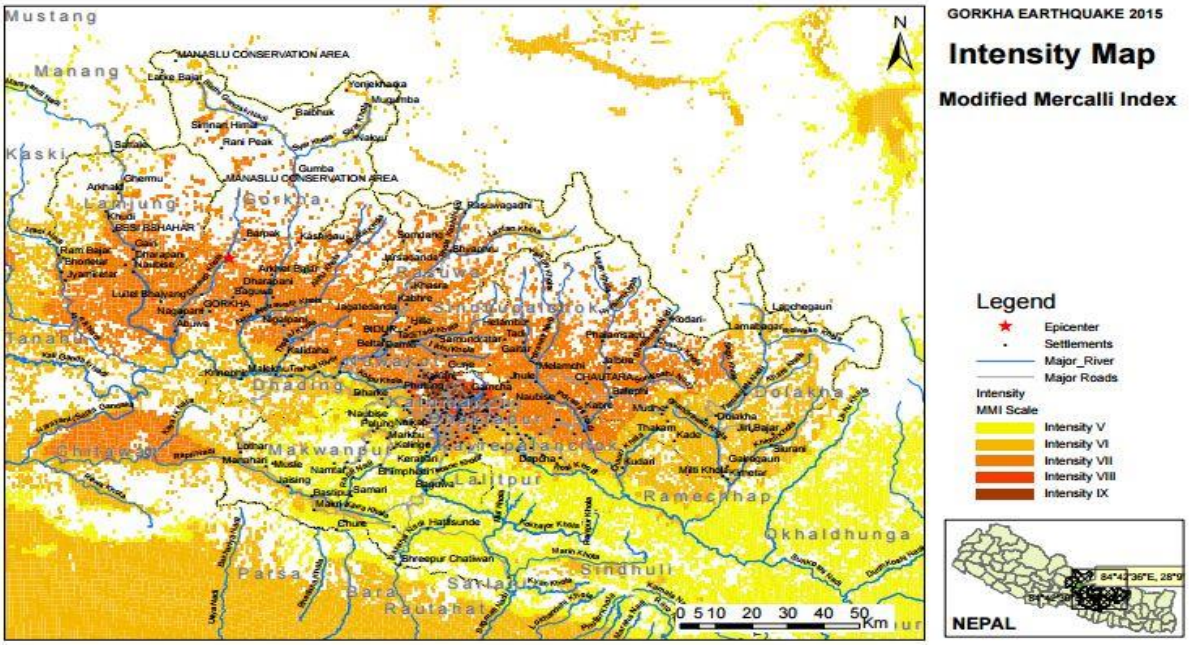

Figure 3.1 Modified Mercalli Intensity map of affected districts by the Gorkha earthquake 2015. (Source: NSET[3])

The main shock of the earthquake had dominant frequencies of roughly 0.23, 0.23 and 0.27 Hz corresponding to the East-West (EW), North-South (NS) and Up-Down (UD) components recorded in Kathmandu. Recorded ground acceleration of the Gorkha earthquake in Kathmandu shows the peak value of less than 200 cm/sec^2 ,Where probabilistic seismic hazard analysis of Nepal suggested that PGA is around 100 cm/sec^2 considering return period of 98 years and 450 cm/sec^2 for return period of 475 years in soft soil areas (Parajuli et al. 2008).

[3] http://www.nset.org.np/nset2012/images/download/Map_Final/Intensity_KV_mmi_DISTRICT.pdf

3.2.1 Ground motions

Nepal does not have a dense network of accelerometers; however, the USGS has established a station (KATNP) that records earthquakes in the capital city, Kathmandu, and data from that station are analyzed in this section. In total, nine independent data sets available from strongmotioncenter.org are analyzed and discussed here.

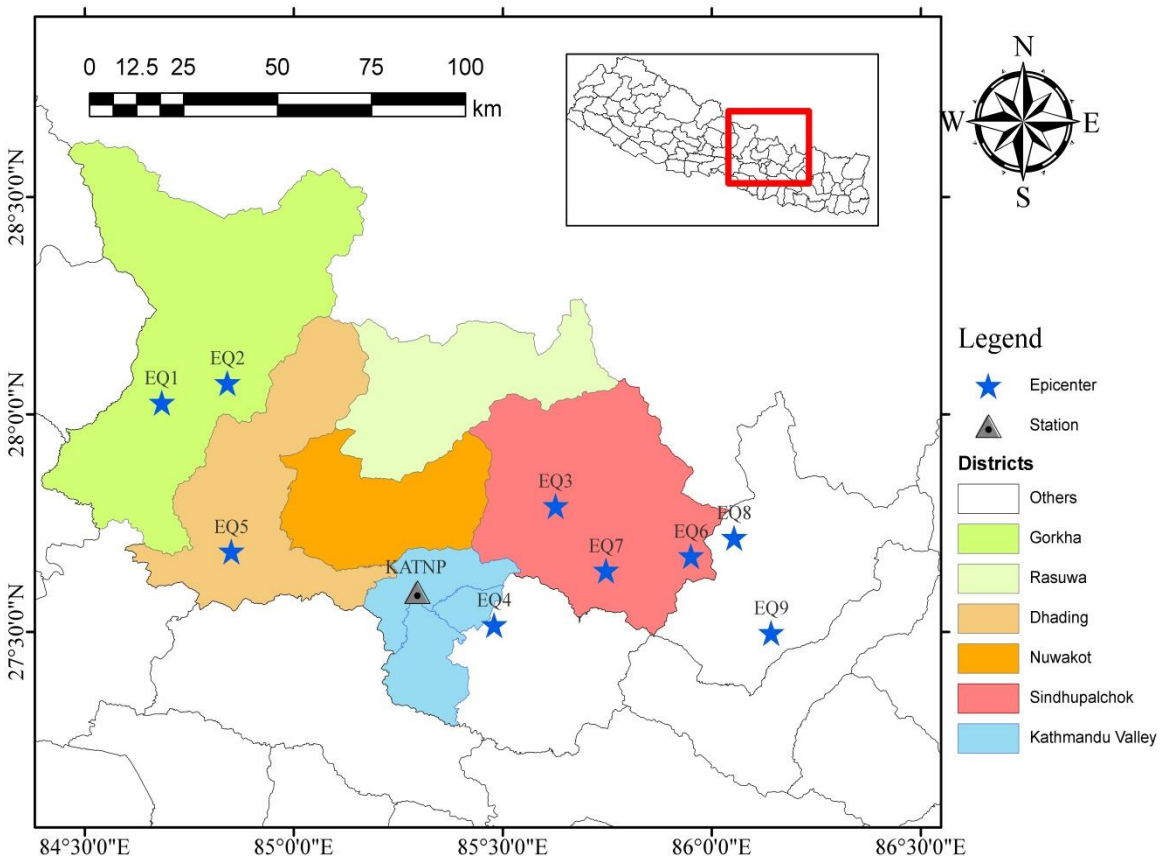

Figure 3.2 Location of main shock and aftershocks epicentres of The Gorkha earthquake 2015 and major affected districts

Table *3*.1 presents detailed information regarding triggered dates and times, moment magnitudes, the locations of epicenters and the epicentral distances from the recording station KATNP (27.7120°N, 85.3155°E). Earthquakes are numbered 1 to 9, with EQ1 representing the main shock, and EQ8 the major aftershock to the east of the fault plane. Earthquake events range from moment magnitude 5.2 to 7.8, with epicentral distances as far as 83.90 km and as near as 18.5 km.

Table 3.1 Location, time and epicentral distances of main shock and aftershocks of The Gorkha earthquake 2015

SN	Description	Time (UTC)	Magnitude (M_w)	Location		Epicentral Distance (km)
				Latitude	Longitude	
1	EQ1	25-04-015 06:11	7.8	28.1473	84.7079	76.86
2	EQ2	25-04-015 06:45	6.6	28.1927	84.8645	69.30
3	EQ3	25-04-015 06:56	5.5	27.9100	85.6501	33.00
4	EQ4	25-04-015 08:55	5.3	27.6364	85.5029	18.50
5	EQ5	25-04-015 23:16	5.2	27.8052	84.8744	43.60
6	EQ6	26-04-015 07:09	6.7	27.7945	85.9739	67.20
7	EQ7	26-04-015 16:26	5.3	27.7612	85.7704	44.80
8	EQ8	12-05-015 07:05	7.3	27.8368	86.0772	75.10
9	EQ9	12-05-015 07:36	6.3	27.6180	86.1659	83.90

The spatial distribution of the earthquakes extends to the east and west of the recording station, which help evaluate the effect of directivity of the seismic waves. Figure 3.2 shows the location of the earthquakes relative to the recording station (KATNP) in Kathmandu. Data are sampled at an interval of 0.005 s, and the length of recorded data varies for each event. For analysis, we have chosen a record length of 81.92 s (16,384 samples). This data selection of 2^{14} samples facilitates using fast Fourier transforms, which require a power of 2 for calculation. Records that are shorter than the required length were extended with null values for the remaining duration.

Ground motion, Fourier spectra and response spectra of the EW components of all earthquake events are shown in Figure 3.3, respectively, from left to right. All of the events are stacked into a single figure where base line accelerations for EQ1, EQ2, EQ3, EQ4, EQ5, E6, EQ7, EQ8 and EQ9 are 0, 300, 400, 500, 600, 700, 800, 900 and 1000 cm/sec^2, respectively, as shown by dotted lines in the figure. The main shock of the Gorkha earthquake had an epicentral distance of 76.86 km NW from KATNP; maximum recorded accelerations were 155, 162 and 184 cm/sec^2 for the EW, NS and UD components, respectively. Fourier transforms to the

frequency domain showed that all three components were dominated by low frequencies. Figure 3.3 clearly shows that the dominant frequencies of large aftershocks (EQ2, EQ6 and EQ8) are low: even the small ones are in a higher range. In contrast with the Fourier spectra, spectral accelerations (Figure 3.3), show aftershock ground motions that are greater and in a higher frequency range, even though the main shock has a higher value over a lower range of frequencies (0.22 Hz).

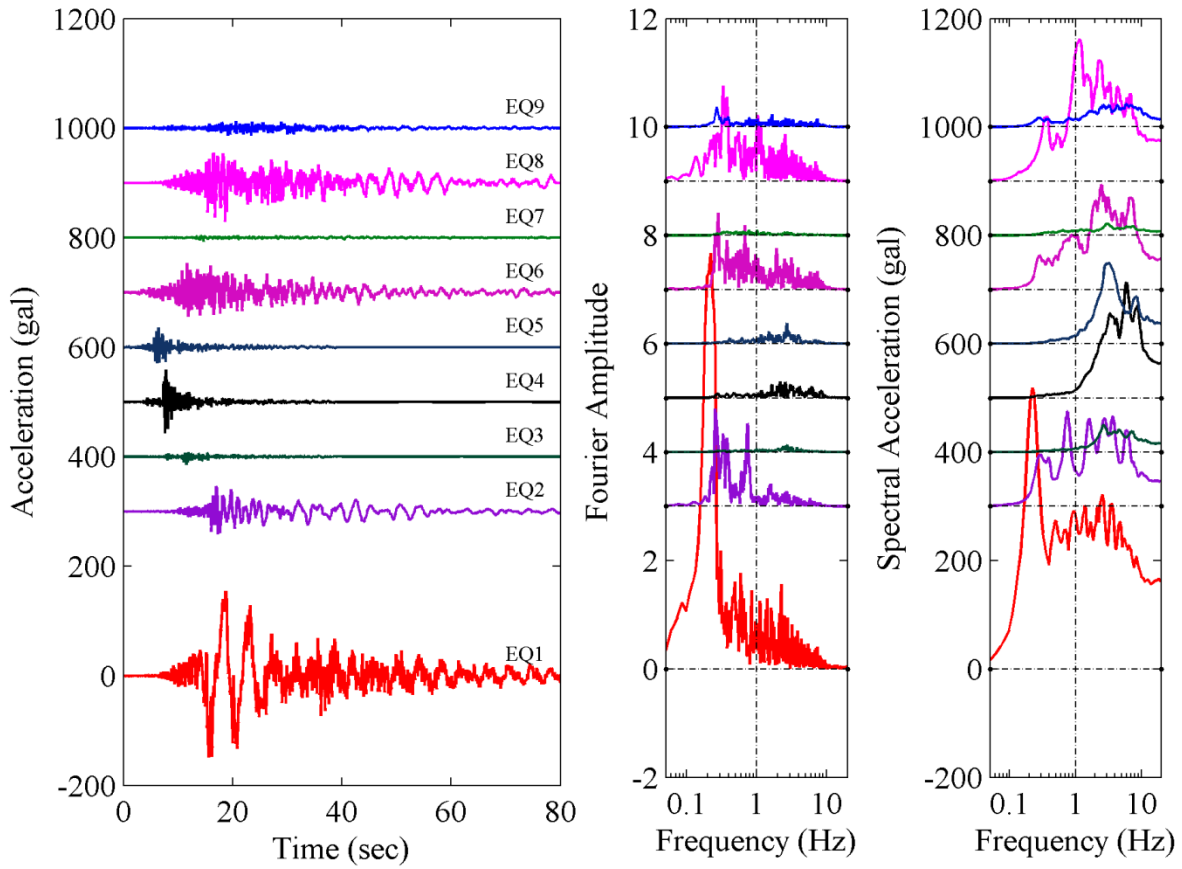

Figure 3.3 Ground motions of the Gorkha earthquake and aftershocks, corresponding Fourier and response spectra of EW component

Figure 3.4 shows the dominant frequencies of all earthquakes in all three directions. In four of the events (EQ1 (M7.8), EQ2 (M6.6) EQ6 (M6.7) and EQ8 (M7.3)), all of the components are dominated by low frequencies ≤1 Hz. Three of the events (EQ3 (M5.5), EQ4 (M5.3) and EQ5 (M5.2)) have dominant frequencies in all three components ≥1 Hz. EQ7 (M5.3) is low-frequency dominant in the EW and NS components, while the UD component had a slightly higher value of 1.26 Hz. The final event, EQ9 (M6.3), has variable frequency content, with peak Fourier amplitudes for the EW component at 0.28 Hz, the NS component at 2.43 Hz, and the UD component at 1.17 Hz.

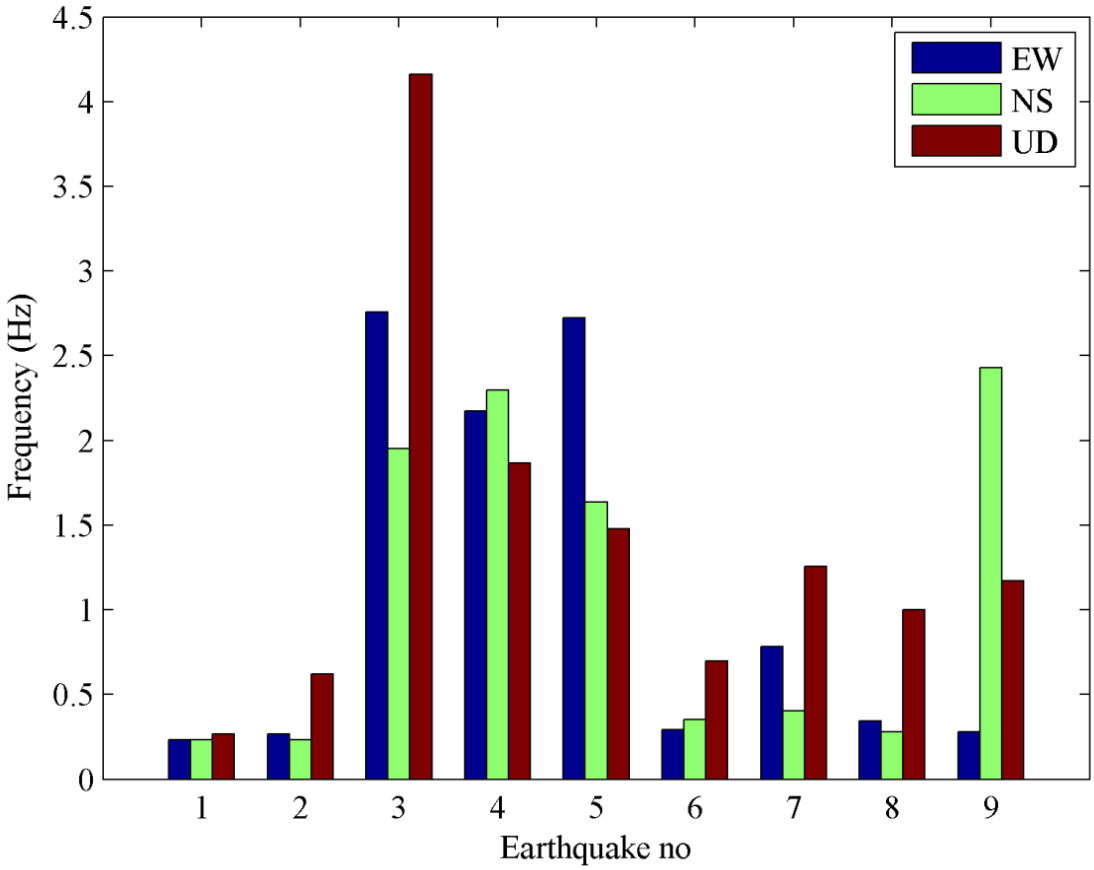

Figure 3.4 Dominant frequencies of the Gorkha earthquake and aftershocks

The response of a structure to earthquake ground motion with a single degree of freedom is represented by response spectra for various natural frequency ranges for the structure. A damping ratio of 5% is assumed in the calculation of response spectra. Figure 3.5 shows the tripartite plot of pseudo velocity spectra (cm/s) with axes for displacement (cm) and pseudo acceleration (cm/sec^2). Four earthquake events (EQ1, EQ2, EQ6 and EQ8) exceeded a velocity of 10 cm/s with peak values in range of 0.2 – 0.5 Hz. Despite of EQ1, the main shock, other earthquake events had a small peak in the higher frequency range of 0.8 – 3 Hz but the main shock surges only at a lower frequency range with crossing value of 100 cm/s in range of 0.08 – 0.2 Hz. EQ9 also has the same trend as the other three stated above, but the value peaks at slightly less than 10 cm/s. Apart from EQ3, EQ7 and EQ8, the other events crossed the spectral acceleration value of 100 cm/sec^2 in the range of 2.5 – 10 Hz; EQ4 and EQ5 have a peak value only in this range.

The response acceleration of the Gorkha earthquake (EQ1) has an almost flat shape in the range of 0.3 to 10 Hz. Maximum displacement during the main shock was nearly 300 cm for the

structure with a frequency of nearly 0.25 Hz at a velocity of 380 cm/s and 500 cm/sec^2 as acceleration.

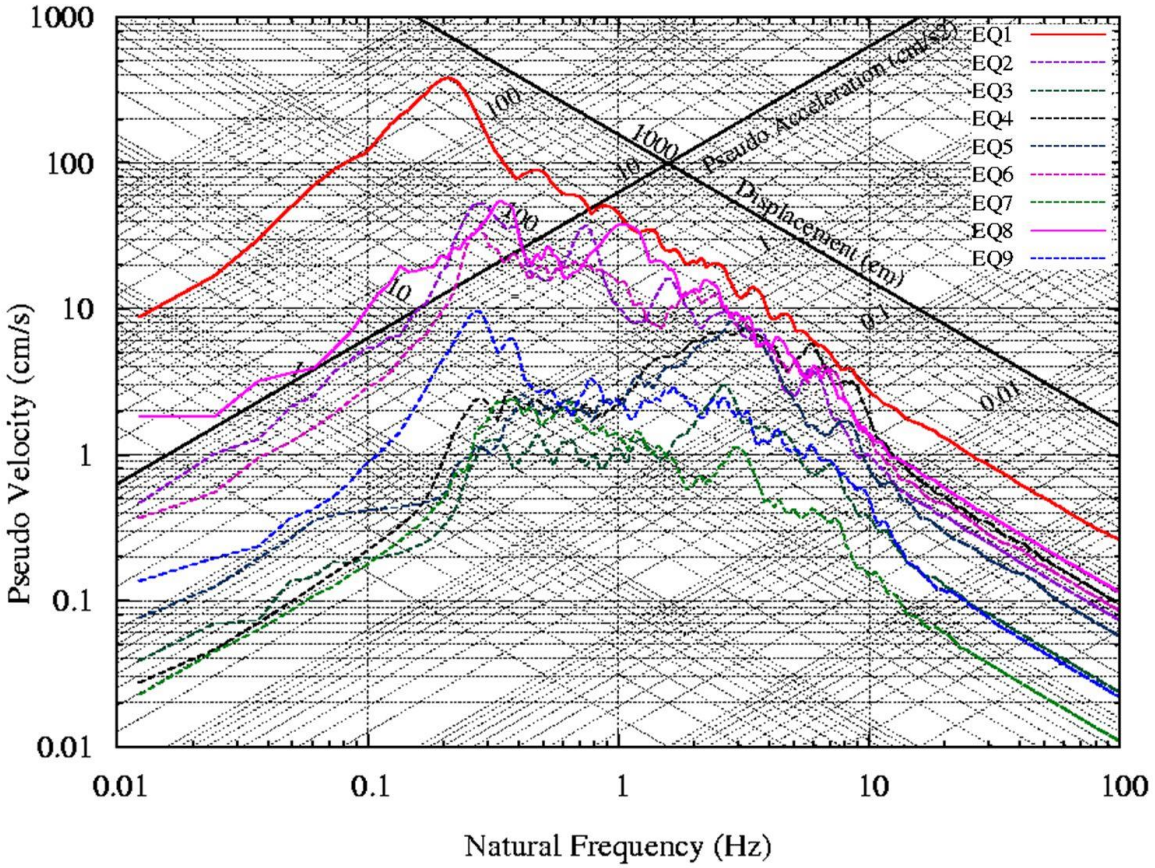

Figure 3.5 Tripartite plot of velocity, displacement and acceleration response spectra of the earthquakes

Recorded ground motion in Kathmandu valley having small PGA but the dominant frequency is lower, cause more response to the vehicles too. Even though the ground acceleration is small enough to get toppled during shaking, but lower frequency push the vehicles to have enough responses. We had spotted most of the two wheelers got laid down to the ground due to shaking. There are several cases of failure of road side structures and down to the road. Photo 3.1 shows the scene of Tripureshwor chowk, one of the major intersections in Kathmandu, where the structure of traffic island collapsed and fell down to the road, a scooter laid down where a car nearly hit it during the earthquake shaking. Analysis on vehicle responses and drivers' behavior are discussed in following section using the recorded videos and interview with the drivers.

Photo 3.1 Scene of Tripureshwor chowk, Kathmandu just after the earthquake shaking

3.2.2 Videos and discussion

There are several videos recorded during earthquake shaking shared in social media. Few of the videos recorded streets and roads are gathered as playlist in YouTube[4] which are considered in the analysis.

Vehicles were moved out of the lane when shaking of ground took place. Photo 3.2 shows some snapshots of the videos those recorded in Kathmandu city roads. Photo 3.2 a, b and c are captures in 15, 18 and 21 seconds of the video, recorded in Maitighar – Koteshwor road. In this photo we can see the position of a motorbike (red circle) that moves to the right lane and again back to the own lane and downed on the road. Similarly, we can see the similar trend of a minibus that run in the same direction. This bus can only see in two clips of 15 and 18 seconds that moved to right lane as shown by blue arrows.

People started to run towards the center of roads in city areas for safety during earthquake shaking. Most of the vehicles got stopped when they feel unusual vibrations or after seeing the shaking of structures in surroundings, people behavior and other vehicles stopped etc. Two wheelers are in higher risk; almost all the two wheelers were laid down on the road. Photo 3.2 d shows the conditions of the vehicles in Bhadrakali roundabout during strong shaking, where all the vehicles stopped.

[4] https://www.youtube.com/playlist?list=PLy9jt4daaZAYd8e3MSfr87Ok6__qHkQsG

Photo 3.2 Snapshots of CCTV footage recorded on roads in city area of Kathmandu during earthquake

Photo 3.3 Snapshots of video recorded in Durbarmarg, Kathmandu during Gorkha earthquake

Response of vehicles in a group represents the overall scenario of seismic response of vehicles. When vehicles are subjected to low frequency dominant ground motion, like main shock of the Gorkha earthquake 2015, we can see the response of the flow of traffic at a glance. Video[5] recorded in Durbarmarg area in Kathmandu shows the flow of traffic responses where two

[5] https://www.youtube.com/watch?v=MiR05bnJIK0

wheelers tracked their path as parallel waves. Photo 3.3 shows the snapshots of the video at duration of 16.00, 17.02, 17.83 and 18.83 seconds. Motorbikes those running on the road towards North/South are in straight track on 16.00 seconds but they are moving towards east at 16.83 seconds. At the time of 17.83, vehicles started to change the direction and started to move on west, we can see in the photo at 18.83 seconds all the vehicles moving in west direction except those stopped already. A car moving North-South, pointed as the tip of the arrow in 16.00 and 17.02 seconds responded as like motorbikes but the displacement is much smaller in quantity.

3.2.3 Interview with drivers

A popular idiom "Experience is the best teacher" applied in all sector. Response of vehicle and drivers' response during the real earthquake shaking is most valuable asset for the student, researcher of this field. The Gorkha earthquake 2015 struck at midday, when many people were in their work, vehicles were running as drivers were on their duty. There were several vehicles running at the time of earthquake struck but the traffic density is very low as the day was Saturday, only a weekend day in Nepal.

On March, 2016, nearly a year later we went to search the drivers who were driving during the shaking. In cooperation with different government and non-government agencies we hardly found thirty drivers who actually felt the shaking during driving and ready to share the experience. We prepared few major questions and did the interview about their experience of earthquake shaking, vehicle behavior and their reaction. There are four major sections covered in the question sheet; information about driver, Information and condition of vehicle, vehicle response during earthquake and driver's reaction and their perception on earthquake risk. The question sheet we used is shown in the Appendix-II.

Interviewees are diverse in age group and driving experience, 50% of the drivers are in age group of 20 – 30 years where other 40% are in 30 – 40 years' rest two are in group of 40-50 and one is older than 50 years. Driving experience can also play the role in controlling the vehicle in danger condition so we also record the driving experience of them. Drivers with experience of 1 – 5 years are 30 %, 5 – 10 years are 36.7%, 10 – 20 years are 26.7% and more than 20 years experienced are just two drivers. Vehicles are categorized in four types during the interview as car, bus, truck and van/micro but in this study, we can consider the van/micro in the car group. No of car, bus and truck are 15, 9 and 6 respectively. Speed of the vehicles grouped in 5 ranges with <10 kmph (3), 10 – 20 kmph (4), 20 – 40 kmph (15), 40 – 60 kmph

(6) and more than 60 kmph(2). The numbers in the bracket denotes the number of vehicles in this speed range. Figure 3.6 shows the bar graph of age and experience of drivers and vehicle type and speed ranges in percentage.

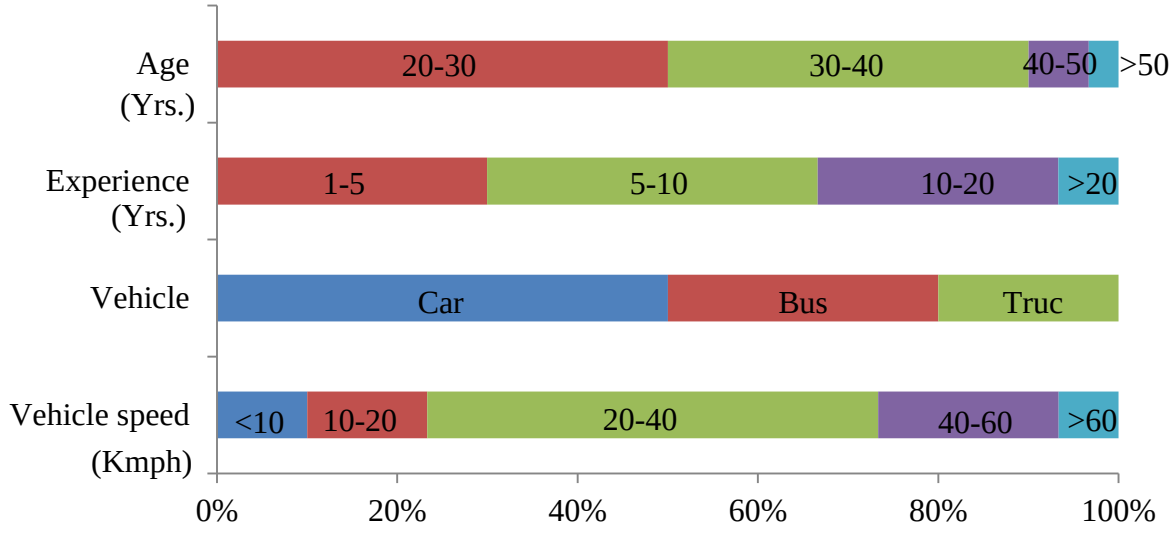

Figure 3.6 Bar graph representing percentage of age group and experience of drivers and vehicles with speed group

Most of the vehicles are in good condition (23 out of 30) where rest of the vehicles are in normal condition. When we ask the drivers "when did you know about the earthquake?" 20% of them said they knew that lately where same no of drivers claimed they knew it initially when it starts shaking. Most of the drivers (60%) knew that there is an earthquake, during the shaking. They knew the triggered earthquake by the unusual behavior of the vehicle in most of the cases (76.67%), only three drivers knew due to shaking in surroundings and four others knew after seeing the damages around.

Vehicle response and displacements are also asked with drivers, how they felt during the shaking. Twenty-one drivers said there was very little response of the vehicle in longitudinal direction where one more driver think same in lateral direction. One driver who was driving on earthen road felt nothing as he supposed the shaking was as usual, who lately know there was earthquake after viewing the damages in the surroundings. Four and five drivers said there was no response of vehicle in longitudinal and lateral directions respectively. Four and two drivers claimed there was significant response of the vehicle in longitudinal and lateral directions respectively. Charts on the figure 3.7 show the feelings of the drivers on vehicle responses during Gorkha earthquake 2015.

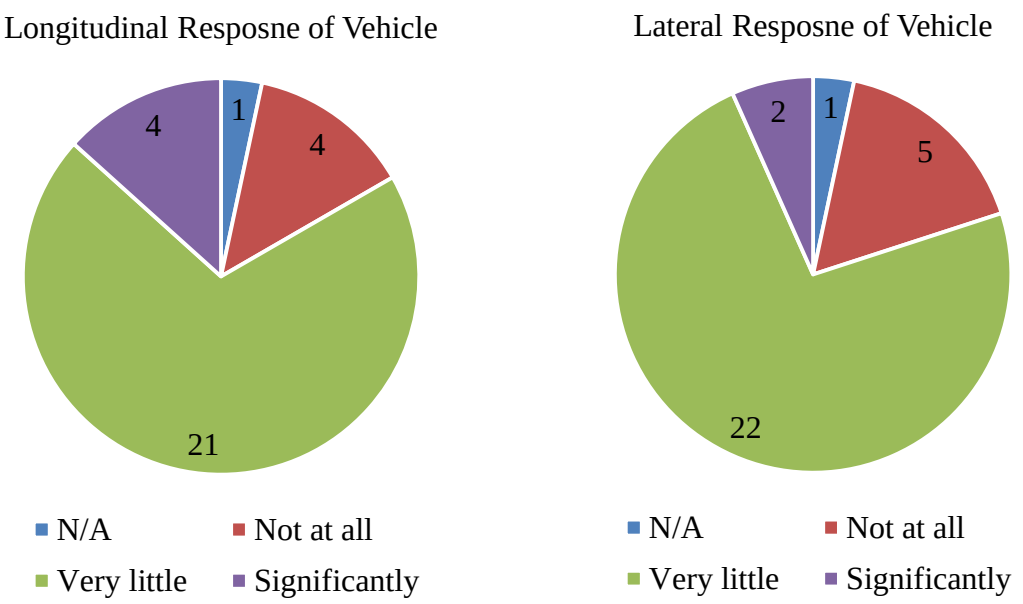

Figure 3.7 Feelings on vehicle responses during Gorkha earthquake in experience of drivers

When we ask about the vehicle displacement in longitudinal and lateral directions, majority of drivers said it was less than 1 meter, 18 and 21 respectively. Six drivers claimed there was about 1 – 2 meters' displacement in longitudinal direction where only two said the similar amount in lateral direction. A driver who was driving near Shantinagar gate of Kathmandu experienced most deviations of vehicle in lateral and longitudinal displacement of 2 – 3 meters. Figure 3.8 shows the charts of longitudinal and lateral displacements experienced by drivers.

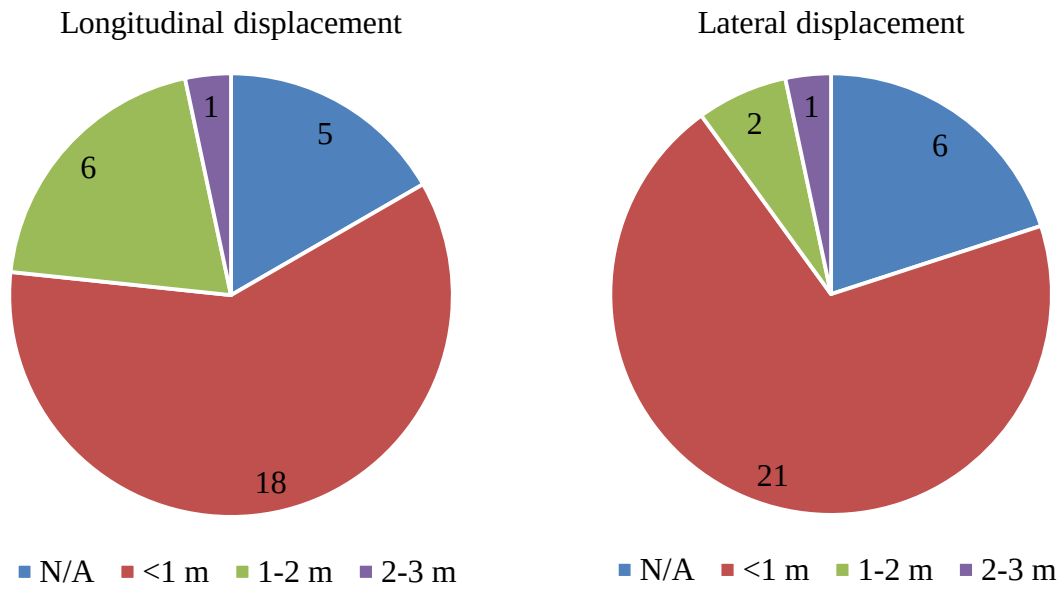

Figure 3.8 Lateral and longitudinal displacements of vehicles during Gorkha earthquake

One of the major factors to be considered in this study is drivers' reaction after they felt the earthquake shaking. We focused on the how they react and what they experienced in controlling the vehicle. Two third of the drivers say it was easy on controlling the vehicle where 20% said it was difficult to control the vehicle. On the same time two persons did not noticed and for two that was not applicable as they did not notice. The action they followed was applying the brake where 23 (76.67%) used the normal brake where 5 (16.67%) used hard brake and it does not apply to rest to drivers.

Half of the drivers interviewed, stopped their vehicle immediately where other 13 (43.33%) slow down the speed. One of the driver said he was in the same speed, interestingly one driver said he had accelerated the vehicle and moved fast. He was driving on the mountainous road, where he saw there were rock falling due to earthquake, to escape from those risks of hitting by the fallen rock, he speeded up his vehicle. 17 drivers stopped the vehicle on the shoulder where 11 others stopped on the lane where they were moving, 2 did not stop. Among thirty interviewees only one driver was in minor accident due to earthquake others did not faced any accident. Three of them said, they saw minor accidents where one driver saw a major accident. A car went down from the road due to the earthquake shaking.

Earthquake early warning system is one tool to mitigate the probable earthquake risk, especially for the drivers it might be more effective based up on their perception and reaction. We had asked them what you would do if you will get notification of upcoming earthquake prior to the shaking. Fifty percent of the drivers said they would stop the vehicle slowly and safely where 46.67% said they would stop the vehicle immediately where one said he would not react on that.

3.3 Kumamoto earthquake 2016

April 16, 2016, M7.3 earthquake struck in Kumamoto of Kyushu region in Japan at depth of about 12 km. The main shock followed the two major foreshocks of M6.4 and M6.5 in 15th and 14th. At least 49 people lost their life with tens of thousands moved to the evacuation centers where thousands of structures got collapsed. JMA seismic intensity due to the main shock was recorded up to 6.5 in Mashiki area at station KMMH16 [35], about 7 km far from the epicenter. Tateno area in Kumamoto, about 26 km NE from the epicenter was hit by the large landslide, triggered due to the earthquake shaking. Structures in Kurokawa, adjacent to Tateno area were also severely damaged where rupture line exposed to the surface. A1 in the

Figure 1 shows the Tateno and Kurokawa area where the fault slip is in range of 4-5 meters and the corresponding values on the surface is in rage of 3-3.5 m [38].

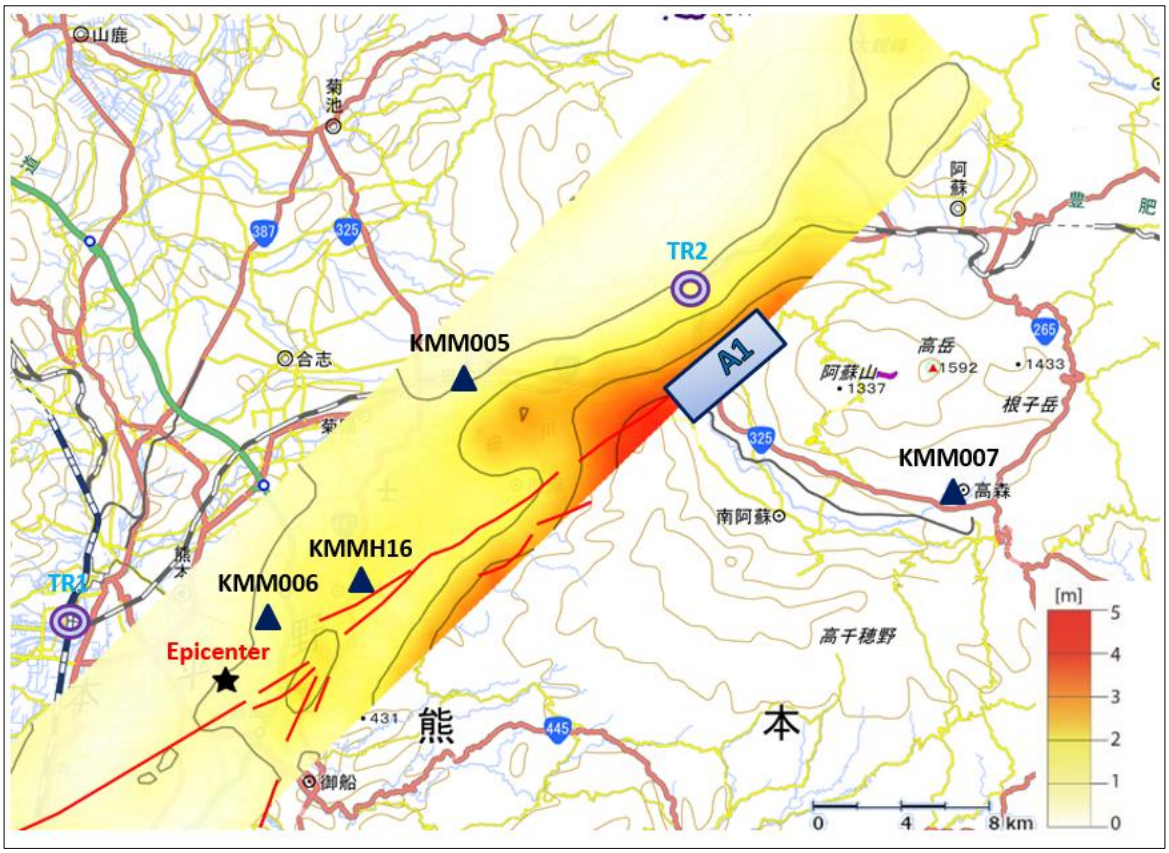

Figure 3.9 Fault slip distribution of Kumamoto earthquake, NIED ground motion record stations, vehicles toppled site and train derailed locations [38]

During the survey in Kurokawa area we found some cars (C1 – C5) toppled on the site due to the earthquake ground motion. The high-speed train (TR1) and normal JR train (TR2) shown in Figure 1 were also derailed at nearby Kumamoto station and Akamizu station respectively. We used the google earth map that updated post-earthquake to find the more cases where we found a truck (TRK) and a car (C6) in Tateno area got toppled on April 16. Locations of all the toppled vehicles and their direction of toppling are also shown by red arrows in the figure 2 along with rupture lines. All the vehicles toppled toward main rupture line (fault normal direction) except one car that toppled in fault parallel direction. Such phenomenon is localized in the distance of about 100 meters from the line of rupture that exposed to the surface in Kurokawa area. Photographs of the toppled vehicles are shown in Figure 3. All the cars toppled are registered with yellow plate that denotes the light vehicles.

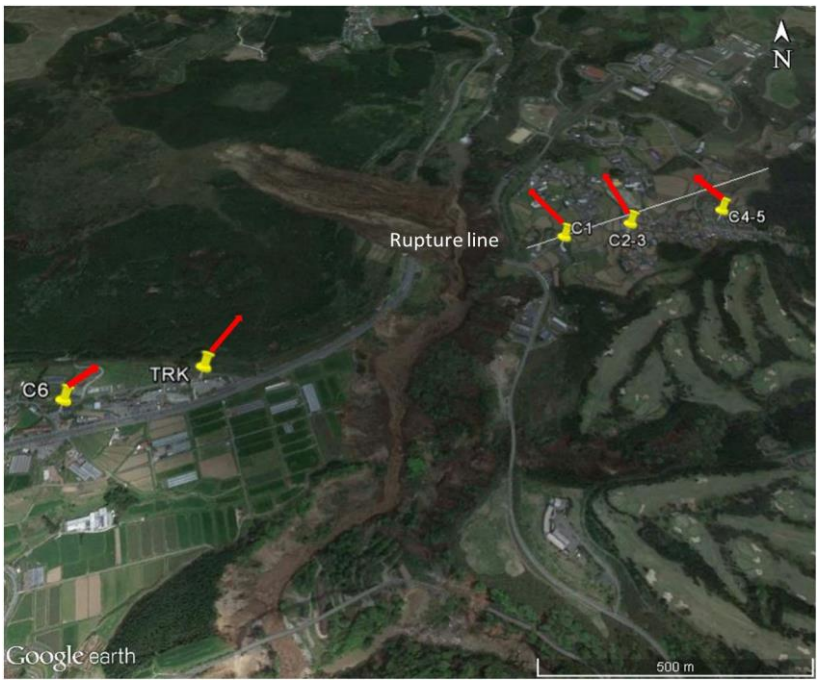

Figure 3.10 Locations of vehicles toppled and toppling direction with surface rupture lines

Figure 3.11 Photos of the toppled cars in Kuorokawa area

Target areas where the vehicles got toppled are Kurokawa and Tateno, about 26 km far from the epicenter. Toppled vehicles are registered with yellow plates those licensed as light cars (under 660 CC). We select a model SUZUKI Every Wagon as the sample car in this study [39]. The total weight of the vehicle is 950 Kg, wheel base is 2.35 m, rear and front treads both are equal of 1.28 meters. Total length, breadth and height of the car is 3.395 m, 1.475 m and 1.87 m respectively. Ground clearance of the car is 0.145 m but we could not found the exact CG location of this car. CG of the vehicle is variable with rotational motion, it has higher variation when subjected to the pitching than in rolling motion[40]. Height of CG of Skoda Yeti car is 0.5642 m and 0.714 m in rolling and pitching where total height of car is 1.671 m with ground clearance of 0.18 m [40]. Ratio of height of CG to body height is 0.3784 excluding the ground clearance when subjected to rolling motion. In case of SUZUKI Every Wagon, configuration of the car is different than the Skoda hence we suppose the height of CG is 20% of height of car body excluding the ground clearance. Now the total height of CG of the car is 0.490 m and b/h ratio is 2.612. We estimate the lateral PGA to topple the car using the regression coefficients stated in chapter 2 and from the analysis using extended CPLM method.

Recorded ground motions are not available in Kurokawa area hence we use the most likely ground motion in the analysis as seed ground motion. NIED has dense network of ground motion recording stations in Japan. KMM005 is the nearest station from the epicenter located in about 5 km. The highest PGA recorded was in station KMMH16, about 7.6 km far from the epicenter, near the fault in the Mashiki town. PGA recorded in KMMH16 are 11.57, 6.53 and 8.73 m/sec2 in EW, NS and UD components [35]. This station is about 18.7 km far from the site (Kurokawa). Locations of the NIED stations, epicenter and Kurokawa area are shown in figure 3.9.

We found from the geological map that the Mashiki area has the similar geological condition with Kurokawa area. Fault slip distribution of Kumamoto earthquake is shown in figure 1. Fault slip in Kurokawa area is about 4 – 5 meters when the value in Mashiki area is about 1 meter [35]. Hence, we used the ground motion record of KMMH16 in the analysis with amplifying factors to get the condition of vehicles to be toppled. We transferred recorded ground motion to the axis of fault parallel and normal supposing the strike angle of fault is N40°E, PGA values now changed to 12.2, 5.34 and 8.73 m/sec2. Ground motion in fault

parallel, fault normal and vertical directions in left, with the corresponding Fourier spectrum in right are shown in figure 3.12.

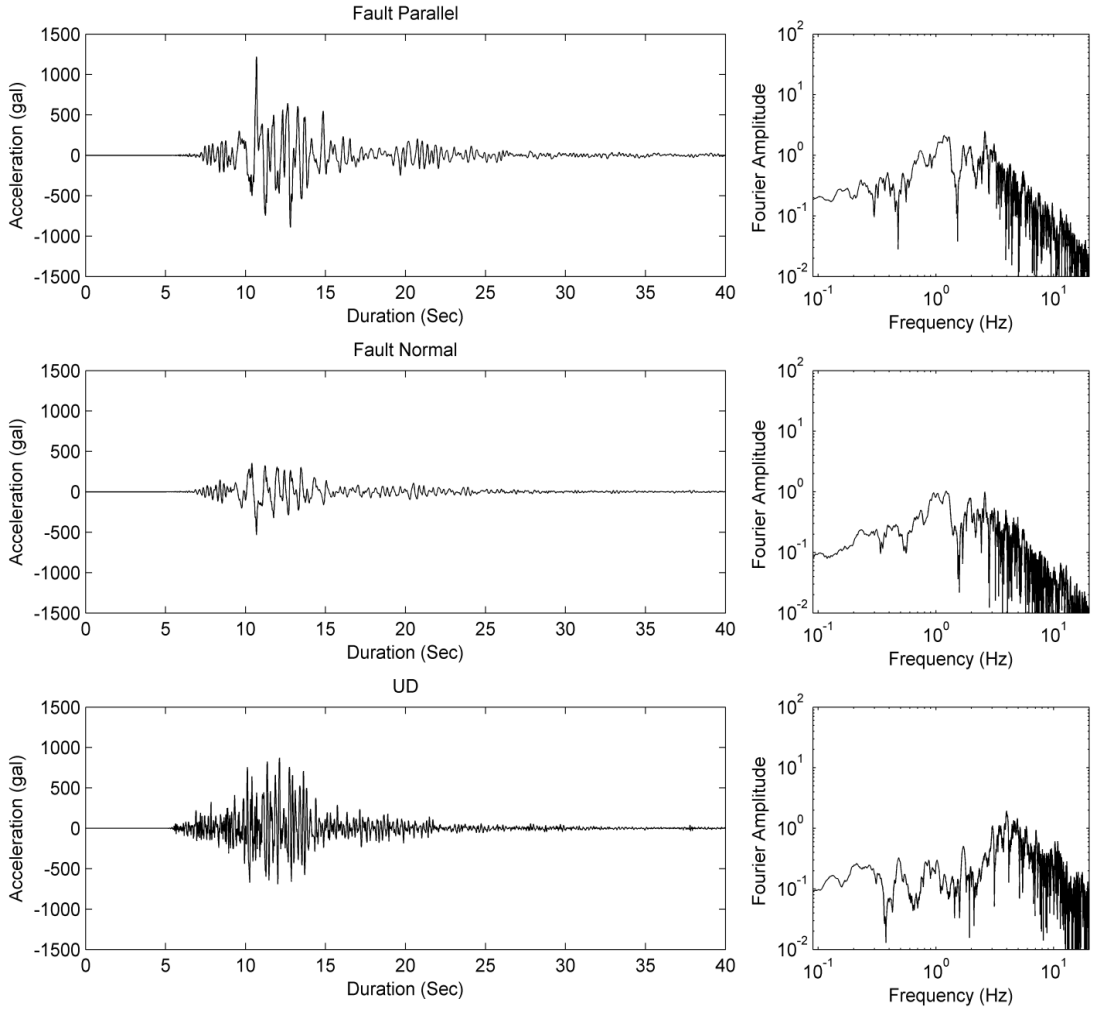

Figure 3.12 Ground motions recorded in KMMH16 and corresponding Fourier spectrum after transferred to the fault parallel and fault normal axes

Vehicle toppling mechanism initiates in the section of ground motion with peak records, we selected the time window of 10.3 – 11.0 sec and found the phase difference and dominant frequency. Figure 3.13 shows the lateral (Y) and vertical (Z) components of acceleration (ACC) and corresponding Fourier spectrum (FOU). Dominant frequency of lateral component is about 1 Hz where vertical has around 10 Hz, phase difference of the lateral and vertical component is 5.146 radian.

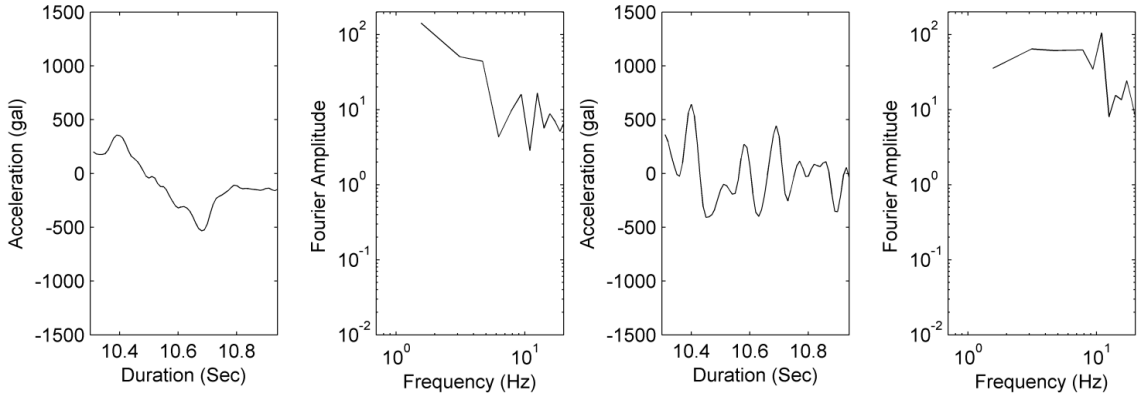

Figure 3.13 Acceleration and Fourier spectrum of the lateral and vertical components in peak time window of 10.3 - 10.94 seconds of recorded ground motion in KMMH16 from left to right

When the vertical amplitude is 8.73 m/sec2, phase difference 5.146 radian and dominant frequency of 1 Hz, PGA to topple the car is just 4.64 m/sec2 and 31.13 m/sec2 for dominant frequency of 10 Hz. Here in Kurokawa, cars were in parking area so ρ_v is taken as unit but we should find ρ_d as dimensional scaling factor. Dimensional parameters d/h ratio is 2.612 and weight is 9.5 KN. ρ_d for dominant frequency of 1Hz is 0.61 and 0.69 for 10 Hz.

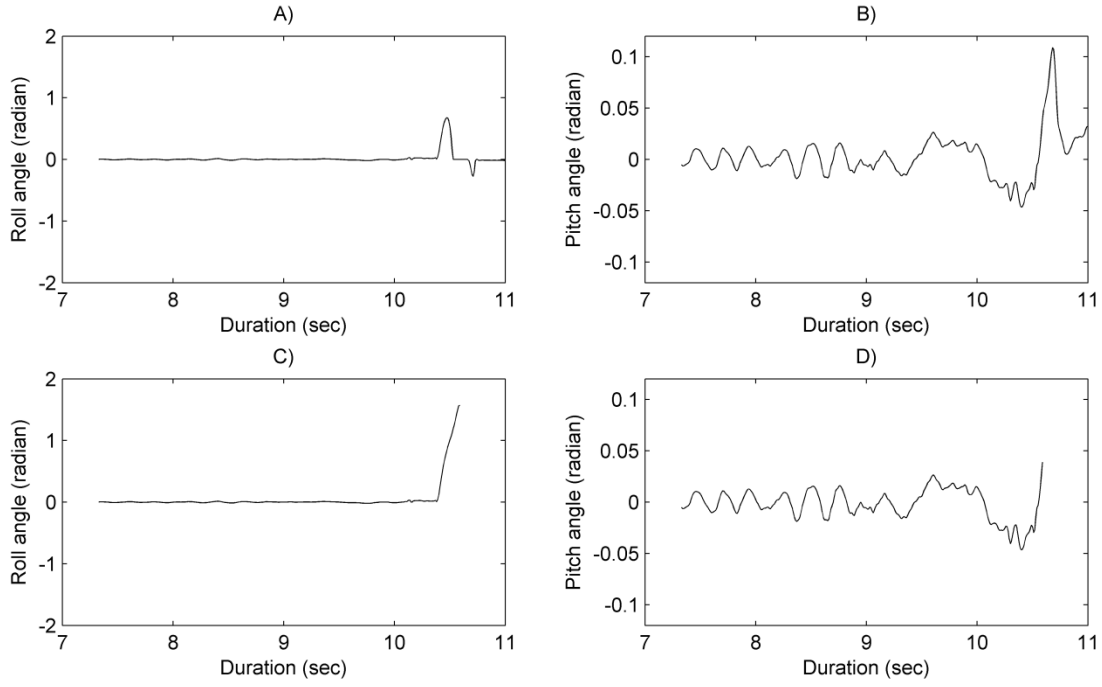

Figure 3.14 Rolling and pitching angles of the vehicle in the time window of 7.34 to 11.00 seconds' duration A) roll angle and B) pitch angle in response for PGA of 13.35 m/sec^2 and C) roll angle and D) pitch angle in response for PGA of 14.172 m/sec^2 of seed ground motion

PGA required to topple the car is 2.83 m/sec2 when considering dominant frequency of 1 Hz and 21.48 m/sec2 for 10 Hz. PGA value to topple the car in smaller frequency with higher vertical amplitude is very small as it considers the same frequency of vertical component. Resonance of the lateral and vertical component is not likely to happen hence we take the average of these two values to introduce the threshold PGA to topple the car is 12.155 m/sec2.

Figure 3.15 Toppling of vehicle in response to PGA value of 13.35 m/se2 of seed ground motion with timestamp

Now, we use the seed ground motions in the analysis, keeping the vertical component constant. The car got toppled when the PGA is 14.172 m/sec2 in 10.86 seconds as scaling factor is 2.654 for lateral component. Fault normal ground motion used in lateral and fault parallel in longitudinal direction of vehicle. When we use the smaller scaling factors then the vehicle starts to tilt in one direction after it crosses the threshold to start toppling but later it comes back to the stable position. Roll and pitch angles under the different PGA of seed ground motion are shown in figure 3.14. When the PGA value of seed ground motion reaches 13.35 m/sec2, it has maximum tilt in 10.48 seconds and it comes back to stable position. Figure 3.15 shows the conditions of the vehicle in different time corresponding to PGA 13.35 m/sec2. Figure 3.16 shows the conditions of the toppled vehicle in different time.

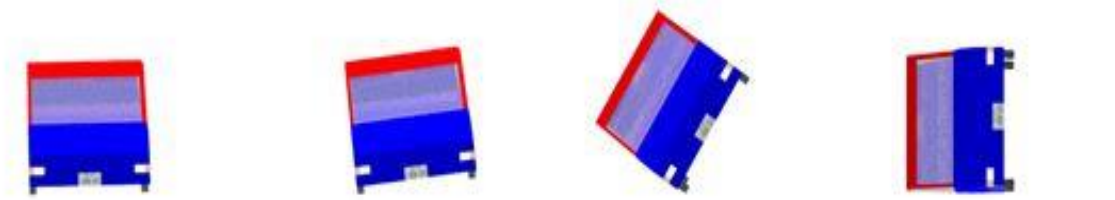

Figure 3.16 Toppling of vehicle in response with PGA of 14.172 m/sec^2 of seed ground motion with timestamp

3.4 Chapter overview

Vehicle responses during the Gorkha earthquake 2015 was done using videos and interview with drivers. Form the video it has clearly seen that two wheelers are in higher risk than four wheelers but four wheelers are also in risk. We found that during the long period ground motion, vehicles get affected even in small PGA value. Interview with drivers revealed that there are various interpretations and perceptions during earthquake shaking which is difficult to define properly. Driver's action after recognition of earthquake are also random, in using of brake and stopping location.

Analysis of toppled vehicle during Kumamoto earthquake in Kurokawa area near the Minami Aaso bridge suggested the PGA value of fault normal is about 14.172 m/sec2, 2.654 times in reference with the Mashiki area. From the calculation using the ground motion and vehicle parameters with regression coefficients provided in this study threshold PGA to topple the car in Kurokawa area is 12.155 m/sec2, around 10% sort of result from analysis. Evidences of large slip and surface rupture along with the damages to the buildings in that area could agree with this level of ground shaking in that area.

4 Vehicle following behavior and drivers' response during earthquake

4.1 Introduction

A single vehicle running on the road surface is subjected to free driving condition where driver's decision in each time follow by the vehicle freely. However, when the same driver driving his vehicle in the group, he could not be able to be free like as single. Drivers must have been influenced by the other vehicles running in front and sometimes back of them. Driver's action to be in the flow of the traffic should be different in several conditions. Moreover, vehicle responses during the events like earthquake affect on the decision making on action. There are several factors those affect the car following behavior which have already been considered in several cars following models. Here we discuss about the existing car following models on brief and use one of the models in the study of vehicle following behavior.

Driving simulator experiment conducted to analyze the driver's behavior in several conditions are presented. Thirty drivers did the driving in our test randomly for different 7 cases where total samples for each driver is fifteen. Behaviors in following the vehicle, using the brake in different conditions are under the study where we propose the brake model under several seismic intensity of earthquake shaking.

4.2 Car following models

Vehicle running on a highway is greatly affected by an immediate vehicle, driver's perception and psychology. The process of the car following the other cars in around is described by the car following models. Vehicle running in a group on a highway, transfer the condition to following vehicles. In general, application of brake and acceleration are considered in car-following models where several criteria considered under different conditions. Mark Brackstone and Mike McDonald reviewed the different car following models [41] which are discussed here in brief.

4.2.1 Gazis – Herman – Rothery (GHR) model

Concept of velocity and distance gap of vehicles are implemented in GHR model almost six seven decades ago. Main formulation of this model is given by equation 4.1.

$$a_n(t) = cv_n^m(t)\frac{\Delta v(t-T)}{\Delta x^l(t-T)} \tag{4.1}$$

a_n = acceleration of vehicle *n* at time *t*

v = speed of the n^{th} vehicle

Δv = velocity gap of n^{th} and $(n\text{-}1)^{th}$ vehicle

Δx = spacing between n^{th} and $(n\text{-}1)^{th}$ vehicle assessed at an earlier time (t-T)

T = Reaction time of driver

c, *m* and *l* are constants to be determined

Table 4.1 Summary of optimal parameter combinations for the `GHR' equation[a]

Source	*m*	*l*	Approach
Chandler et al. (1958)	0	0	Micro
Gazis, Herman and Potts (1959)	0	1	Macro
Herman and Potts (1959)	0	1	Micro
Helly (1959)	1	1	Macro
Gazis et al. (1961)	0–2	1–2	Macro
May and Keller (1967)	0.8	2.8	Macro
Heyes and Ashworth (1972)	–0.8	1.2	Macro
Treiterer and Myers (1974) (dcn/acn)	0.7/0.2	2.5/1.6	Micro
Ceder and May (1976) (Single regime)	0.6	2.4	Macro
Ceder and May (1976) (uncgd/cgd)	0/0	3/0–1	Macro
Aron (1988) (dcn/ss/acn)	2.5/2.7/2.5	0.7/0.3/0.1	Micro

Ozaki (1993) (dcn/acn)	0.9/-0.2	1/0.2	Micro

[a] Key: dcn/acn: deceleration/acceleration;
brk/no brk: deceleration with and without the use of brakes;
uncgd/cgd: uncongested/congested;
ss: steady state.

Chandler, Herman and Montroll [10] proposed the first car following model in 1958 based on the hypothesis of acceleration applied by the driver is proportional to the speed of the vehicle or following distance. They had performed the test of 8 test objects in the speed range of 10 – 80 mph over 30 minute in test track. Form the result they found that the distance gap could be neglected in the formulation ($l = m = 0$) where scaling constant has the variation in range of 0.17 – 0.74 seconds as reaction time of 1.0 – 2.2 seconds. Herman, Montroll, Potts and Rothery subsequently proposed new values and considerations in 1959 and proposed new values of *l*, *m* and *c* [14]. Several studies following these did their best to improve the formula and getting finer results [42][43][15][44][45][46][16][17][18]. Table 4.1 shows the estimations of the constants from different study. Most reliable estimates of the parameters are from micro approach (except Aron (1988)) of the study as per the review of Brackstone and McDonald[41].

4.2.2 Collision avoidance model

Driving with the conception of safety, keeping the safe distance between cars to avoid from the collision is collision avoidance model. This concept was formulated by Kometani and Sasaki in 1959[11]. Main concept of the formulation is providing safe distance between vehicles using Newton's equations of motion as shown in equation 4.2.

$$\Delta x(t-T) = \propto v_{n-1}^2(t-T) + \beta_1 v_n^2(t) + \beta v_n(t) + b_0 \qquad 4.2$$

Where $\propto$, β_1, β and b_0 are constant coefficients. From the test of vehicles with maximum speed of 45 kmph in about 200 meters long strip of road, 22 test runs and data captured by camera up to about 310 seconds deduced the parameters value as follows:

T = 0.5

$\propto$ = -0.00028

β_1 = 0.00028

β = 0.585

b_0 = 4.1

R^2 value of the data from the experiment with coefficients is 0.75. In other tests, there are different values with varied fitness. This model was further improved by Gipps in 1981 by considering several aspects [47]. It can be used in the propagation of the disturbances for the group of vehicles.

4.2.3 Linear model

Linear model attributed by Helly in 1959 [12] is taken as the first linear model in vehicle following research, although GHR model of first purposed was also linear. Helly added the acceleration term to be used according to the braking action of front vehicle. The basic model equation is shown in equation 4.3 to find the acceleration.

$$a_n(t) = C_1 \Delta v(t-T) + C_2\big(\Delta x(t-T) - D_n(t)\big) \quad 4.3$$

Where C_1 and C_2 are constants, D_n is desired following distance, can be calculated from equation 4.4.

$$D_n(t) = \propto + \beta v(t-T) + \gamma a_n(t-T) \quad 4.4$$

There are several improvements in this model by Hanken and Rockwell (1967) [48], Bekey, Burnham and Seo (1977) [49], Aron (1988) [17] and Xing (1995) [50]. Optimal parameter values of those studies are shown in table 4.2.

Table 4.2 Optimal parameters for linear model

Source	$\boldsymbol{C_1(\Delta v)}$	$\boldsymbol{C_2(\Delta x)}$
Helly (1959)	0.5	0.125
Hanken and Rockwell (1967)	0.5	0.06
Bekey, Burnham and Seo (1977)	0.5	1.64
Aron (1988) (dcn/ss/acn)	0.36/1.1/0.29	0.03/0.03/0.03
Xing (1995)	0.5	0.05

4.2.4 Psychophysical model

This model of vehicle following explains the perception of the driver with the size of the front vehicle and act on acceleration or deceleration accordingly. Michaels in 1963 [13] put forward this idea in vehicle following model. He considered the relative velocity of front vehicle by view of subtended angle of the driver. When certain threshold of the angle exceeds then drivers starts to decelerate. There are several other improvements in this model as like others thereafter.

4.2.5 Fuzzy logic model

The concept of human perception and action on the vehicle that drag the vehicle path as car following is used in this model. Perception and decision making of the driver is taken as the main parameters. Logic thought of the human is qualitative where communication is not precise. Hence, the process of perception, decision and action process of human fits in the fuzzy logic. This model firstly use by Kikuchi and Chakroborty in 1992 [51]. This model has been updating by several researchers in the following days.

4.2.6 Autonomous Decentralized Mechanism (ADM) model

Doustari, M. A. and Sannomiya, N. in 1993 proposed the model of autonomous decentralized mechanism (ADM) model for the fish behavior [52]. They used the water tank experiment to formulate the model using different forces that plays the role in fish behavior. The relationships of forces that act in the movement are shown in following equations.

$$m_i \cdot \ddot{x}_i(t) = F_{i1} + F_{i2} \tag{4.5}$$

$$F_{i1} = a_1^i\left(|\dot{x}_i(t)| - a_2^i\right)\left(|\dot{x}_i(t)| - a_3^i\right)\dot{x}_i(t) \tag{4.6}$$

$$F_{i2} = \sum b_i\left(r_{ij}\right)\frac{x_{ij}}{r_{ij}} + \sum c_i\left(r_{ij}\right)\frac{\dot{x}_j(t) - \dot{x}_i(t)}{M_c} \tag{4.7}$$

$$x_{ij} = x_j(t) - x_i(t) \tag{4.8}$$

$$r_{ij} = \left|x_{ij}\right| \tag{4.9}$$

$$b_i\left(r_{ij}\right) = \begin{cases} \frac{\left(k_{bi}^4 - k_{bi}^3\right)r_{ij}}{\beta_{i1}} + k_{bi}^3 & \left(0 \le r_{ij} \le \beta_{i1}\right) \\ k_{bi}^4 & \left(\beta_{i1} \le r_{ij} \le \beta_2\right) \\ 0 & \left(r_{ij} > \beta_2\right) \end{cases} \tag{4.10}$$

$$c_i(r_{ij}) = \begin{cases} k_{ci} & (0 \le r_{ij} \le \delta) \\ 0 & (r_{ij} > \delta) \end{cases} \tag{4.11}$$

A formation of order by interacting among individuals in fish group is quite similar to maintaining the stability of traffic flow. Equations (4.5) - (4.11) shows the formulation of ADM model. When ADM model is applied to car-following model, F_{i1} is regarded as force for free flow and F_{i2} is regarded as interaction between vehicles in equation of motion. Equation (4.7) defined interaction between vehicles, the first term is attraction between vehicles adjusts a distance between front vehicle and rear vehicle, and the second term is force to control a group adjusts relative velocity and direction.

This model is now further modified by adding the brake force depending on the seismic intensity of the shaking and brake level to use in the simulation of vehicle behavior during earthquake.

4.3 Driving simulator experiment

Driving likely in real situation using the mechanical and instrumental setup inside the laboratory is driving simulator experiment. In this set up road display in the screen, steering, accelerator, gear and braking systems are similar to the real vehicle. Driving simulator experiment is popular in analysis of driver's behavior in several conditions. We can design the driving background where several vehicles, obstacles can be placed. Photo 4.1 shows the driving simulator in Kyoto University.

Photo 4.1 Driving simulator, screens in the blue

We use driving simulator experiment to analyze the driver's behavior during earthquake shaking, mainly focusing on the application of brake. Total thirty drivers are involved in the test, where mainly two levels of shaking as earthquakes are used. Several four conditions with both level of shaking was sampled randomly with all drivers. Analyses on car following and application of braking are modeled from the result. Driving simulator experiment has conducted in Intelligent Transport Systems (ITS) laboratory in Kyoto University.

4.3.1 Experimental setup and sampling

Driving simulator with six actuators is all set to observe the driving behavior and response of driver under different conditions. Driving environment is set in the computer connected to the simulator where the road and its background are designed for target. When the driver sit on the driving seat, he/she can feel the real driving situation with audio visual system.

Photo 4.2 Driver drives on driving simulator experiment

Drivers are selected based on their experience of driving and license issued year, we have selected the drivers who has license at least more than a year with driving experience of at least one year. Total thirty drivers have registered to take part in the driving simulator experiment. Photo 4.2 shows a person driving in the driving simulator.

All the drivers are set to drive on the fixed segment of the road that set on the simulator. Total length of the road section is about 1300 meters where all the drivers are asked to drive with nearly constant speed of 80 kmph. Earthquake excitations are given in terms of displacements in the section of 700 meters as there was technical problem on excitation with acceleration.

Hence, we provide the displacements on the road surface where the vehicle subject to the shaking for about 30 seconds. In many cases, some drivers stopped the car, some did not respond and some react gently on braking. Total 15 sets of data are collected under different conditions for one driver as shown below.

- Without shaking: 3 sets
- Lower level of shaking
  - Without front vehicle: 2 sets
  - With front vehicle (Stopped): 2 sets
  - With front vehicle (Not stopped): 2sets
- Upper level of shaking
  - Without front vehicle: 2 sets
  - With front vehicle (Stopped): 2 sets
  - With front vehicle (Not stopped): 2sets

Where upper level of the shaking corresponds to the seismic intensity (SI) level of equal or more than 6 and lower level corresponds to the SI level of less than 6. We provided displacements in lateral direction and vertical where external acceleration in longitudinal direction is null except the brake applied by driver.

Driver's reaction upon triggering of the earthquake is the main purpose of the study; hence we are considering the time span of about 15 seconds after the threshold value crosses. In this study, earthquake shaking started in about 10 seconds from the time of origin. Figure 4.1 shows the plot of velocity over time in the case of normal condition, i.e. without the shaking. Most of the drivers almost maintained the speed of about 80 kmph throughout the total length of road.

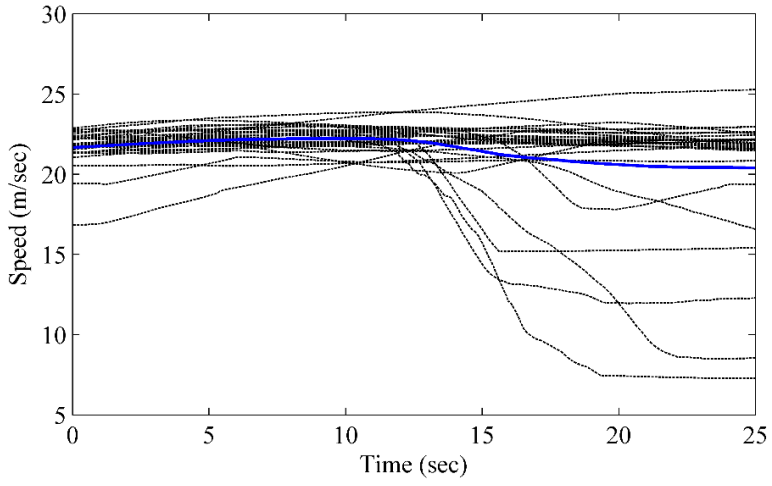

Figure 4.1 Speed trajectories of test samples for normal condition

Figures 4.2 (a – c) show the similar plot of vehicle speed over the time under lower level of shaking for conditions of without front vehicle, with front vehicle stopped and with front vehicle keeping on running during shaking. Speeds of the vehicles over the time for all three cases under upper level of shaking are shown in Figures 4.3 (a – c).

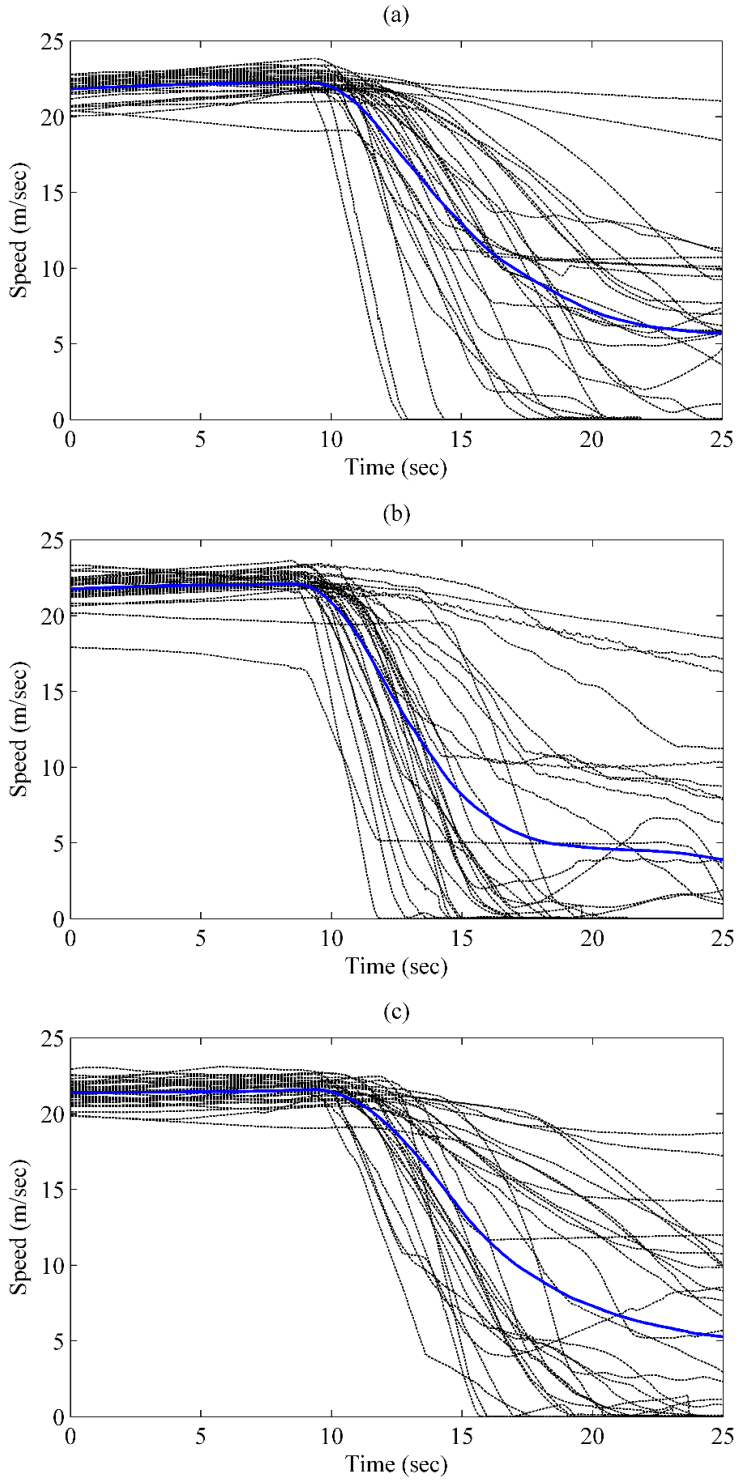

Figure 4.2 Speed of vehicles under lower level of shaking under cases of (a) No front vehicle, (b) Front vehicle stopped and (c) Front vehicle not stopped

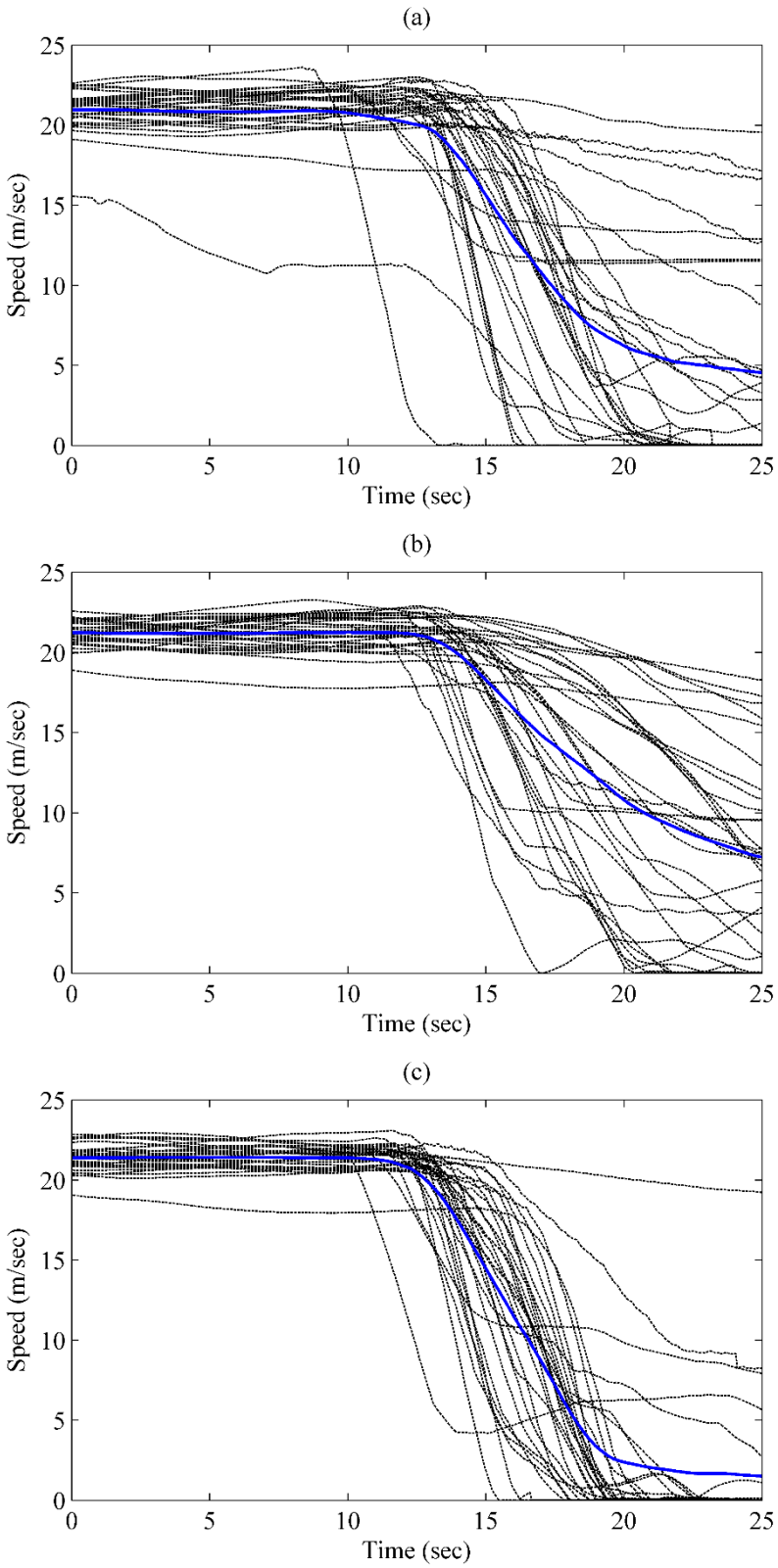

Figure 4.3 Speed of vehicles under upper level of shaking under cases of (a) No front vehicle, (b) Front vehicle stopped and (c) Front vehicle not stopped

Changes on the speeds of the vehicles under three cases of both higher and upper level of shaking are following similar trend for all drivers. When there is no front vehicle in upper and lower level of shaking, drivers tend to slow down the speed. However, some of the drivers stopped the vehicle under lower level of shaking where the rate is higher when shaking level is higher. For the case of front vehicle stopped, the rate of vehicle stopped in lower level of shaking is lower; they intend to pass the front vehicle. Similarly, under the higher level of shaking drivers follow that trend. For the case of front vehicle do not stop, in lower shaking level it seems less number of drivers stopped as compared to the front vehicle stopped in contrast with the case of upper level of shaking, stopped vehicle samples goes up.

4.3.2 Brake level and reaction time

Braking action under several conditions by the drivers are now in discussion. All three cases under both shaking level are in focus of the study. We have selected the threshold of the lateral acceleration of 0.5 m/sec2 for the reaction of the driver against the shaking. When the vehicle is in speed, it itself is in shaking mode due to internal springs and road undulations. We have also checked the recorded data when the drivers are getting active to press the brake paddle. We first find the time of threshold acceleration (first absolute value of 0.5 m/sec2), supposed to trigger by the earthquake, then analyze the brake level and time correspondingly.

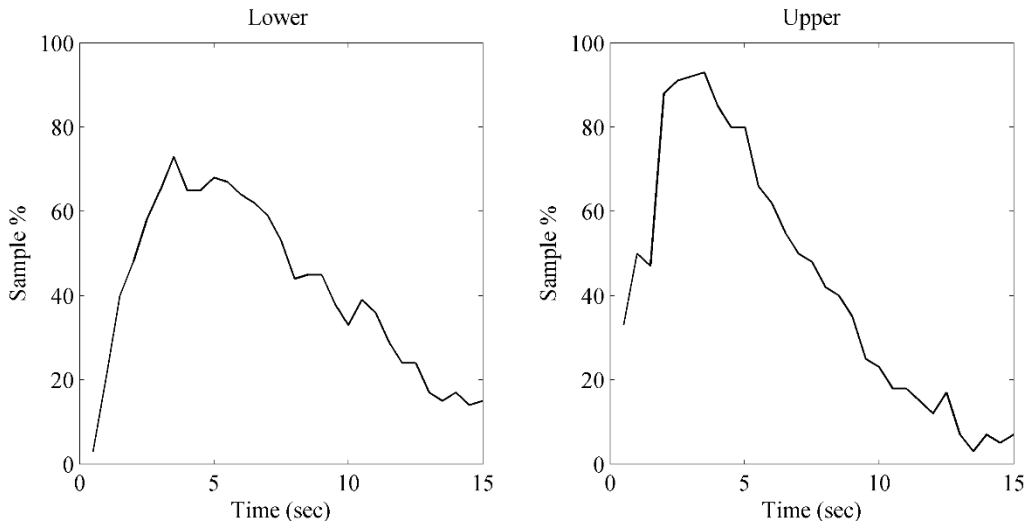

Figure 4.4 Engagement of driver in braking paddle (Percentage of drivers applied brake more than 0.05 m/sec^2) in the case of without front vehicle under lower (left) and upper (right) level of shaking

Brake levels are selected in ranges from 2 – 8 m/sec^2 at interval of 1.0 m/sec^2 and observed the percentage of drivers' engagement, moreover the engagement of certain level of brake over the time are calculated. Figure 4.4 shows the engagement of the drivers over time as braking action,

percentage of drivers who applied the brake at corresponding time for cases without front vehicle. Braking action of drivers totally depends on the level of shaking, when there is low level of shaking there are less numbers of drivers applied brake than the case of upper level of shaking. Time of maximum engagement on brake is higher for lower shaking level where it is shorter in case of higher shaking level. Similarly, for the cases with front vehicle stopped and front vehicle did not stop are shown in figures 4.5 and 4.6 respectively.

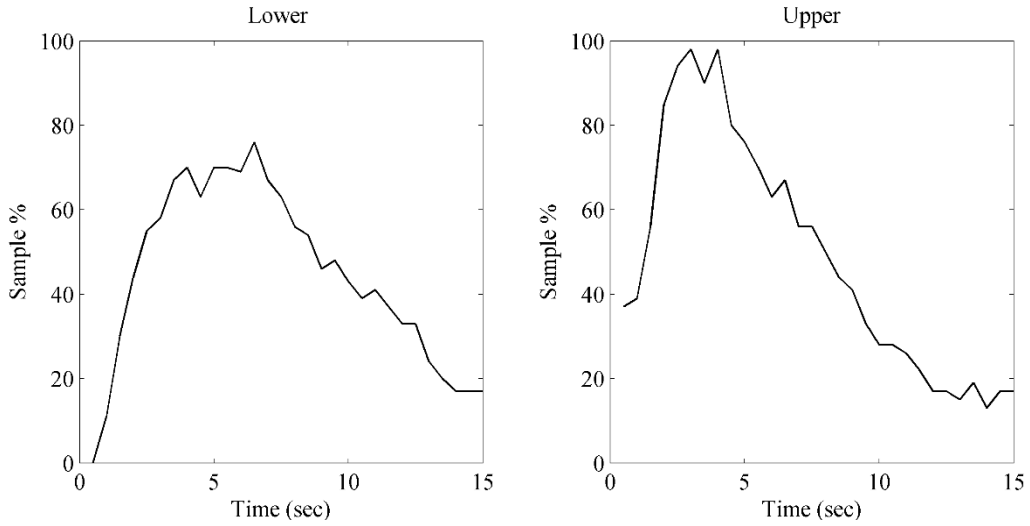

Figure 4.5 Engagement of driver in braking paddle (Percentage of drivers applied brake more than 0.05 m/sec^2) in the case of with front vehicle stopped under lower (left) and upper (right) level of shaking

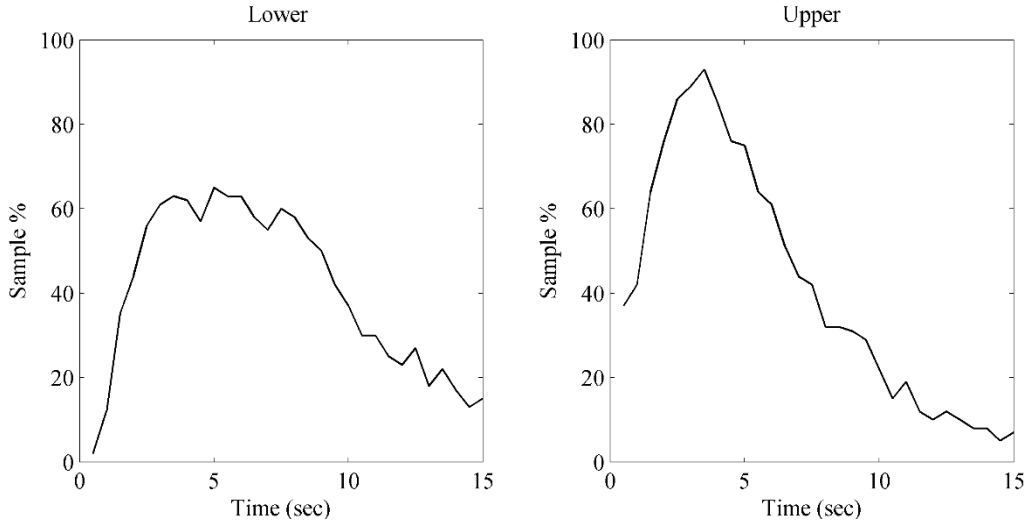

Figure 4.6 Engagement of driver in braking paddle (Percentage of drivers applied brake more than 0.05 m/sec^2) in the case of with front vehicle did not stopped under lower (left) and upper (right) level of shaking

Reaction time and brake level for all cases and all level of brakes are also presented in this study. Figures of the driver's engagement in braking for all cases and all level of brakes (2, 3, 4, 5, 6, 7 and 8 m/sec^2) are provided in annex III.

4.4 Brake model

This section focus on the brake model to be used in the simulation of multiple vehicle. In all cases, driver's reaction on braking varied widely that we could not specify the fixed brake level for certain case. Using the stochastic method, we gathered the maximum usage of brakes for all three cases under lower and upper level of shaking. We found that the exceedance of brake level follows normal distribution as engagement. Figure 4.7 shows the experimental observation and corresponding cumulative normal distribution fit under lower and upper level of shaking. Mean values are 3.8 and 5.95 for lower and upper level of shaking correspondingly however standard deviation is similar with value of 2.5.

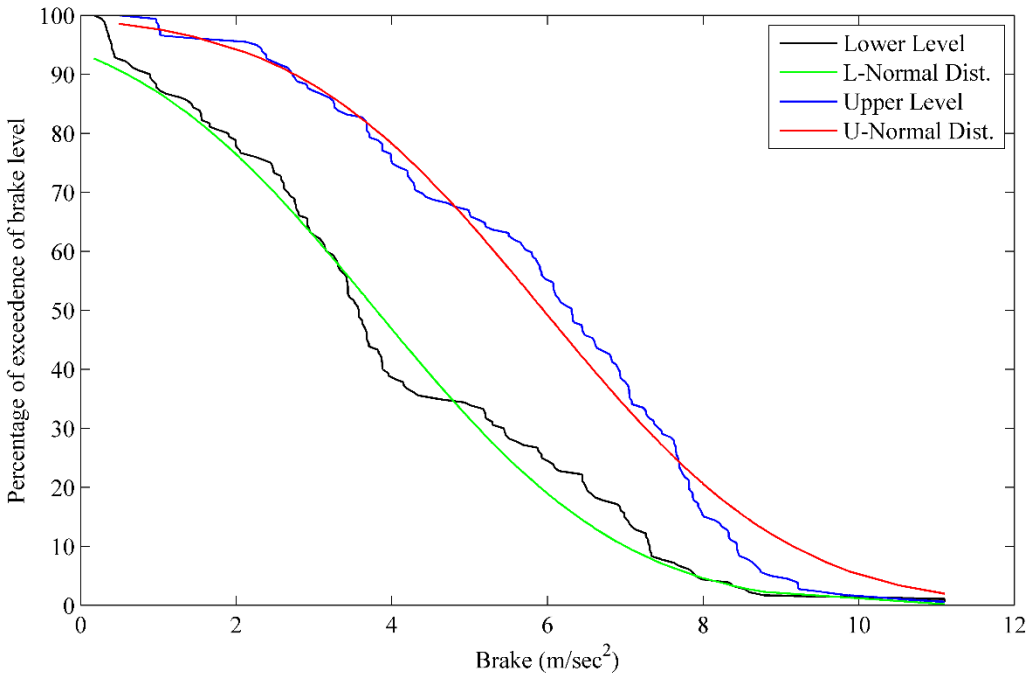

Figure 4.7 Percentage of exceedance of brake level under lower and upper level of shaking

Time corresponding to the maximum engagement of the drivers for all brake levels under all cases are now plotted. We have neglected the first few seconds' peak for smaller value of brake levels because many of those corresponds to the steps of the higher brake levels. Figures 4.8,

4.9 and 4.10 show the time of corresponding brake level under lower level of shaking in left and higher level of shaking in right. We find there is linear relationship of brake and applied time those represented by trend line in each figure.

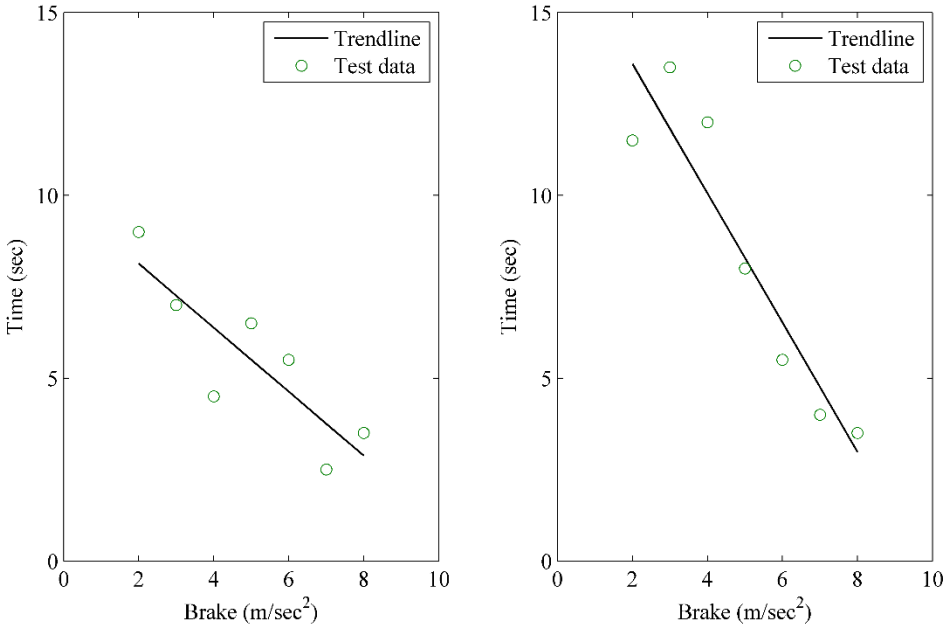

Figure 4.8 Relationship of maximum brake level and time for the case of free vehicle

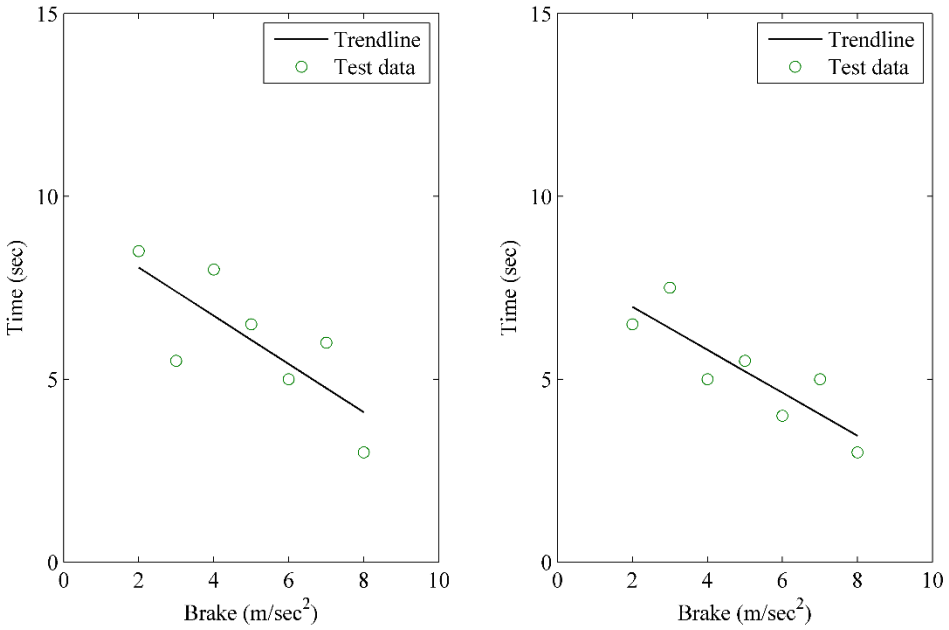

Figure 4.9 Relationship of maximum brake level and time for the case of front vehicle stopped

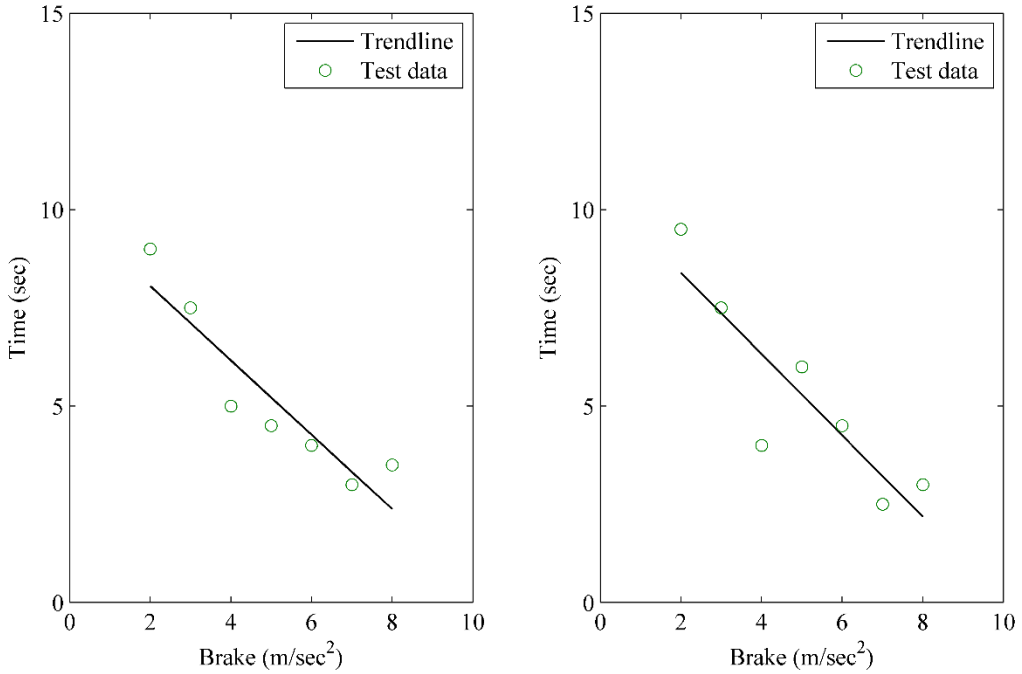

Figure 4.10 Relationship of maximum brake level and time for the case of front vehicle did not stopped

Table 4.3 Coefficients of relationship between brake and time of application

S.N.	Cases	Coefficients		
		M	C	R^2
1	Without front vehicle			
	Lower level of shaking	-0.875	9.875	0.7267
	Higher level of shaking	-1.76786	17.125	0.8714
2	Front vehicle stopped			
	Lower level of shaking	-0.66071	9.375	0.5901
	Higher level of shaking	-0.58929	8.160714	0.7241
3	Front vehicle did not stopped			
	Lower level of shaking	-0.94643	9.946429	0.8522
	Higher level of shaking	-1.03571	10.46429	0.7816

Application of brake by the drivers after the earthquake seems dependent on the condition of the vehicle position and other vehicles with their state. When there is no front vehicle or free flow of the vehicle exist, drivers applied higher level of brake sooner but the execution time of

soft brake is relatively late in higher level of shaking condition. In contrast with higher level of shaking, soft brakes are executed faster in lower shaking condition are observed. However, the application of soft brake seems almost similar in case of front vehicle keep moving but sooner they used hard brake in strong shaking. When the front vehicle stopped after the earthquake, faster they applied the brake during strong shaking rather than of moderate one.

Now, we can use the random sampling of brake level for different vehicles using the distribution for the case of either lower or upper. After getting the maximum brake level of corresponding vehicle, time of application of maximum brake can be determined by using the relationship of brake and time as shown above using the equation 4.12 (a). Where M and C are, coefficients given in table 4.3, T_m is time of maximum brake, B_r is brake level. 4.12 (b) shows the relationship of brake level to the standard deviation.

$$T_m = M.B_r + C \qquad 4.12(a)$$

$$SD_m = -0.2215.B_r + 2.8066 \qquad 4.12(b)$$

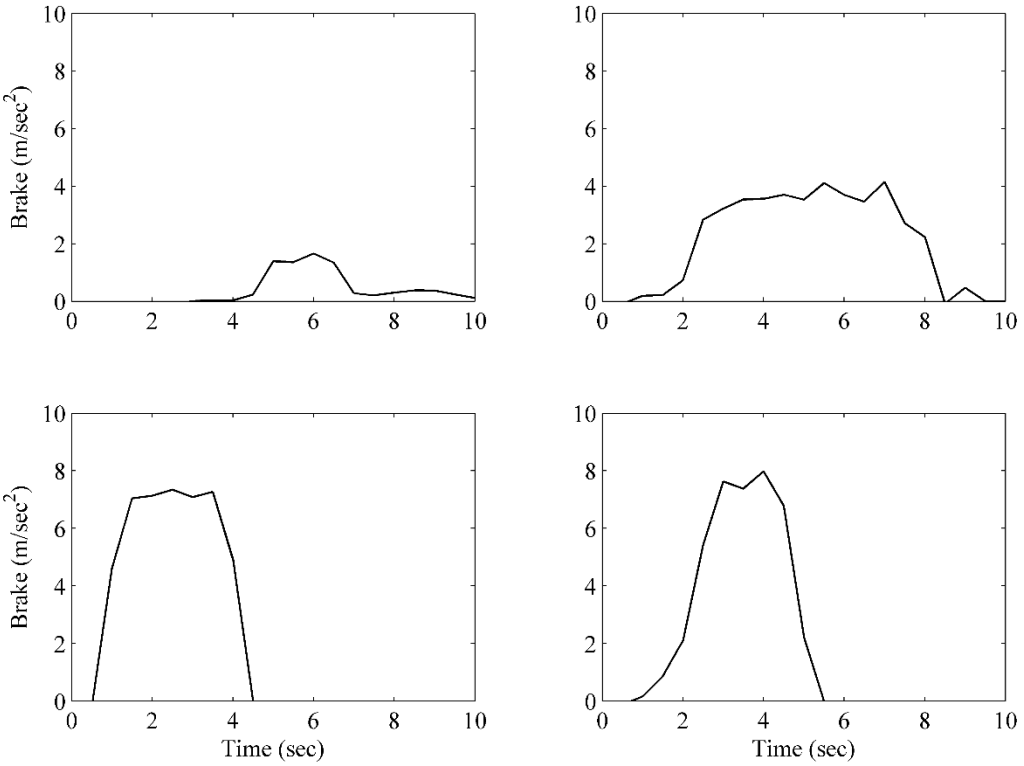

Figure 4.11 Application of brake by drivers during experiment

Application of the brake by the drivers are also varied widely but the trend of application follows normal distribution for about 74%. We have checked the individual trend and find the standard deviation which varied with brake level. Figure 4.11 shows the samples of application of brake by drivers during experiment, which nearly follows the trend of normal distribution.

4.5 Car following model under earthquake shaking

Driver's behavior during earthquake shaking depends on the individual, perfect modeling of human behavior is difficult. Hence, we extend the ADM model with introduction of the extra force that developed due to braking of vehicle under several conditions. Now the equation 4.5 can be modified as equation 4.13.

$$m_i \cdot \ddot{x}_i(t) = (F_{i1} + F_{i2})(1 - \alpha) + F_{i3}\alpha \qquad 4.13$$

Where F_{i3} is, force induced by the application of brake, α is the priority factor of braking. When the driver use hard brake level then priority of driver will shift to application of braking rather than caring of other factors, in contrast it will be down for soft brake.

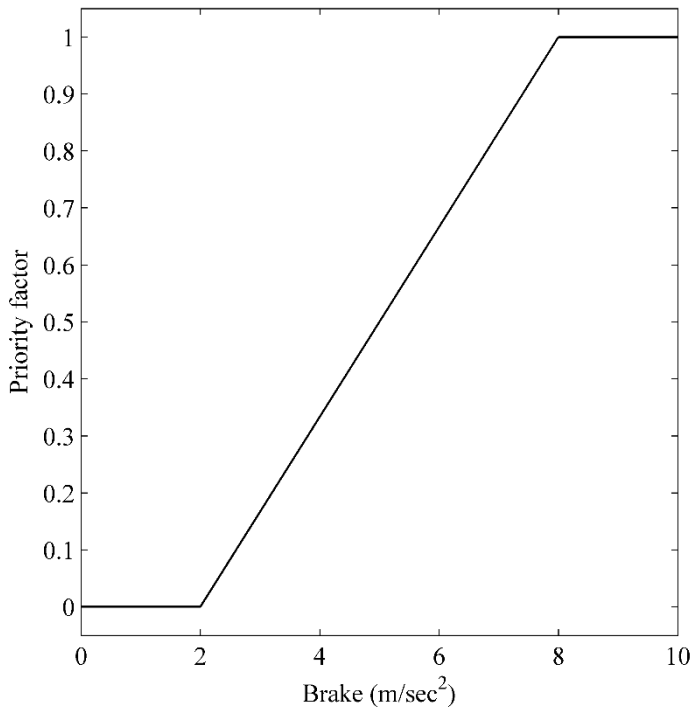

We assume the linear function of priority factor that considering the lower level of braking is 2.0 m/sec2 and upper level of 8.0 m/sec2. However, the cases of braking level under 2.0 m/sec^2

exists, the effect will accommodate in terms of repulsion force that accommodate in the term F_{i2} in ADM model.

Car following behavior are now discussed using extended ADM model in case of earthquake shaking. Firstly, we tested the model for the cases of varying initial speed, no earthquake excitation and corresponding brake level defined for vehicles. Five vehicles with initial speed of 20.0, 22.0, 24.0, 22.0 and 20.0 m/sec are running with initial gap of 40.0 m each, the car following state is shown in Figure 4.12. Car2 and Car3 have higher speed than the vehicle in front that cause them decelerate and manage the target speed, which was set as 20.0 m/sec. Car4 and Car5 have lower speed than front vehicle so firstly they started to accelerate but later again they use brake and reduce the speed which ultimately take them to more lower speed and again try to back to target speed. This phenomenon of changing in speed is like a dropping of a ball.

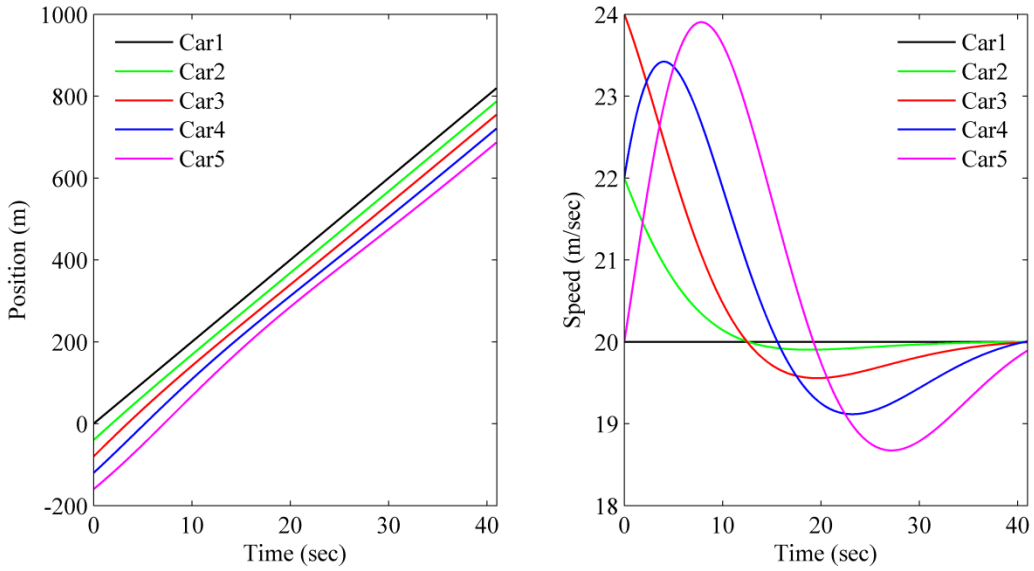

Figure 4.12 Position (left) and velocity (right) of the cars using ADM model under ideal case

Now we use the earthquake excitation for the same cars but now we supposed that drivers will not respond to the earthquake shaking effect hence we do not provide the brake level for them. Totally the car following state will be as the normal but vehicle response will make differences in speed. Earthquake motion from Kumamoto earthquake that shown in section 3.3 is used in this analysis.

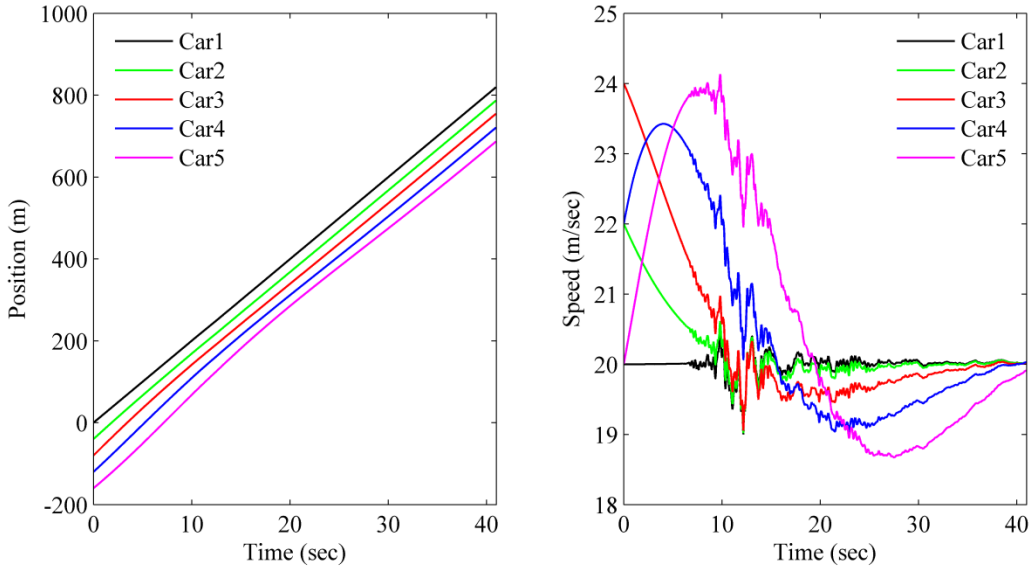

Figure 4.13 Position (left) and velocity (right) of the cars using ADM model under the excitation of earthquake, without driver's reaction on brake

When earthquake struck then longitudinal speed of the vehicle got affected by the shaking. However, the braking reaction of the driver is not considering, almost the vehicle following phenomenon is similar to that of without the earthquake. Figure 4.13 shows the positions of the vehicles and corresponding speeds.

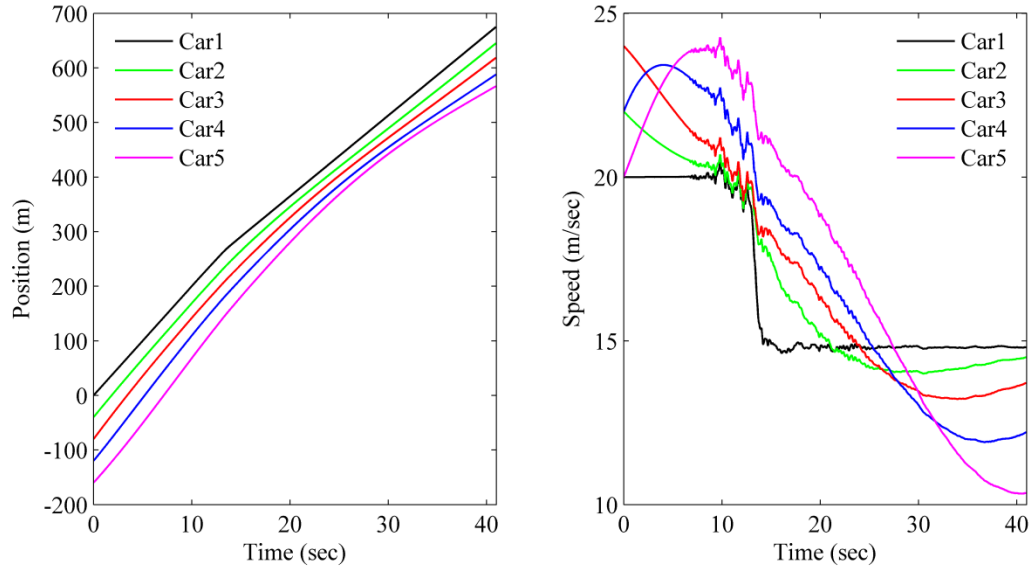

Figure 4.14 Position (left) and velocity (right) of the cars using ADM model under the excitation of earthquake, with brake level of 4.0 m/sec^2

When we consider the reaction from the driver, there will be certain brake level that will use by the driver. Brake level here is defined as the maximum value that used as reaction after the shaking acceleration exceed 50 gal (0.5 m/sec^2). Positions and the speeds of the vehicles are shown in figure 4.14, when we assign the same brake level of 4.0 m/sec2 as supposed reaction from the driver. First car (Car1) has only applied the provided brake level where it follows normal distribution but other vehicles got affected by the brake of immediate front vehicle, which clearly seen in the figure.

4.6 Chapter overview

This chapter provide insight in the car following model that to be used in the cases of earthquake shaking. When the vehicle starts to vibrate, driver's reaction under this situation is crucial in the safety of vehicle and driver. Driving simulator experiment provide the trends of driver's reaction during earthquake shaking. However, these results are based on the reaction of a single driver with other automated cars. Brake action by the drivers are varied widely even though we can model the percentage of exceedance of brake levels follow the normal distribution. Application of brake by the drivers also follows the normal distribution where mean value of time is different, which can be determined form the relationship proposed for different brake levels under varying cases.

Introduction of the additional force factor due to the earthquake in ADM model can be used in the case of vehicle follow study under earthquake shaking. Priority factor during the application of brake is also introduced on the assumption of perception during hard brake and soft brake.

5 Elevated structures and vehicle response

5.1 Introduction

Mega cities are spreading as the urban population escalating year by year. Transportation facilities in megacities are now expanding in vertical direction as it limits in lateral. Tunnels and elevated structures are built rapidly to cater the traffic of city along with link to countryside. City expressways are dominated by elevated structures rather than surface road. Hanshin expressway that serves in Kansai region of Japan is of total about 250km in length. It comprises of about 80% of steel and concrete bridges, another about 10% of surface road and rest 10% of tunnel structures standing to complete the network. Pie chart in figure 5.1 shows the distribution of road structures in Hanshin expressway, Kansai Japan.

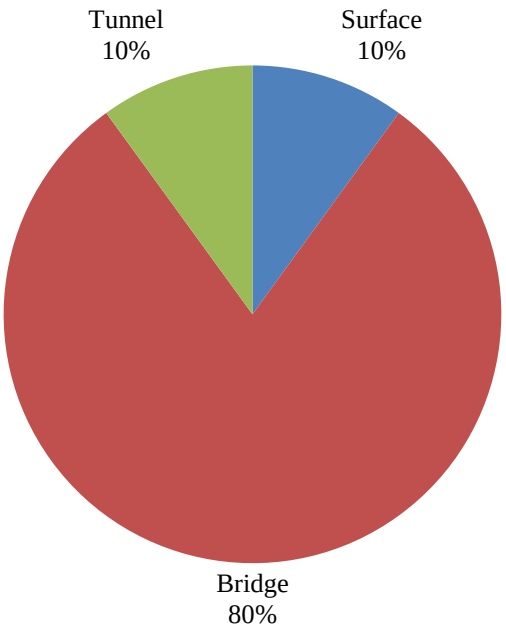

Figure 5.1 Road structures in Hanshin expressway, Kansai, Japan

Risk associated to the vehicles those running on the surface road is not similar to the vehicles those using elevated structures. Earthquake ground motion that propagates through the ground surface will be different in the road surface where it passes via bridges or viaducts depending on structural response. Seismic response analysis of vehicle considering earthquake ground motion on surface would not be enough explaining the real scenario of vehicle behavior for

elevated structures. Method of vehicle risk analysis running on the elevated structures will be discussed in this chapter.

A symmetrical cable-stayed bridge model is used as a sample elevated structure having total length of 1330 m. Dynamic analysis of the bridge with input ground motion in base of piers had given nodal acceleration response in bridge deck. Interpolation of nodal acceleration for each vehicle in each time step of calculation gives input ground motion for each vehicle which depends on the location of it. Vehicle response analysis was already discussed in chapter two. This chapter mainly focuses on extraction of the input seismic motion for vehicle those running through elevated structures.

Interpolation of the nodal responses of bridge structure for input to the vehicle has done and shown the interpolated acceleration for different cases of speed and location of the vehicle. Responses of car, bus and truck in the longitudinal and lateral directions for several conditions using the interpolated earthquake accelerations are shown. The relationships between the vehicle's responses with the speed and peak ground acceleration (*PGA*) were also investigated.

5.2 Bridge modelling

A virtual cable-stayed symmetrical bridge of total length 1330 m was modeled with nodal distance of 5 m between central three nodes and 15 m in rest of the part except two nodal distances of 7.5 m in both sides near short piers in between long and edge piers. Central span of bridge is 580 m long with three columns on each side as shown in Figure 5.2. Total numbers of nodes in bridge deck level are 91. Cables are connected to the deck from two main towers in sides. Bridge supported by the cables with two main towers in center where there are another two piers supported in each side. 2D model of the bridge has longitudinal direction in *X* axis where vertical axis denoted as *Z*. The analysis was performed using commercial software Forum 8, Engineering Studio. Dynamic analysis of bridge with input ground motions as shown in Figure 5.3, in base of piers give nodal acceleration response. Nodal response accelerations of bridge model were later used in the determination of earthquake motion for analysis of vehicle behavior.

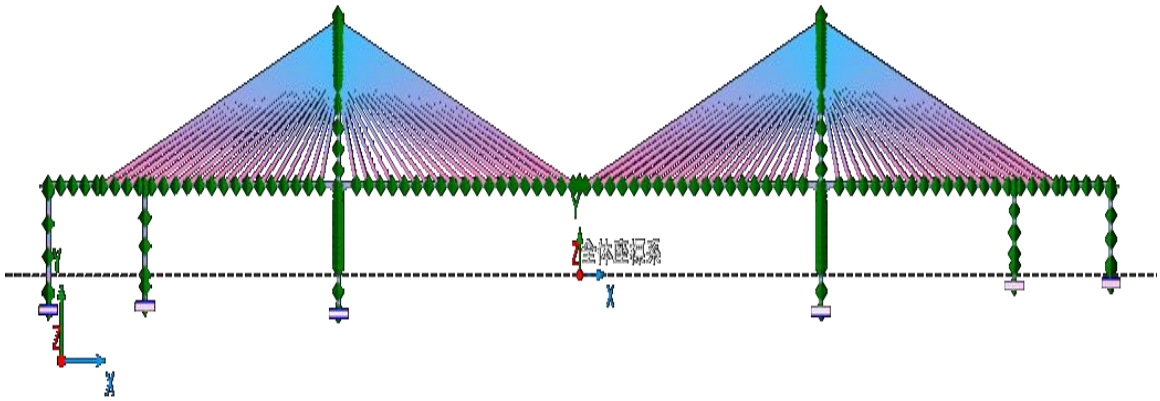

Figure 5.2 – Cable-stayed bridge model

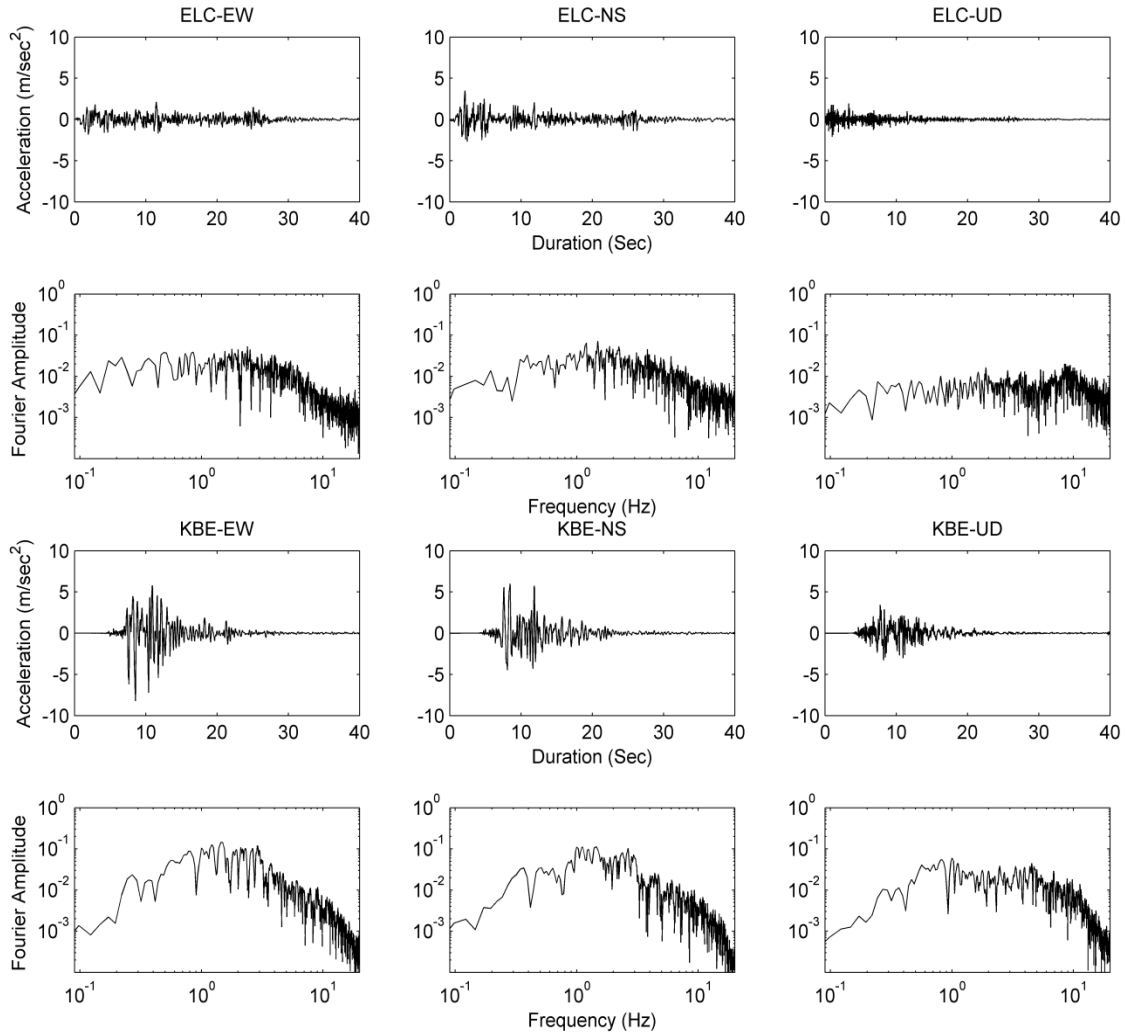

Figure 5.3 – Input ground motions (first and third row) and corresponding Fourier spectrum (second and fourth row) of Elcentro and Kobe earthquake

5.3 Interpolation of earthquake motion

Speed and origin of vehicle vary in each case for multiple vehicle analysis, which leads to variation of real exciting earthquake motion depends on the response of bridge where the vehicle stands at that particular moment of time. Analysis of the responses of the vehicles running over the elevated structures having similar location of nodes of structural element with individual vehicle position is almost impossible hence we should use the structural analysis results for each vehicle. The real earthquake shaking for individual running vehicle can find from interpolation of bridge response. Here we discuss the responses of the bridge with Kobe earthquake ground motion in this section.

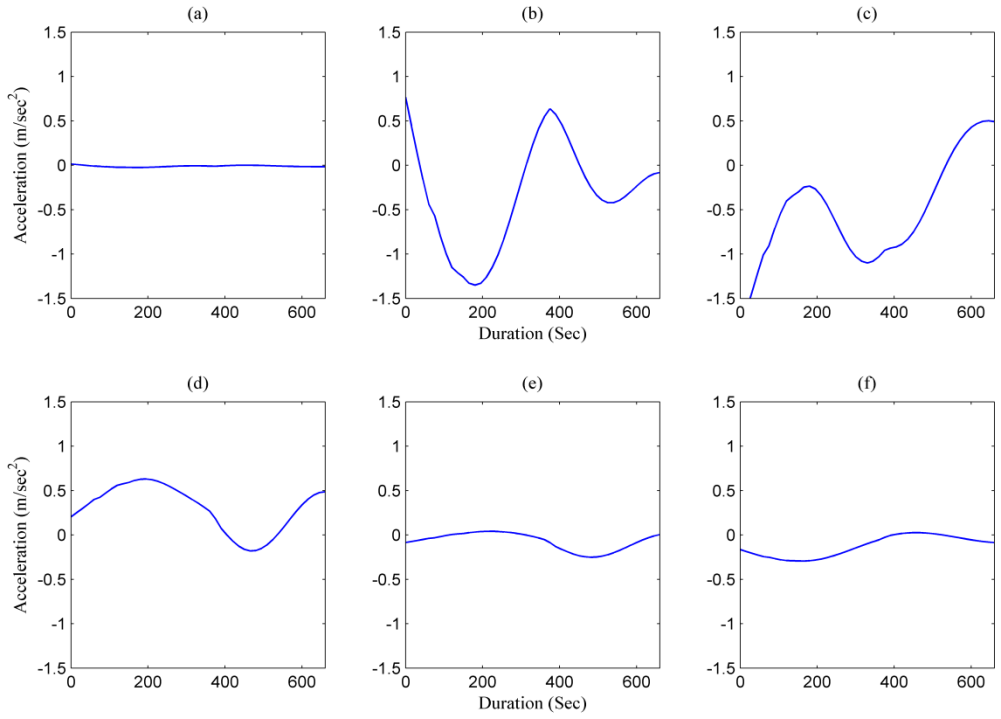

Figure 5.4 Lateral response acceleration on bridge locations for the time of 1, 4, 8, 12, 16 and 20 seconds (a), b), c), d), e) and f) respectively)

We check the longitudinal distribution of response acceleration on structures that shows the cubical variation. Figure 4.4 shows the lateral response accelerations of bridge along its length in 1, 4, 8, 12, 16 and 20 seconds respectively in a), b), c), d), e) and f) respectively. Bridge deck has the structural elements of maximum 15 m in length where the function can be defined by cubic polynomial function. From the above condition, we can use the interpolation considering three points around the location of vehicle. Lagrange's interpolation, considering the known three points (nodes), can find the new value for new location with in this range. This form of interpolation is suitable in case of cubic or square parabolic functions. Lagrange's form of

polynomial interpolation is combination of linear functions. In our case as nodal distances are maximum of 15 meters and the relation of data to three points (45 m) are seemed cubic functions, Lagrange's three-point interpolation had chosen.

Three points interpolation using Lagrange's interpolation of (x_0, y_0), (x_1, y_1) and (x_2, y_2) for $x_0 \leq x \leq x_2$ is given by equation 5.1 and 5.2.

$$L(x) = \sum_{k=0}^{n} y_k l_k(x) \qquad (For\ n+1\ data) \qquad (5.1)$$

$$l_k(x) = \frac{(x - x0)}{(x_k - x0)} \dots\dots \frac{(x - x_{k-1})}{(x_k - x_{k-1})} \frac{(x - x_{k+1})}{(x_k - x_{k+1})} \dots\dots\dots \frac{(x - x_n)}{(x_k - x_n)} \qquad (5.2)$$

Three-point interpolation formula can get from these two equations (5.1) and (5.2) as per our condition of finding response of vehicle location. Figure 5.5 shows a simple condition of vehicle and nodal locations. Let suppose a car moving from one end of the bridge (X_1) to the other end with designated speed. Nodes are denoted by X_1, X_2 and X_3 in the figure which are fixed when we model the structure. L_1, L_2, L_3 and L_4 denotes the locations of the vehicle in predefined time steps (after each 1 second in this figure) in the dynamic analysis which are totally dependent of vehicle speed.

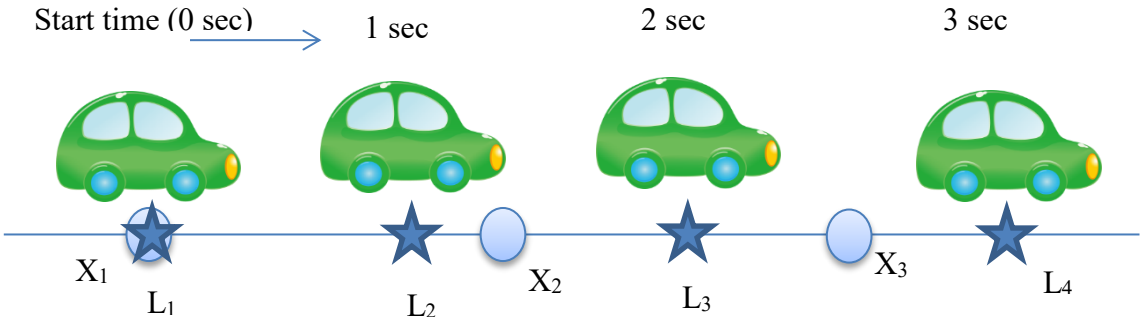

Figure 5.5 vehicle and nodal locations in the structure

Vehicle location in particular time and corresponding nearest three nodes can be defined as shown in figure 5.6. Ordinates of response accelerations and the corresponding nodes are represented as a_1 in x_1, a_2 in x_2 and a_3 in x_3. We can now interpolate the unknown response acceleration A at point L using the equation 5.3.

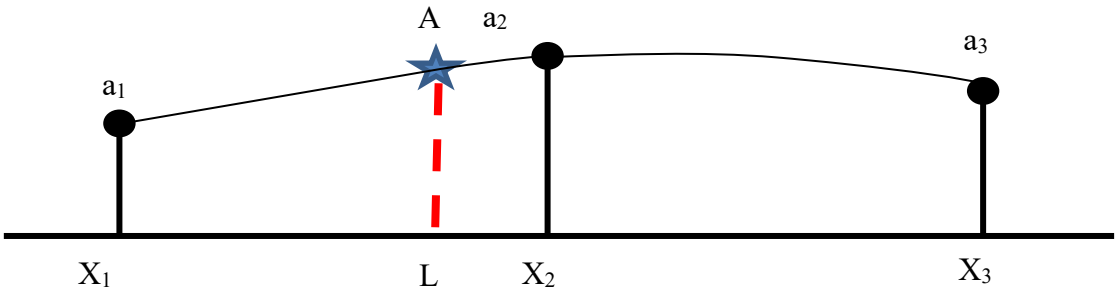

Figure 5.6 Ordinates for Interpolation

$$A = a1\frac{(L-x2)}{(x1-x2)}\frac{(L-x3)}{(x1-x3)} + a2\frac{(L-x1)}{(x2-x1)}\frac{(L-x3)}{(x2-x3)} + a3\frac{(L-x2)}{(x3-x2)}\frac{(L-x1)}{(x3-x1)} \quad (5.3)$$

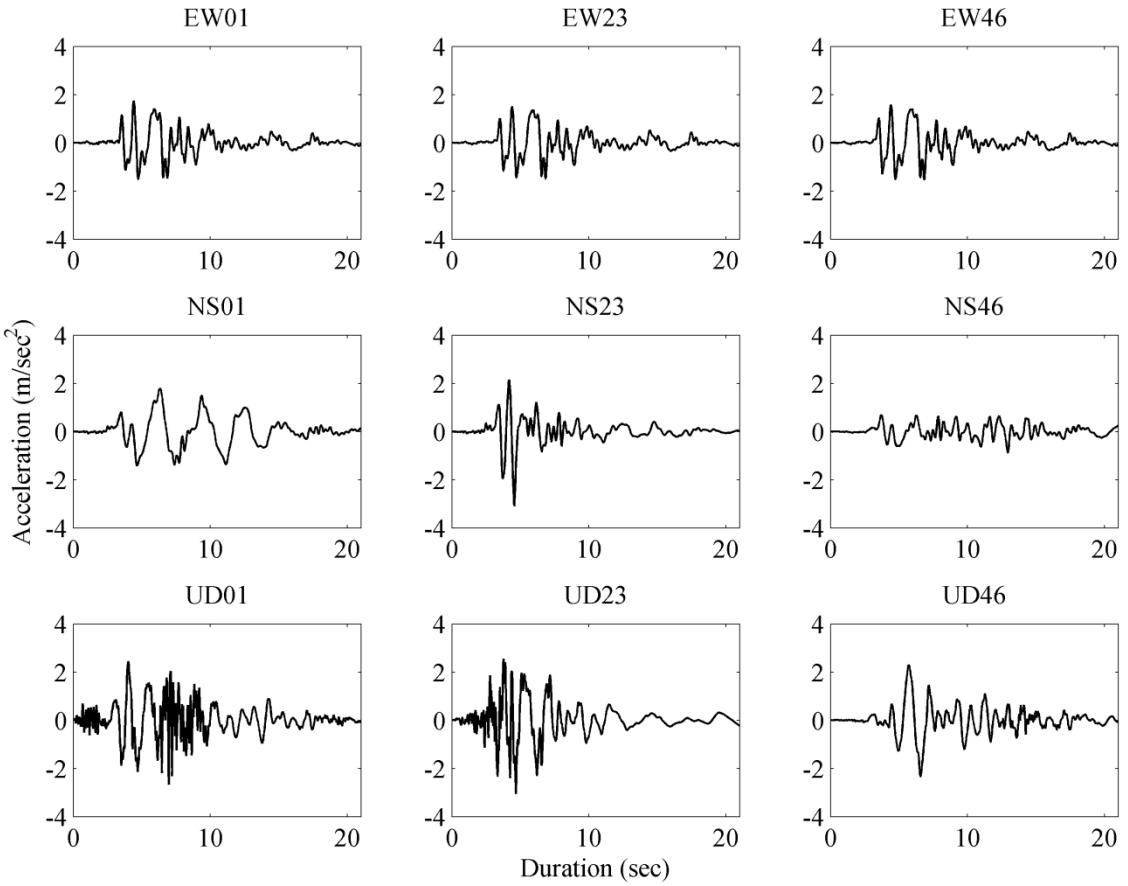

Figure 5.7 Interpolation of earthquake motion for a vehicle with speed 20 m/sec originate from 01, 23 and 46 nodes (Kobe earthquake response)

Figure 5.7 shows the input ground motion from Kobe earthquake that excites in the foundation of bridge model as shown in Figure 5.2. Nodal responses at bridge deck level are listed and

interpolated for the vehicle with the constant speed of 20.0 m/sec. Figure 5.7 and 5.8 shows the interpolated acceleration when the vehicle is just entering the bridge, on quarter of the bridge length and on the center of the bridge with node values 01, 23 and 46 for Kobe and Elcentro earthquakes respectively. These earthquake motions that excite the vehicle, varies with the location, not only in amplitude but also in the frequency of the wave.

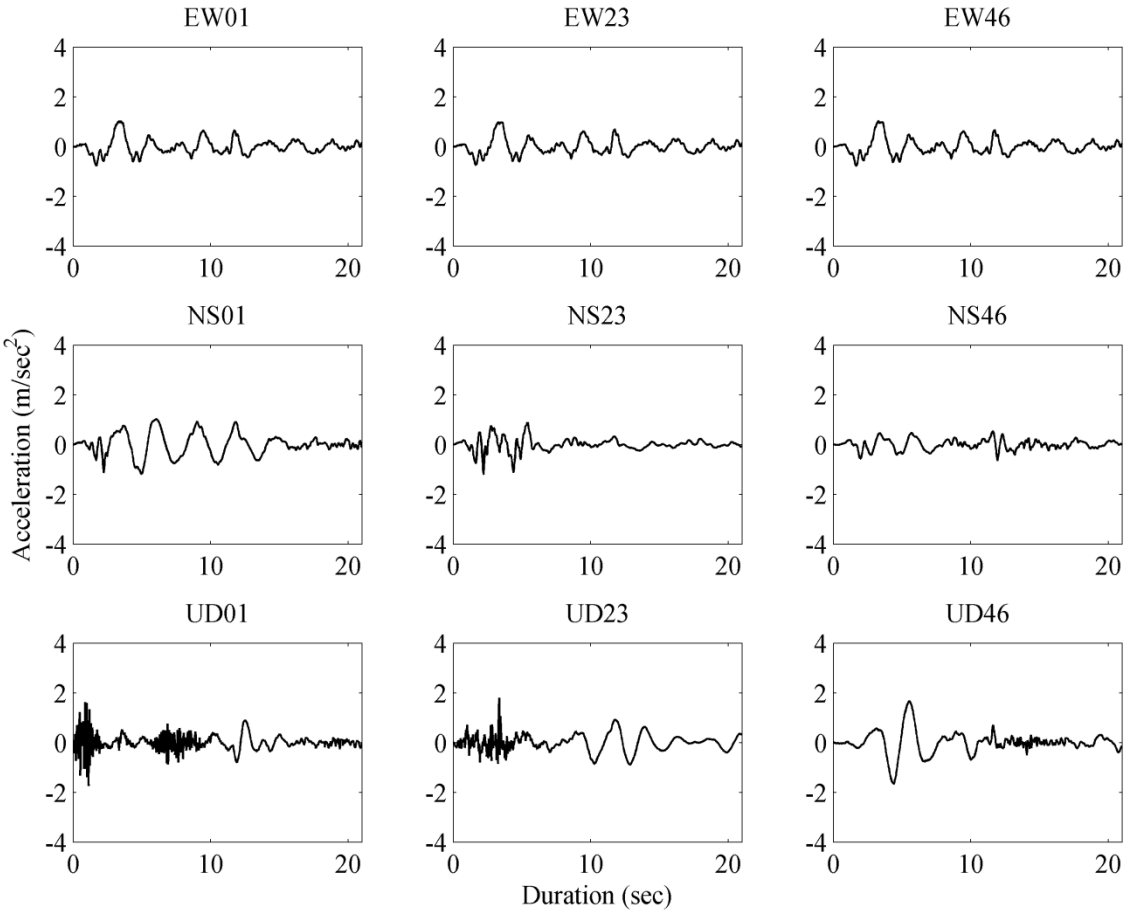

Figure 5.8 Interpolation of earthquake motion for a vehicle with speed 20 m/sec originate from 01, 23 and 46 nodes (Elcentro earthquake response)

Similarly, when we consider the vehicles with different running speed, originated from the same location, amplitude and frequency of the wave will be different as shown in Figures 5.9 and 5.10 for Kobe and Elcentro earthquake response of bridge. Where we show the result of interpolated wave for the vehicle at rest and with speed of 14.0 m/sec and 30.0 m/sec, assuming all the vehicles originate from same point, entry point of bridge as earthquake shaking starts.

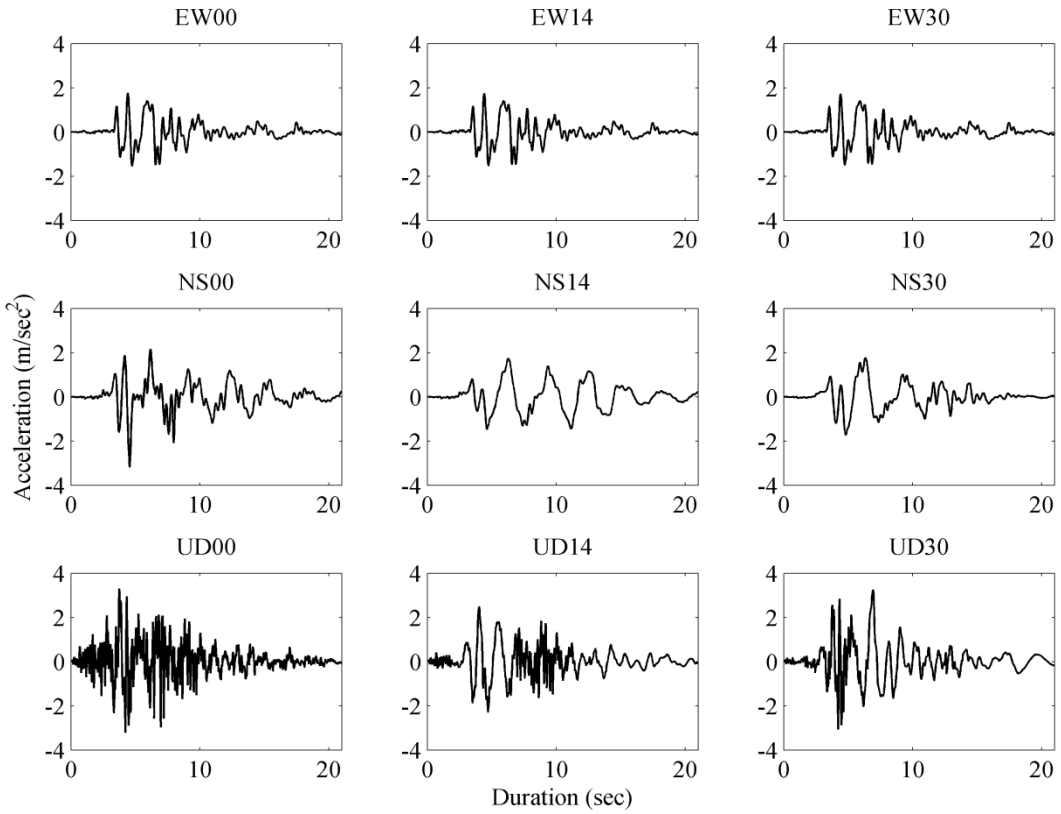

Figure 5.9 Interpolation of earthquake motion for different speed of vehicle (0.0, 14.0 and 30.0 m/sec) (Kobe earthquake response)

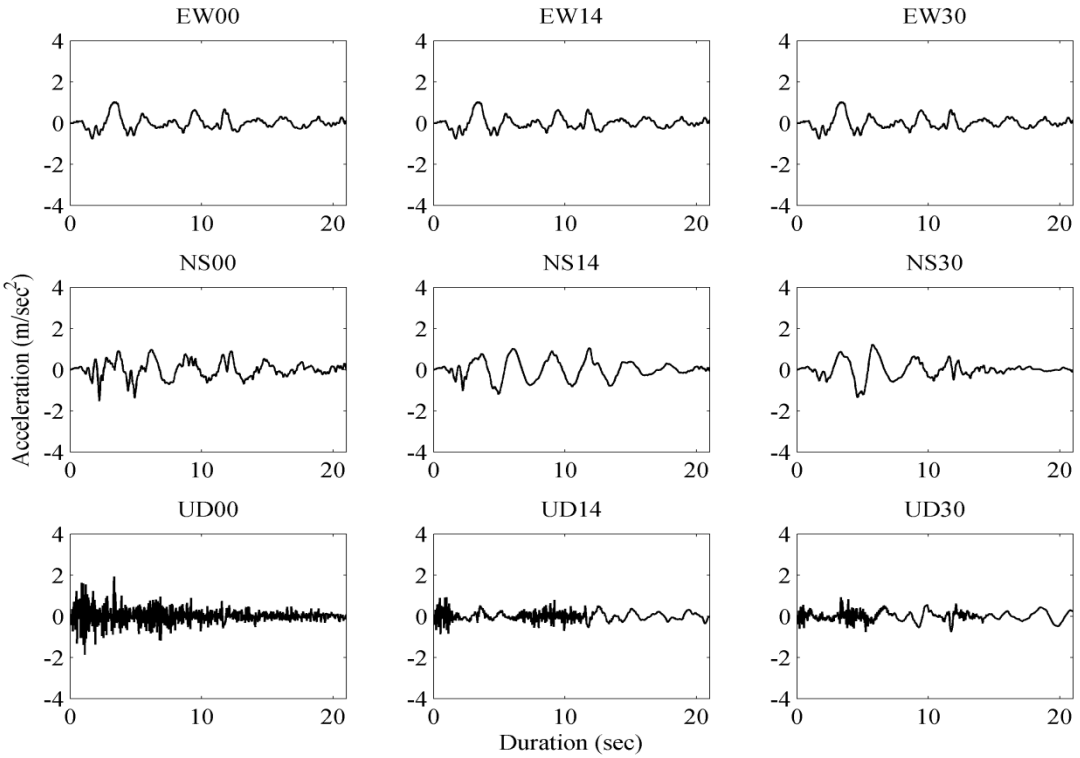

Figure 5.10 Interpolation of earthquake motion for different speed of vehicle (0.0, 14.0 and 30.0 m/sec) (Elcentro earthquake response)

5.4 Risk analysis of vehicle running on the elevated structure

Vehicles of three categories, car, bus and truck are analyzed using the CPLM method[53] with interpolated earthquake excitation. We considered two variables as location of the vehicle and speed of the vehicle for two different earthquakes, Kobe and El Centro. Maximum lateral displacements for the fixed time window (time of PGA plus 5 seconds) of earthquake motion were calculated.

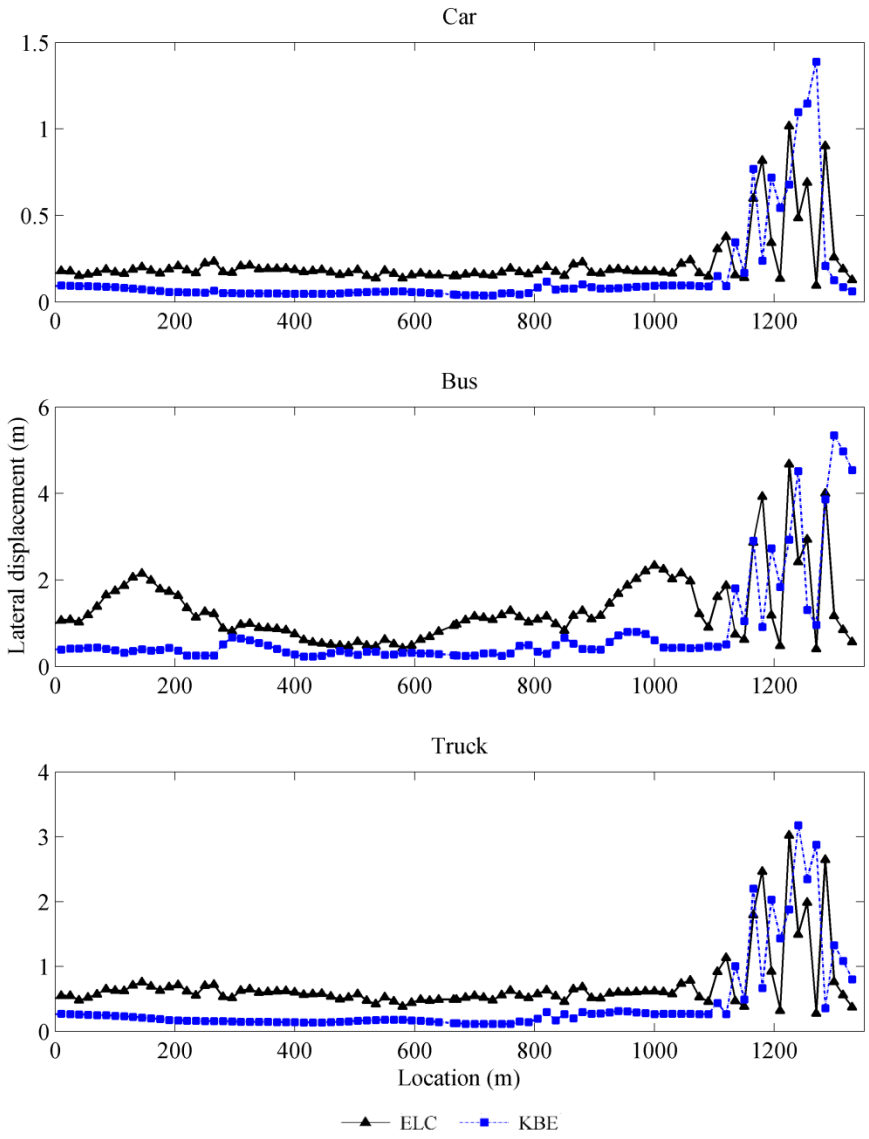

Figure 5.11 Lateral displacement of vehicles for different locations of origin

Figure 5.11 shows the results for the maximum lateral displacements with various origins of the vehicle with constant speed of 20.0 m/sec. Location of the vehicle at the time of triggering

by earthquake plays a role on lateral response of vehicle. Bus is more critical on risk of misalignment than truck and car on the sides, where all the vehicles have low level of effect on lateral movement when they are at the center of the bridge. In the case of bus, maximum lateral movement form the moving direction is more than four times when the bus is in the chainage of 0+200 than in the center of bridge (0+400 to 0+600 from entry side). Similar trend of responses is followed by the car and truck even though the values are small. Response of the vehicles seems much higher when the location during triggering of earthquake is near to the exit point due to the higher values of ground acceleration. When the vehicle exit from the bridge, it responds to the ground acceleration despite of structural response, whose PGA is much higher than that of nodal responses of bridge. Figure 5.12 shows the difference on ground motion when the vehicle is near to the exit point, nodes 81, 86 and 91 respectively (chainage of 1+180, 1+255 and 1+330).

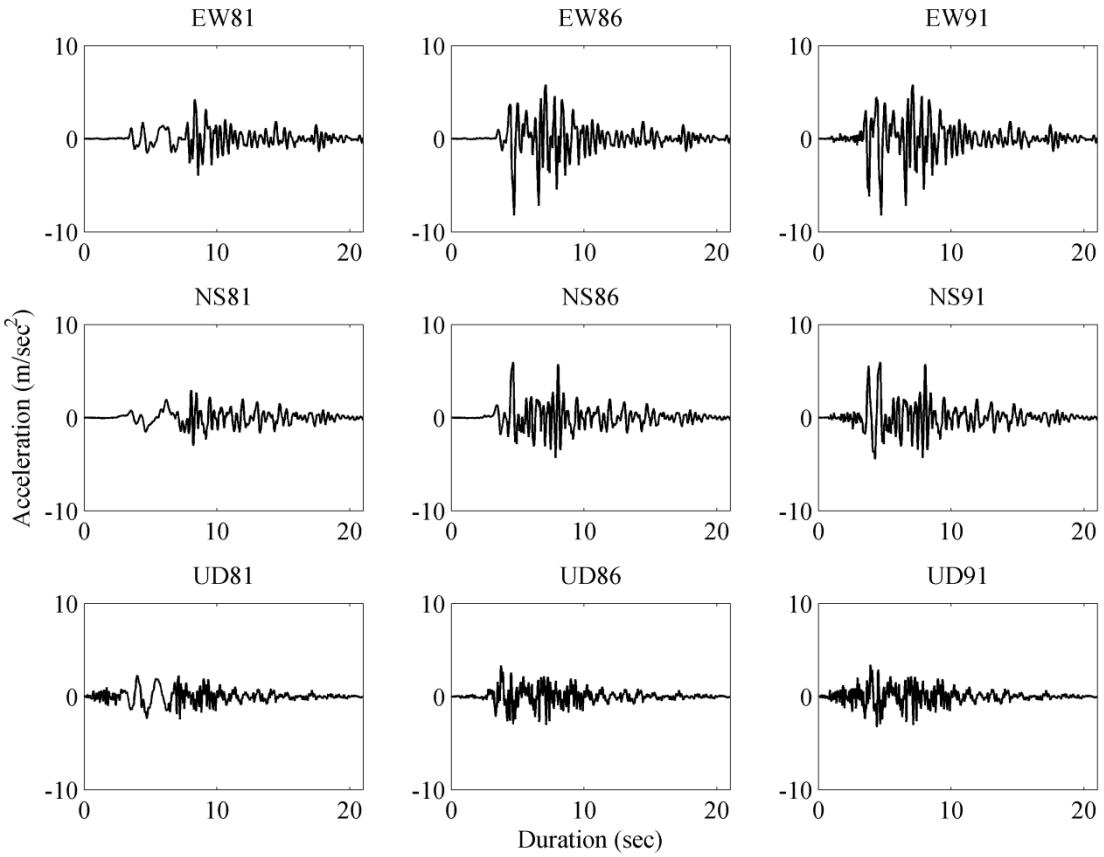

Figure 5.12 Interpolation of earthquake motion for a vehicle with speed 20 m/sec originate from 81, 86 and 91 nodes (Kobe earthquake response)

When the vehicle originates from the chainage of 1+180, node 81 in the model, it experiences the structural response up to 7.5 seconds and then it starts to move on ground which is subjected to the recorded ground motion. Similarly, in the case of vehicle start from node 86 (chainage

of 1+255) experiences structural response for just 3.75 seconds where the vehicle at the exit point experience ground shaking instead of structural response during shaking of all time.

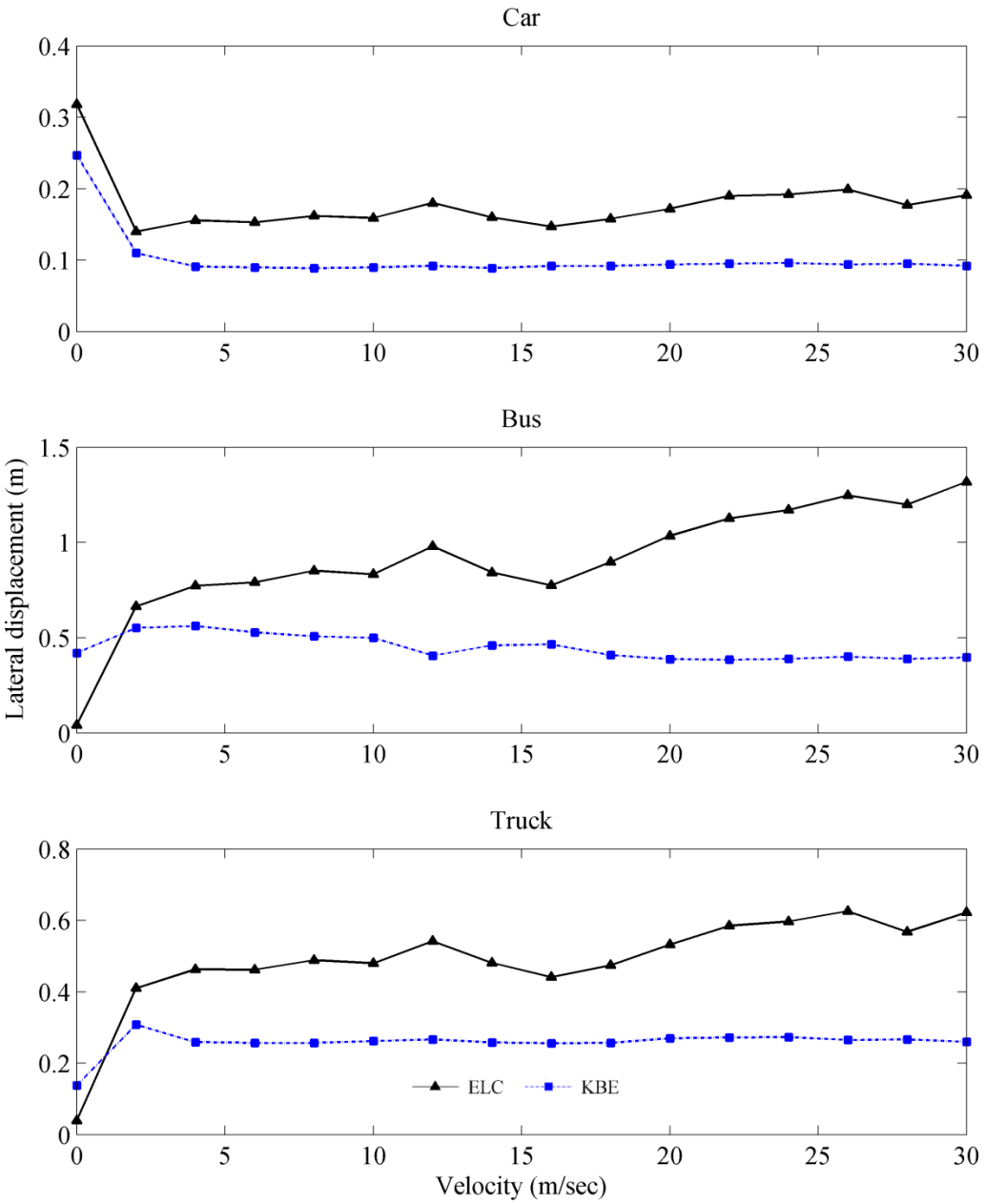

Figure 5.13 Lateral displacement of vehicles for different speed

Responses of the vehicles vary with the speed of the vehicle it run on the bridge. Figure 5.13 shows the results for the maximum lateral displacements for cases of rest to the speed up to 30.0 m/sec in increment of 2.0 m/sec. Velocity of the vehicles also play a vital role along with the characteristics of earthquake motion, in general as the speed of the vehicle increases, lateral

response of the vehicle is also ascending in case of El Centro but it is slightly descending for the case of Kobe when the speed crosses 4.0 m/sec.

5.5 Chapter overview

Earthquake motion to analyze the vehicle response running on the bridge or any elevated structures is essential to consider the response of the structure. Interpolation of the structural responses is useful to find the actual excitation of the vehicle due to earthquake. The speed of the vehicle determines the actual excitation that depends on the location of vehicle along the section of structure. Frequency and the amplitude of the earthquake motion are varied with the speed of the vehicle for the same structure. Vehicles running on the cable stayed bridge deck are subjected to higher risk when they are near to the entry point but the same vehicle could have exposed to lower risk if that will be in the center. Speed of the vehicle is also responsible on the risk of lateral deviation. Vehicles with higher speed are in more risk than that of lower in some cases like El Centro earthquake case but the trend of the maximum lateral displacements for the case of Kobe earthquake motion is almost constant, negligibly varying after the speed of 4.0 m/sec.

We can conclude here that the risk associated with the vehicles running on the long span cable-stayed bridge is depending on the location of the vehicle during the earthquake and the speed of the vehicle. Structural and the ground motion characteristics variations are another key parameter which are not considered in this study.

6 Earthquake early warning and its effectiveness on expressway drivers

6.1 Introduction

Early warnings are most popular in mitigation of the risk from natural disasters. When the event supposed to be occur or hazard due to possible event supposed to strike, dissemination of information regarding the risk is early warning. These days due to the advancement in science, weather forecast, early warnings of heavy rain, flood, typhoons, tornedos, tsunami etc. are issued effectively. Those events related to phenomenon which can be forecasted effectively are issuing early warnings precisely. However unpredicted events those spread the hazard rapidly are almost impossible to predict till the date but the warning to the distant locations from the epicenter of large event is possible. The information dissemination of possible risk at the location before the earthquake shaking to start is earthquake early warning. Early warning for earthquakes are placed in some countries around the world. Figure 6.1 shows the status of the earthquake early warning systems placement, where places/countries with blue letters indicate the systems issuing warnings and with green letters represents the places/countries with real time testing as of 2009 [21].

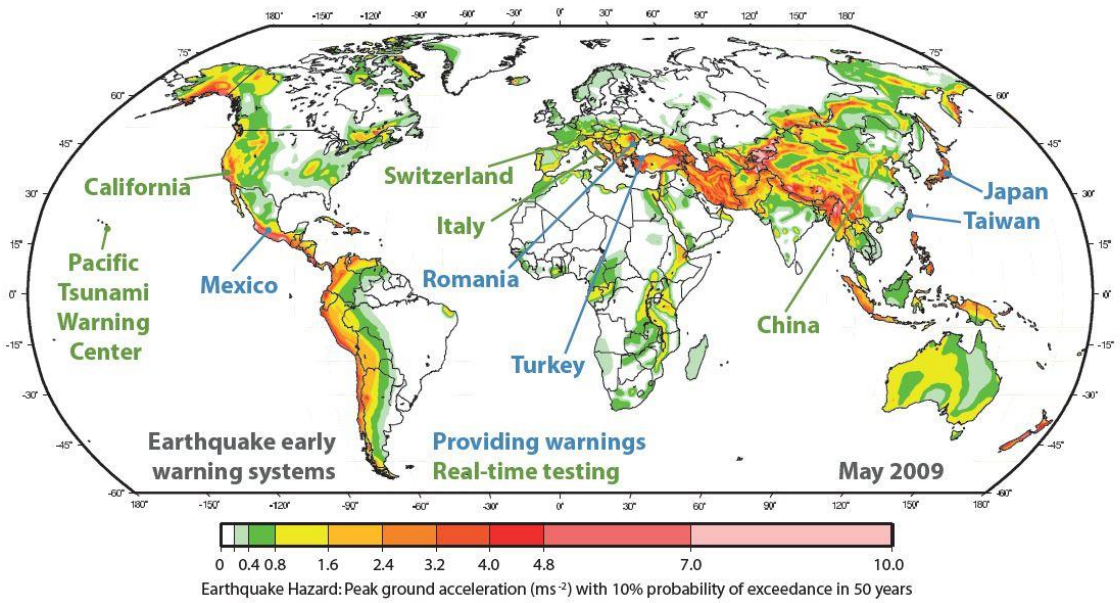

Figure 6.1 Status of earthquake early warning system usage around the world as of 2009 [21]

Vehicle responses and driver's behavior during earthquake have already discussed including the cases of bridge. This chapter mainly focus on the effect of early warning to the drivers in expressways. When the early warning issue, all the drivers could not get the information at the same time, perception and reaction time and action of individual driver's variation can also lead to accidents. Several scenarios of driver's reactions and use of early warnings are considered in this study to find the level of risk.

6.2 Earthquake early warning

There are mainly two systems of Earthquake Early Warning (EEW), one is on site early warning and other one is regional early warning system. Onsite early warning system solely depends on single seismometer which provide the warning when it receives P-wave signals. The time for issuing a warning is about 3-4 seconds. This type of warning system can be effective when the target location is at least 20 km far from the epicenter. Industries, Hospitals and other major properties can use this system privately, wherever the regional system exists or not. Regional earthquake early warning system, with dense network of seismometers demand more epicentral distance for effective warning but the lead time of regional system is higher for distant locations than onsite system [54].

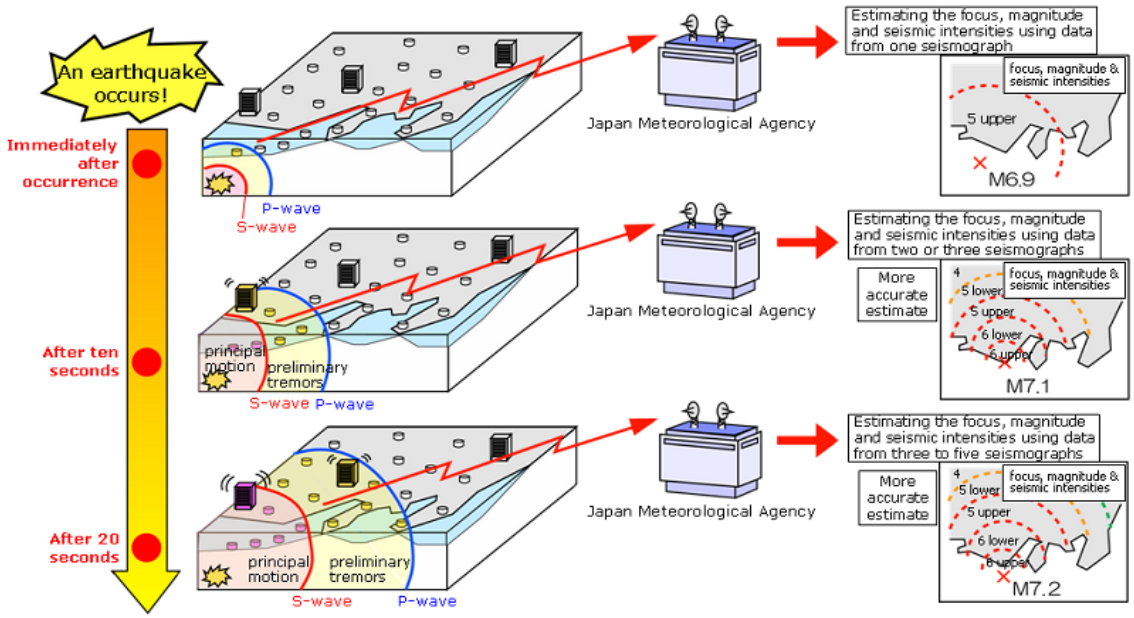

Figure 6.2 Basic system of earthquake early warning system (Figure by JMA[6])

[6] Japan Meteorological Agency http://www.jma.go.jp/jma/en/Activities/eew1.html

Figure 6.2 shows the basic system of the EEW, prepared by Japan Meteorological Agency. Japan having dense network of seismometers, has regional system of earthquake early warning. It started to issue earthquake early warning from 2007. During Tohokhu earthquake 2011, JMA system issued first forecast to advanced users at 14:46:45.6 where the first warning to general public issued at 14:46:48.8. For distant locations, like Tokyo, first information disseminate at 14:47:10.2 [55]. When the earthquake struck in any place, after at least three sensors recognized the P-wave arrival then the warning system activate and send messages to smart phones, televisions, radios and other messaging and warning systems.

Earthquake early warning system can work precisely for areas where it will have more lead time. Prediction of long period ground motion on issuing the early warning is also important to avoid the unnecessary alarms as well as to have the essential warnings. Long period ground motion prediction algorithms are used to provide warnings for locations with large epicentral distance, in cases of large events [56].

6.3 Application of EEW to drivers on expressway

Highways and expressways are equipped with information systems, boards, radios are commonly used in highways in Japan. There are several factors which cause dilemma whether the early warning issuance to driver is favorable or not. Mainly we can consider the human and mechanical factors in reaction to any events during driving. When we focus on the earthquake early warning then we should consider the dissemination of information that we should ensure all drivers get information at the same time. Information received as early warning can be taken in different level by individual drivers which leads the variation in taking action. When some of the driver perceive as a normal event and try to move normally but immediate front vehicle driver taken it as warning of danger and try to stop immediately, there is possibility of accident.

Maruyama et al. in 2009 [57] did the driving simulator experiment using the obstruction in the road. They found that when a vehicle is running individually EEW can reduce the risk of accidents but it is not well effective when they used three synchronized simulators with part of cars given the warning. In real scenario, the information gap with drivers can create the similar environment. They suggested the best way of disseminating information by using hazard lamp on by the vehicles.

Interview with drivers in Nepal, as discussed in previous chapter also indicated the random perception and action when they feel earthquake. In any case of similar perception of the drivers and mechanical efficiency, there will not be any accident even all the drivers used hard brake. This is an ideal situation except for the case of automated cars. When vehicles in group moving on the road with almost similar speed; if they applied same level of brake at the same time then there is very less chance of collision.

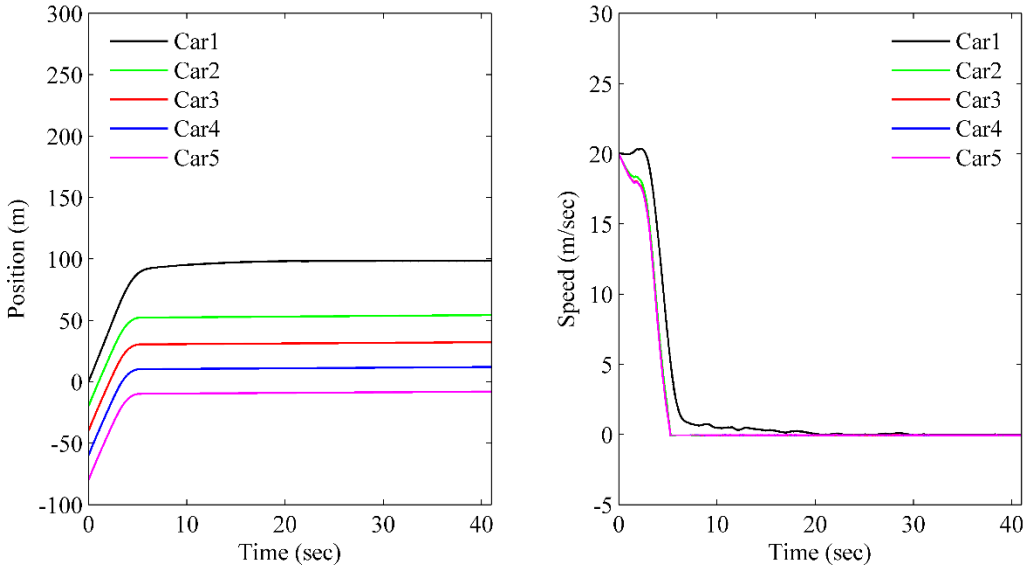

Figure 6.3 Position (left) and speed (right) of vehicle states for case of initial speed 20.0 m/sec, gap 20.0 m and similar brake level of 8.0 m/sec^2

Result for the case of ideal situation shows that there is no any collision if the vehicles in the group are moving with same initial speed and gap with same brake level. When we assign the different brake levels as nearly real situation there is chance of collision when front vehicle associated with higher brake level than immediately followed one. Different scenario of positions, brake levels and locations are now discussed in the following section.

6.4 Risk analysis

Risk associated with vehicles during earthquake are uncertain, few cases of group of vehicles are considered in this study. We compare the situations when the vehicles are running on the ground surface and elevated structures. Changing on information dissemination time are also under study which supposed to provide the effectiveness of early warning to avoid effect of shaking in running vehicle.

At first, we considered the vehicles running on the ground surface, where the shaking due to the earthquake is not varying. When we use Kobe and Elcentro earthquake data as input, initial condition of vehicles with speed of 20.0 m/sec, gap of 20.0 m of each vehicle; same brake level of 8.0 m/sec^2. Result of location and velocity are shown in figures 6.4 and 6.5 respectively. There is no any collision between the cars in cases of Elcentro earthquake and Kobe earthquake under similar condition of braking action.

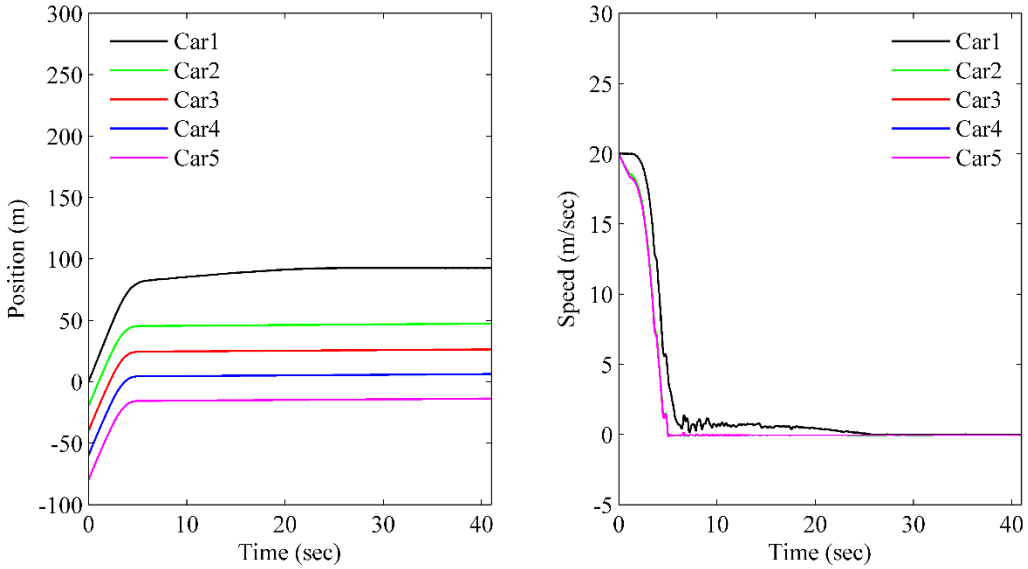

Figure 6.4 Position and velocity of vehicles running on the surface road with same brake level (Kobe)

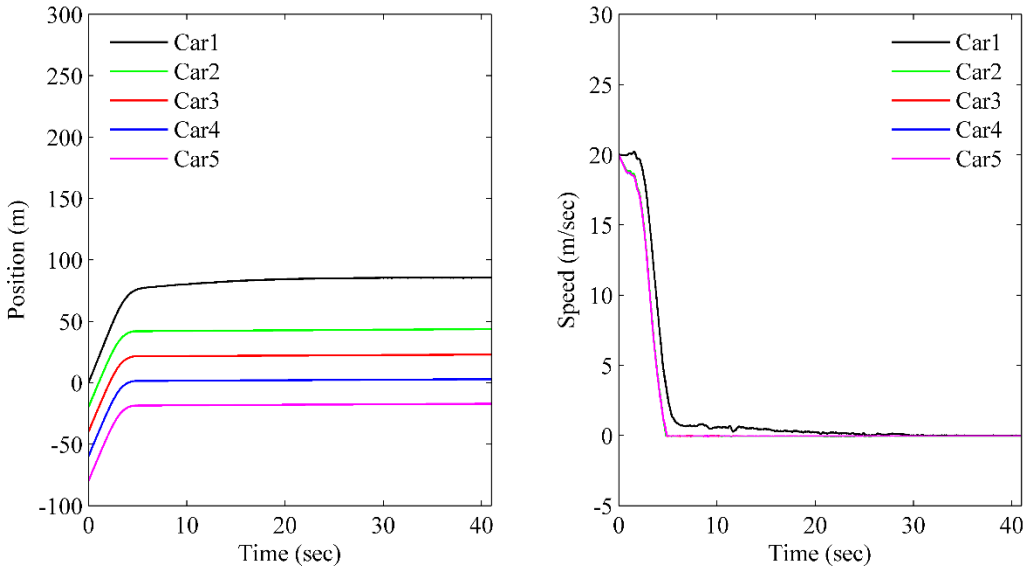

Figure 6.5 Position and velocity of vehicles running on the surface road with same brake level (Elcentro)

When we assign the varied brake levels with same other conditions, all cars got collided with immediate front cars, in both earthquake excitations. Brake levels are set higher (8) for front car and reduced in order of 1 for all other rare cars respectively. Figure 6.6 shows the position and the velocity of the vehicles when assigned for different brake level with Kobe earthquake.

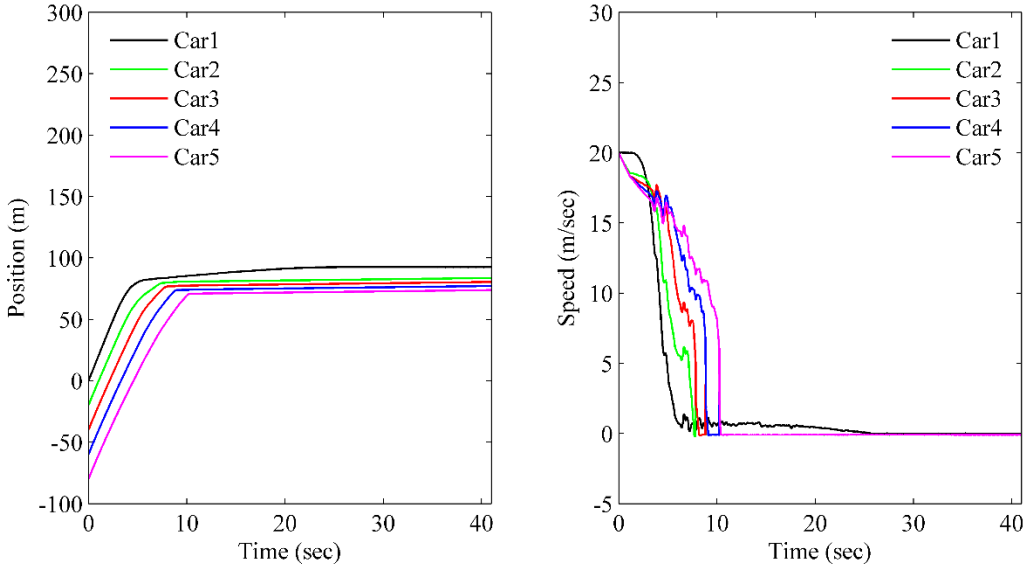

Figure 6.6 Position and velocity of vehicles running on the surface road with different brake level (Kobe)

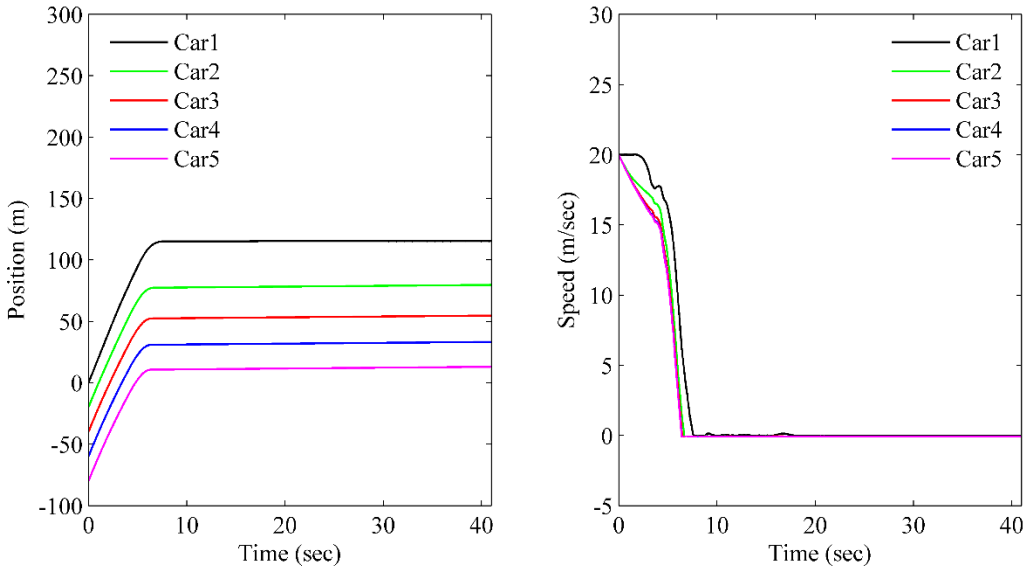

Figure 6.7 Position and velocity of vehicles running on the bridge with same brake level (Kobe)

Risk of the vehicle moving on the bridge is different. We use the same bridge that specified in chapter 5 and see the risk of vehicle collision under different cases as stated before for surface road condition. There is no collision with the input of Kobe earthquake with same brake level and gap of vehicles that same for Elcentro too. When the brake level is assigned in low order from the front, all vehicles got collided as like the same case of surface road. Figures 6.7 and 6.8 show the locations and the speed of the vehicles over time with Kobe earthquake excitation for same brake level of 8.0 m/sec^2 and different brake levels respectively.

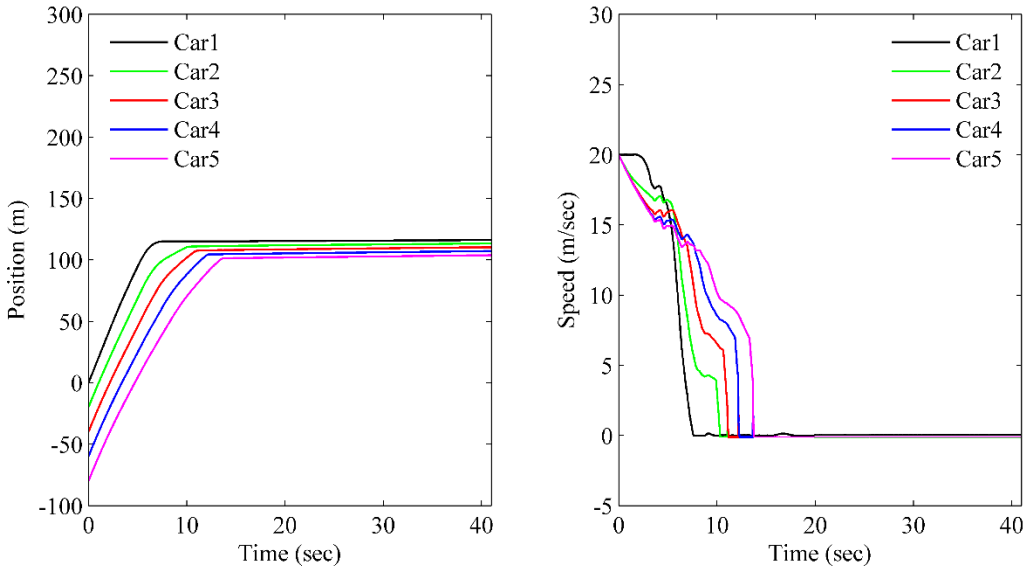

Figure 6.8 Position and velocity of vehicles running on the bridge with different brake level (Kobe)

In this analysis, we use cars, in a single lane, with constant initial gap of vehicles which is ideal situation that is hard to find in the road.

6.5 Chapter overview

Earthquake early warning and its usage in highways are discussed in this chapter. EEW are emerging in disaster mitigation in these days but regarding the usage in highways, it depends on the interpretation and action by drivers after receiving the message. When vehicles are moving with smaller gap between them, there is more chance of collision. When the brake level of vehicles assigned randomly, depending on the speed and gap, there is high chance of

collision between two vehicles of higher brake level with immediate front and lower brake level of following one. If we use same brake level and safe gap between vehicles, there is rare chance of getting collision between them. Hence dissemination of information and action by the drivers in precise way can reduce the accident during earthquake shaking.

7 Summary and Conclusion

7.1 Summary

New method on seismic response analysis of vehicle is put forward by validating the analytical result with vehicle response during the real earthquake shaking. This method can be used for the wide range of vehicle state as in rest and running condition. Vehicle toppling risk associated with ground motion characteristics and vehicle parameters shows more insight in the quick risk estimation of vehicles during earthquake. Regression relationships of ground motion characteristics and vehicle parameters for toppling risk are proposed. Case studies of vehicle responses during recent earthquakes have been analyzed with video analysis, interview with drivers and survey of vehicle toppling with analysis. Videos recorded during shaking of the Gorkha earthquake showed the responses of the moving vehicles. Vehicles responded and followed the path of wave due to earthquake, where most of the two wheelers laid down on the road due to shaking. Most of the drivers felt earthquake during shaking and used normal brake but few drivers used hard brake where fifty percent of drivers stopped immediately after they felt the shaking. Earthquake was noticed by unusual behavior of vehicle for most of the drivers. At least seven cars found toppled in Kurokawa and Tateno area after the 2016 Kumamoto earthquake. Peak ground acceleration of the Kurokawa and Tateno area is estimated as 14.172 m/sec^2.

Car following behavior under earthquake shaking considering the braking action of driver is introduced with brake model. ADM model, which was extended with additional earthquake force in the following behavior is used. Driving simulator experiment was conducted for thirty drivers under different conditions of shaking level and arrangement. Result from the experiment suggests most of the drivers used brake that follows normal distribution curve. Activity of drivers and maximum brake levels used by drivers are also modeled for vehicle following mechanism. Priority factor of using brake is also introduced to accommodate the effect of brake level.

Interpolation of structural responses on analysis of vehicles running on the bridge is introduced on risk analysis. Risk of vehicles depends on the location of vehicle, speed and ground motion characteristics along with structural parameters. Vehicle risk of car, bus and truck are shown for Kobe and Elcentro earthquakes.

Earthquake early warning system for highways are analyzed on risk of collision of vehicles. Brake levels used by the drivers and gap between vehicles play the role on collision between vehicles when considering a single lane flow of vehicles. Brake level and reaction on brake application from the driver might put the vehicle in collision danger in case of random use of brake.

7.2 Conclusion and recommendation

CPLM method can be used on seismic response analysis of vehicles for all conditions. Toppling risk of any vehicle can be calculated for several conditions. Moreover, we can estimate the PGA on the areas where record ground motions are not available from vehicle response. Recognition of the earthquake by drivers during driving is uncertain along with the action taken by the driver is solely depend on individual. Two wheelers are in higher risk during earthquake shaking where toppling and derailment might happen for large vehicles which found in recent earthquakes.

Car following mechanism considering the earthquake shaking level is proposed with priority factor on braking. Brake model was proposed with reaction time as mean and SD for brake function from the analysis of experiment result. Application of brake during shaking is random but we can model the percentage of drivers acting on the certain level of brake. This phenomenon can be defined as the cumulative normal function.

Risk of vehicles running on the elevated structures are depending on the structural parameters, ground motion characteristics, speed and location of the vehicle during shaking. Earthquake early warning system can be used to reduce the risk of vehicles but public awareness on its interpretation and action should be in similar range. If the vehicle in front used hard brake and rear one used to try a soft brake, depending on gap between them, there might be collision. Dissemination of information on time and limited the reaction on slow breaking despite of overreaction can reduce the risk of collision during earthquake.

Further study recommended on development of the CPLM method, mainly considering the steering angles by drivers, minimum free rotation of front tyres under slow speed of vehicle to use as centripetal radius. Car following mechanism can be improved by more experiments and observations in real situation. Vehicle responses in elevated structures could be analyzed in detail with several arrangements.

8 Bibliography

[1] S. E. Chang and N. Nojima, “Measuring lifeline system performance: highway transportation systems in recent earthquakes,” *Proc. 6 th Natl. Earthq. Conf. Earthq. Eng.*, no. 70, p. Paper No.70, 12p, 1998.

[2] A. J. DeBlasio, T. J. Regan, M. E. Zirker, K. S. Fichter, and K. Lovejoy, “Effects of catastrophic events on transportation system management and operations: Comparative analysis,” 2004.

[3] Time.com, “Magnitude 5.1 Earthquake Strikes Los Angeles,” 2014. [Online]. Available: http://time.com/42612/earthquake-los-angeles/. [Accessed: 10-Sep-2016].

[4] A. Kiremidjian, J. Moore, Y. Y. Fan, O. Yazlali, N. Basoz, and M. Williams, “Seismic Risk Assessment of Transportation Network Systems,” *J. Earthq. Eng.*, vol. 11, no. 3, pp. 371–382, May 2007.

[5] JMA, “The Japan Metereological Agency (JMA) seismic intensity scale,” 1996. [Online]. Available: http://www.jma.go.jp/jma/kishou/know/shindo/index.html (in Japanese). [Accessed: 20-Mar-2016].

[6] K. Kawashima, H. Sugita, and T. Kanoh, “Effect of earthquake on driving of vehicle based on questionnaire survey,” *Struct. Eng./Earthquake Eng.*, vol. 6, no. 2, pp. 405–412, 1989.

[7] Y. Maruyama and F. Yamazaki, “Relationship Between Seismic Intensity and Drivers’ Reaction in the 2003 Miyagiken-Oki Earthquake,” *Struct. Eng. / Earthq. Eng.*, vol. 23, no. 1, p. 69s–74s, 2006.

[8] Y. Maruyama and F. Yamazaki, “Seismic response analysis on the stability of running vehicles,” *Earthq. Eng. Struct. Dyn.*, vol. 31, no. 11, pp. 1915–1932, Nov. 2002.

[9] Y. Maruyama and F. Yamazaki, “Fundamental study on the response characteristics of drivers during an earthquake based on driving simulator experiments,” *Earthq. Eng. Struct. Dyn.*, vol. 33, no. 6, pp. 775–792, 2004.

[10] E. W. Chandler, R. E., Herman, R.,Montroll, “Traffic Dynamics: Studies in Car

Following," *Oper. Res.*, vol. 6, pp. 165–184, 1958.

[11] E. Kometani and T. Sasaki, "Dynamic behaviour of traffic with a nonlinear spacing-speed relationship," in *Proceedings of the Symposium on Theory of Traffic Flow*, 1959, pp. 105–119.

[12] W. Helly, "Simulation of Bottlenecks in Single Lane Traffic Flow," in *Proceedings of the Symposium on Theory of Traffic Flow*, 1959, pp. 207–238.

[13] R. M. Michaels, "Perceptual factors in car following," in *Second International Symposium on the Theory of Road Traffic Flow*, 1963, pp. 44–59.

[14] R. W. Herman, R., Montroll, E. W., Potts, R. B., & Rothery, "Traffic dynamics: analysis of stability in car following," *Oper. Res.*, vol. 7, pp. 86–106, 1959.

[15] R. W. Gazis, D. C., Herman, R., & Rothery, "Nonlinear follow the leader models of tra□ffic flow," *Oper. Res.*, vol. 9, pp. 545–567, 1961.

[16] A. ceder, "The accuracy of tra• ffic flow models: a review and preliminary investigation," *Traffic Eng. Control*, pp. 541–544, 1978.

[17] M. Aron, "Car following in an urban network: simulation and experiments," in *Seminar D, 16th PTRC Meeting*, 1988, pp. 27–39.

[18] H. Ozaki, "Reaction and anticipation in the car following behaviour," in *13th International Symposium on Tra• c and Transportation Theory*, 1993, pp. 349–366.

[19] J. M. E. Aranda, a. Jimenez, G. Ibarrola, F. Alcantar, a. Aguilar, M. Inostroza, and S. Maldonado, "Mexico City Seismic Alert System," *Seismol. Res. Lett.*, vol. 66, no. 6, pp. 42–53, 1995.

[20] J. A. Strauss and R. M. Allen, "Benefits and Costs of Earthquake Early Warning."

[21] R. M. Allen, P. Gasparini, O. Kamigaichi, and M. Bose, "The Status of Earthquake Early Warning around the World: An Introductory Overview," *Seismol. Res. Lett.*, vol. 80, no. 5, pp. 682–693, 2009.

[22] E. R. Burkett, D. D. Given, and L. M. Jones, "ShakeAlert — An Earthquake Early Warning System for the United States West Coast," 2016.

[23] Y. Fujinawa and Y. Noda, “Japan’s earthquake early warning system on 11 March 2011: Performance, shortcomings, and changes,” *Earthq. Spectra*, vol. 29, no. SUPPL.1, pp. 3–25, 2013.

[24] Y. Jibiki, M. Ohara, A. Tanaka, and T. Furumura, “東日本大震災における高速道路走行中の運転者の行動に関する分析 Analysis of Drivers ’ Behaviors on Highways in Great East Japan Earthquake (in Japanese),” *J. Inst. Soc. Saf. Sci.*, no. 26, pp. 1–9, 2015.

[25] Japan Meteorological Agency, “Earthquake Early Warnings: Dos and Dont’s,” 2009. [Online]. Available: http://www.jma.go.jp/jma/en/Activities/EEWLeaflet.pdf.

[26] H. B. Pacejka, *Tyre and Vehicle Dynamics*. 2006.

[27] A. V. Alagappan, K. V. N. Rao, and R. K. Kumar, “A comparison of various algorithms to extract Magic Formula tyre model coefficients for vehicle dynamics simulations,” *Veh. Syst. Dyn.*, vol. 53, no. 2, pp. 154–178, 2014.

[28] M. Guiggiani, *The science of vehicle dynamics: Handling, braking, and ride of road and race cars*. Springer Netherlands, 2014.

[29] J. Y. Wong, *THEORY OF GROUND VEHICLES*, Third., vol. 1. John Wiley & Sons, 2001.

[30] L. Li, K. Yang, G. Jia, X. Ran, J. Song, and Z. Q. Han, “Comprehensive tire-road friction coefficient estimation based on signal fusion method under complex maneuvering operations,” *Mech. Syst. Signal Process.*, vol. 56, no. June 2016, pp. 259–276, 2015.

[31] AASTHO, *A Policy on Geometric Design of Highways and Streets*. 2001.

[32] R. R. Parajuli and J. Kiyono, “Ground motion characteristics of the 2015 gorkha earthquake, survey of damage to stone masonry structures and structural field tests,” *Front. Built Environ.*, vol. 1, no. 23, 2015.

[33] Toyota, “Toyota HiAce specifications,” 2015.

[34] USGS, “Center for Engineering Strong Motion Data.” 2015.

[35] NIED, “Strong-motion Seismograph Networks (K-NET, KiK-net),” 2016. [Online]. Available: http://www.kyoshin.bosai.go.jp/. [Accessed: 01-Aug-2016].

[36] USGS, “M7.8 Nepal Earthquake of 25 April 2015,” 2015.

[37] H. Parajuli, J. Kiyono, Y. Ono, and T. Tsutsumiuchi, “Design Earthquake Ground Motions From Probabilistic Response Spectra : Case Study of Nepal,” *J. Japan Assoc. Earthq. Eng.*, vol. 8, no. 4, 2008.

[38] NIED, “Fault slip distribution map of Kumamoto earthquake 2016.04.16,” 2016. [Online]. Available: http://map03.ecom-plat.jp/map/map/?cid=20&gid=587&mid=2963. [Accessed: 08-Aug-2016].

[39] Car sensor Lab, “Suzuki Every Wagon catelog,” 2016. [Online]. Available: http://catalog.carsensorlab.net/suzuki/every_wagon/f001/m006/g003/. [Accessed: 01-Aug-2016].

[40] P. Hejtmanek, O. Blatak, and J. Vancura, “New approach to measure the vehicle center of gravity height,” *Perner’s Contacts*, vol. X, no. 4, pp. 18–27, 2015.

[41] M. Brackstone and M. McDonald, “Car-following: a historical review,” *Transp. Res. Part F Traffic Psychol. Behav.*, vol. 2, no. 4, pp. 181–196, 1999.

[42] R. B. Gazis, D. C., Herman, R., & Potts, “Car following theory of steady state traffic flow,” *Oper. Res.*, vol. 7, pp. 499–505, 1959.

[43] L. C. Edie, “Car following and steady state theory for non-congested traffic,” *Oper. Res.*, vol. 9, no. 66–76, 1960.

[44] H. E. M. May, Jr., A. D, & Keller, “Non integer car following models,” *Highw. Res. Rec.*, vol. 199, pp. 16–32, 1967.

[45] R. Heyes, M. P., & Ashworth, “Further research on car following models,” *Transp. Res.*, vol. 6, pp. 287–291, 1972.

[46] A. D. Ceder, A., & May, Jr., “Further evaluation of single and two regime tra• ffic flow models,” *Transp. Res.*, vol. 567, pp. 1–30, 1976.

[47] P. G. Gipps, “A behavioural car following model for computer simulation,” *Transp. Res. B*, vol. 15, pp. 105–11, 1981.

[48] A. Hanken and T. H. Rockwell, “A model of car following derived empiriacally by piece-wise regression analysis,” in *3rd International Symposium on the Theory of traffic Flow*, 1967, pp. 40–41.

[49] G. A. Bekey, G. O. Burnham, and J. Seo, “Control theoretic models of human drivers in car following,” *Hum. Factors*, vol. 19, no. 4, pp. 399–413, 1977.

[50] J. Xing, “A parameter identication of a car following model,” in *Second World Congress on ATT*, 1995, pp. 1739–1745.

[51] C. Kikuchi and P. Chakroborty, “Car following model based on a fuzzy inference system,” *Transp. Res. Rec.*, vol. 1365, pp. 82–91, 1992.

[52] M. A. Doustari and N. Sannomiya, “Autonomous decentralized mechanism in fish behavior model,” in *International Symposium on Autonomous Decentralized Systems*, 1993, pp. 414–420.

[53] R. R. Parajuli and J. Kiyono, “Circular Path and Linear Momentum Method for Seismic Response Analysis of Vehicles,” *Front. Built Environ.*, vol. 2, no. 16, 2016.

[54] C. Satriano, Y. M. Wu, A. Zollo, and H. Kanamori, “Earthquake early warning: Concepts, methods and physical grounds,” *Soil Dyn. Earthq. Eng.*, vol. 31, no. 2, pp. 106–118, 2011.

[55] E. Yamasaki, “What We Can Learn From Japan’s Early Earthquake Warning System,” *Momentum*, vol. 1, no. 1, 2012.

[56] Y. P. Dhakal, W. Suzuki, T. Kunugi, and S. Aoi, “Ground Motion Prediction Equations for Absolute Velocity Response Spectra (1-10 S) in Japan for Earthquake Early Warning,” *J. Japan Assoc. Earthq. Eng.*, vol. 15, no. 6, pp. 91–111, 2015.

[57] Y. Maruyama, M. Sakaya, and F. Yamazaki, “Effects of earthquake early waring to expressway drivers based on driving simulator experiments,” *J. Earthq. Tsunami*, vol. 3, no. 4, pp. 261–272, 2009.

Appendix I: Magic formula model

The longitudinal and transverse forces acting on each tyre along with the self-aligning moment are calculated using the MFM (Eqs. (I.1)–(I.3)) considering pure slip conditions.

$$y(x) = D\sin[C\arctan\{Bx - E(Bx - \arctan(bx))\}] \quad \text{(I.1)}$$

$$Y(x) = y(x) + S_v\,, \quad \text{(I.2)}$$

$$x = X + S_h, \quad \text{(I.3)}$$

Where X is the input variable: the slip angle θ and the slip ratio. Y is the output variable. B, C, D and E are the stiffness factor, shape factor, peak value and curvature factor, respectively. These factors are calculated for pure slip conditions based on the TRR algorithm, which showed the best performance compared with other algorithms. The coefficients used to calculate the MFM parameters are shown in Table A.0.1 [27]. The pressure on the tyres is calculated considering the static pressure as well as the effects of the rolling, pitching and vertical motion of the vehicle [8].

Table I.0.1 Coefficients used to calculate the MFM parameters

Longitudinal force		Lateral force		Self-aligning torque	
Coefficient	**Value**	**Coefficient**	**Value**	**Coefficient**	**Value**
$\mathbf{p_{Cx1}}$	1.121	p_{Cy1}	1.193	q_{Bz1}	8.976
$\mathbf{p_{Dx1}}$	0.907	p_{Dy1}	-0.990	q_{Bz2}	-1.098
$\mathbf{p_{Dx2}}$	-0.003	p_{Dy2}	0.145	q_{Bz3}	-0.852
$\mathbf{p_{Ex1}}$	-3.246	p_{Ey1}	-1.003	q_{Bz9}	20.766
$\mathbf{p_{Ex2}}$	-0.553	p_{Ey2}	-0.537	q_{Bz10}	-0.211
$\mathbf{p_{Ex3}}$	2.813	p_{Ey3}	-0.083	q_{Cz1}	1.185
$\mathbf{p_{Ex4}}$	-0.226	p_{Ky1}	-14.95	q_{Dz1}	0.101
$\mathbf{p_{Kx1}}$	15.725	p_{Ky2}	2.130	q_{Dz2}	-0.001

$\mathbf{p_{Kx2}}$	0.008	p_{Ky4}	2.000	q_{Dz6}	-0.008
$\mathbf{p_{Kx3}}$	0.121	p_{Hy1}	0.003	q_{Dz7}	0.000
$\mathbf{p_{Hx1}}$	-0.001	p_{Hy2}	-0.001	q_{Ez1}	-1.514
$\mathbf{p_{Hx2}}$	0.001	p_{Vy1}	0.045	q_{Ez2}	-0.340
$\mathbf{p_{Vx1}}$	0.000	p_{Vy2}	-0.024	q_{Ez3}	0.002
$\mathbf{p_{Vx2}}$	0.002			q_{Ez4}	0.184
				q_{Hz1}	0.007
				q_{Hz2}	-0.002

In details for calculation of output forces, for pure slip condition [26] following equations were used.

Longitudinal force (pure longitudinal slip)

$$F_{X0} = D_x \sin[C_x \arctan\{B_x k_x - E_x(B_x k_x - \arctan(B_x k_x))\}] + S_{Vx}$$

$$k\_(x) = k + S\_Hx$$

$$C_x = p_{Cxl}.\lambda_{Cx} \qquad (> 0)$$

$$D_x = \mu_x.F_z.\varsigma_1 \qquad (> 0)$$

$$\mu_x = (p_{Dxl} + p_{Dx2}df_z).\lambda^*_{\mu x} \qquad (> 0)$$

$$E_x = (p_{Exl} + p_{Ex2}df_z + p_{Ex3}df^2).\{1 - p_{Ex4}\mathrm{sgn}(k_x)\}.\lambda_{Ex} \quad (\leq 1)$$

$$K_{xk} = F_z.(p_{Kxl} + p_{Kx2}df_z).\exp(p_{Kx3}df_z).\lambda_{Kxk}$$

$$(= B_x C_x D_x = \frac{\partial F_{x0}}{\partial k_x} \quad \text{at } k_x = 0) \quad (= C_{Fk})$$

$$B_x = \frac{K_{xk}}{(C_x D_x + \in_x)}$$

$$S_{Hx} = (p_{Hx1} + p_{Hx2}\, df_z).\lambda_{Hx}$$

$$S_{Vx} = F_z..(p_{Vx1} + p_{Vx2} df_z).\left\{\frac{|V_{cx}|}{(\epsilon_{Vx} + |V_{Cx}|)}\right\}.\lambda_{Vx}.\lambda'_{\mu x}.\varsigma_1$$

Lateral force (pure side slip)

$$F_{y0} = D_y \sin[C_y \arctan\{B_y\alpha_y - E_y(B_y\alpha_y - \arctan(B_y\alpha_y))\}] + S_{Vy}$$

$$\alpha_y = \alpha^* + S_{Hy}$$

$$C_y = P_{Cy1}.\lambda_{Cy} \quad (>0)$$

$$D_Y = \mu_y.F_z.\varsigma_2$$

$$\mu_y = \left\{\frac{(p_{Dy1} + p_{Dy2} df_z)}{(1 + P_{Dy3}\gamma^{*2})}\right\}.\lambda_{\mu y}{}^* \qquad (>0)$$

$$E_y = (p_{Ey1} + p_{Ey2} df_z)\{1 + P_{Ey5}\gamma^{*2} - (p_{Ey3} + p_{Ey4}\,\gamma^*) sgn(\alpha_y)\}.\lambda_{Ey} \qquad (\leq 1)$$

$$K_{y\alpha} = p_{Ky1} F'_{z0}\, sin[p_{Ky4} arctan\{F_z/((p_{Ky2} + p_{ky5}\gamma^{*2})F'_{z0})\}]/(1 + p_{ky3}\gamma^{*2}).\varsigma_3.\lambda_{Ky\alpha}$$

$$\left(= B_y C_y D_{y=} \frac{\partial F_{y0}}{\partial \alpha_y} \quad at\ \alpha_y = 0\right)$$

$$(if\ \gamma \neq 0 \coloneqq K_{y\alpha 0} = C_{F\alpha})$$

$$(ususally : P_{Ky4} = 2)$$

$$B_y = \frac{K_{y\alpha}}{(C_y D_y + \epsilon_y)}$$

$$S_{Hy} = (p_{Hyl} + p_{Hy2}\, df_z).\lambda_{Hy} + (K_{y\gamma 0}\gamma^* - S_{Vy\gamma}).\left\{\frac{\varsigma_0}{(K_{y\alpha} + \epsilon_K)}\right\} + \varsigma_4 - 1$$

$$S_{Vy\gamma} = F_z.(p_{Vy3} + p_{Vy4} df_z)\,\gamma^*.\lambda_{K\gamma y}.\lambda'_{\mu y}.\varsigma_2$$

$S_{Vy} = F_z.(p_{Vy1} + P_{Vy2}df_z).\lambda_{Vy}.\lambda'_{\mu y}.\varsigma_2 + S_{Vy\gamma}$

$K_{y\gamma 0} = F_z.(p_{Ky6} + p_{Ky7}df_z).\lambda_{Ky\gamma}\ \left(= \sim\frac{\partial F_{y0}}{\partial \gamma}\ \ at\ \alpha = \gamma = 0\right)\ (= C_{F\gamma})$

Aligning Torque (pure side slip)

$M_{z0} = M'_{z0} + M_{zr0}$

$M'_{z0} = -t_0.F_{y0}$

$t_0 = t(\alpha_t) = D_t cos\left[C_t arctan\left\{B_t\alpha_t - E_t\left(B_t\alpha_t - arctan(B_t\alpha_t)\right)\right\}\right].\cos'\alpha$

$\alpha_t = \alpha^* + S_{Ht}$

$S_{Ht} = q_{Hz1} + q_{Hz2}df_z + (q_{Hz3} + q_{Hz4}df_z)\gamma^*$

$M_{zr0} = M_{zr}(\alpha_r) = D_r cos[C_r arctan(B_r\alpha_r)]$

$\alpha_r = \alpha^* + S_{Hf}\quad (=\alpha_f)$

$S_{Hf} = S_{Hy} + \frac{S_{Vy}}{K'_{y\alpha}}$

$K'_{y\alpha} = K_{y\alpha} + \in_K$

$B_t = (q_{Bz1} + q_{Bz2}df_z + q_{Bz3}df_z^2).\left(1 + q_{Bz5|\gamma^*|} + q_{Bz6}\gamma^{*2}\right).\lambda_{Ky\alpha}/\lambda^*_{\mu y}$ (>0)

$C_t = q_{Cz1}$ (>0)

$D_{t0} = F_z.\left(\frac{R_0}{F'_{z0}}\right).(q_{Dz1} + q_{Dz2}df_z).\lambda_t.\mathrm{sgn}V_{cx}$

$D_t = D_{t0}.(1 + q_{Dz3}|\gamma^*| + q_{Dz4}\gamma^{*2}).\varsigma_5$

$E_t = (q_{Ez1} + q_{Ez2}df_z + q_{Ez3}df_z^2)\ \left\{1 + (q_{Ez4} + q_{Ez5}\gamma^*)\frac{2}{5}arctan(B_tC_t\alpha_t)\right\}$ (≤ 1)

$B_r = \left(q_{Bz9}.\lambda_{Ky\alpha}/\lambda^*_{\mu y} + q_{Bz10}B_yC_y\right).\varsigma_6$ (Preferred: $q_{Bz9} = 0$)

$C_r = \varsigma_7$

$$D_r = F_z.R_0\{(q_{Dz6} + q_{Dz7}df_z)\lambda_{Mr}.\varsigma_2 + (q_{Dz8} + q_{Dz9}df_z)\gamma^*\lambda_{Kzy}\varsigma_0 + (q_{Dz10} + q_{Dz11}df_z)\gamma^*|\gamma^*|\varsigma_0\}\cos'\alpha.\lambda^*_{\mu y}\mathrm{sgn}V_{cx} + \varsigma_8 - 1$$

Figure I.0.1 shows the variation of the longitudinal and lateral forces for a range of tyre slip ratios and slip angles, respectively, for three cases of vertical loading (5.88 kN, 3.92 kN and 1.96 kN) (from left to right). Figure on left shows the variation of the self-aligning torque with slip angles for the same cases. We selected an R15 tyre, where the nominal load is taken as 6.15 kN for calculation of MFM parameters [27].

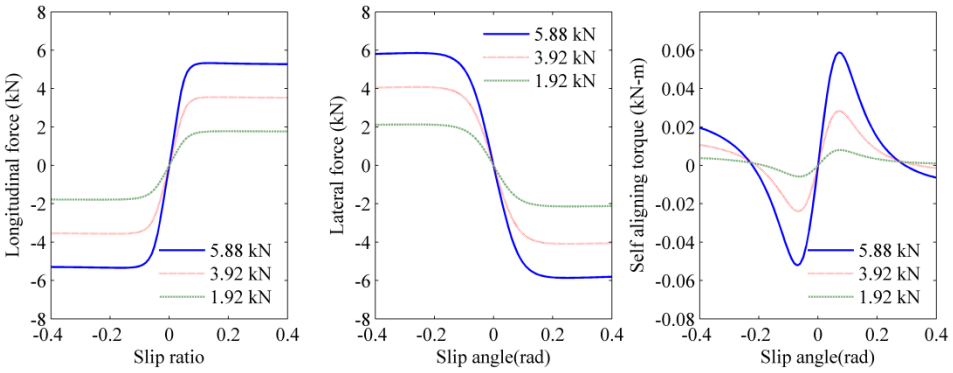

Figure I.0.1 Magic formula parameters

Appendix II: Major interview questions for drivers

Vehicle No:

Age:	☐ Less than 20	☐ 20-30	☐ 30-40	☐ More than 40
Driving Experience:	☐ Less than 1 yrs.	☐ 1-5 yrs.	☐ 5-15 yrs.	☐ More than 15 yrs.

1. Which vehicle were you driving?

☐ Car, Taxi ☐ Bus ☐ Truck ☐ Microbus/Van ☐ Tempo

2. Condition of vehicle

☐ Bad ☐ Normal ☐ Good

3. Where were you driving during earthquake?

District: Area:

4. When did you know the earthquake shaking?

☐ initially ☐ During strong shaking ☐ Lately

5. How did you know there was the earthquake?

☐ Unusual behavior of vehicle ☐ Shaking of surroundings ☐ Damages at surrounding

6. How was the response of vehicle?

a) Moved Backward/forward? ☐ Not at all ☐ Very little ☐ Significantly

b) Moved laterally? ☐ Not at all ☐ Very little ☐ Significantly

7. How much the vehicle moved due to earthquake?

Longitudinal: ☐ less than 1 m ☐ 1-2 m ☐ 2-3 m ☐ More than 3 m

Lateral: ☐ less than 1 m ☐ 1-2 m ☐ 2-3 m ☐ More than 3 m

8. What did you feel to control the vehicle?

☐ Difficult ☐ Easy control ☐ Did not notice

9. What did you do just after you knew the earthquake?

☐ Stopped ☐ Slow but moving ☐ same speed ☐ Moved faster

10. If you stopped, how did you stop the vehicle?

a) How you used brake? ☐ Used hard brake ☐ Normal braking

b) Where did you stop? ☐ on the lane ☐ On shoulder

11. Did you have accident on that time?

☐ No, it was Safe ☐ Minor ☐ Major

12. Had you seen any other vehicle accident due to earthquake?

☐ No ☐ Yes

If yes, How many accidents? :

What was the condition? :

13. What you will do if you get earthquake early warning just before main shaking?

☐ Stop immediately ☐ stop slowly ☐ No reaction

We really appreciate your cooperation.

Thank you.

Appendix III: Brake activity of drivers

Case 1: Without front vehicle

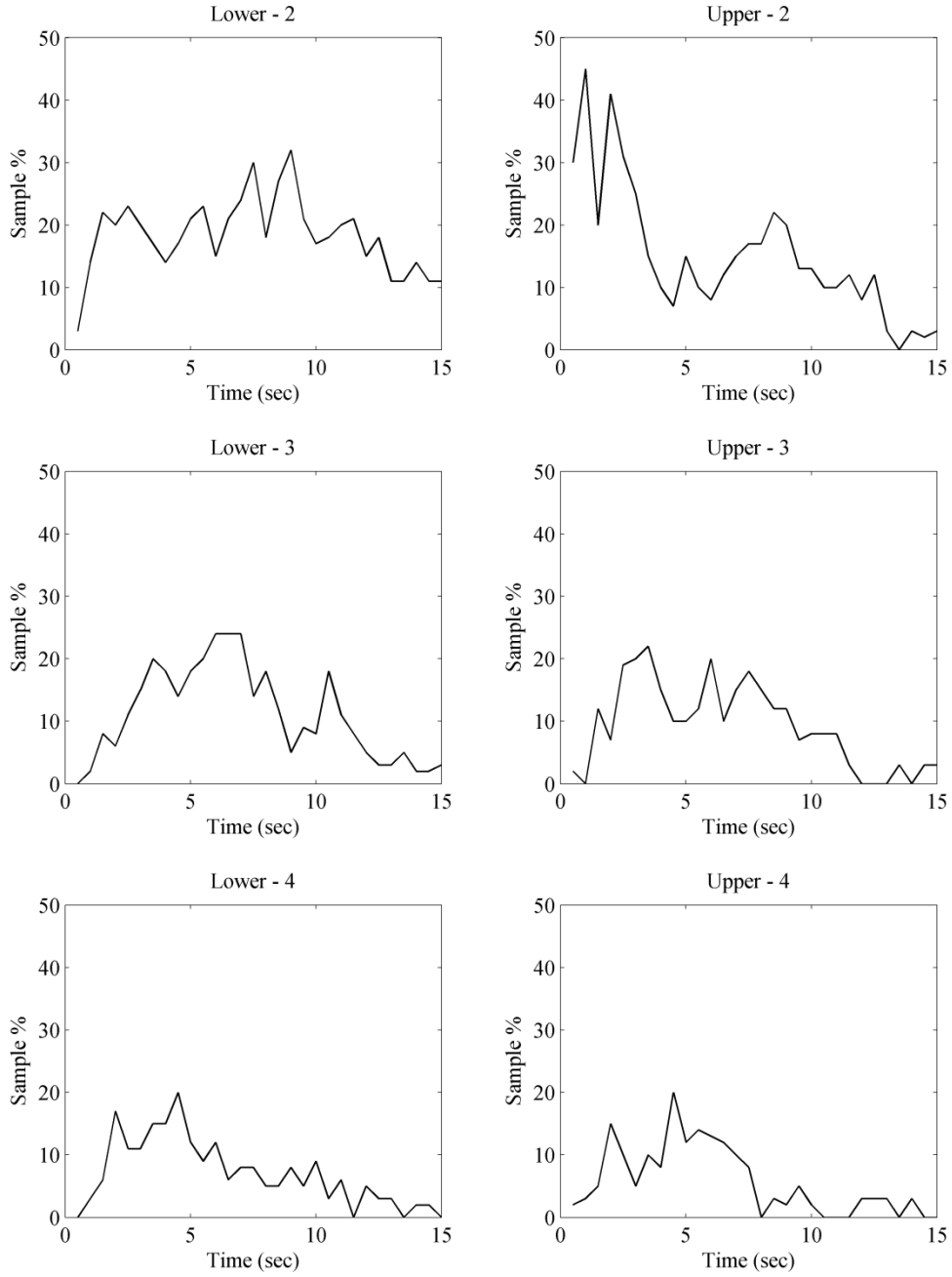

Figure III.0.1 Brake activities of drivers without front vehicle (brake level 2, 3 and 4 m/sec^2 respectively)

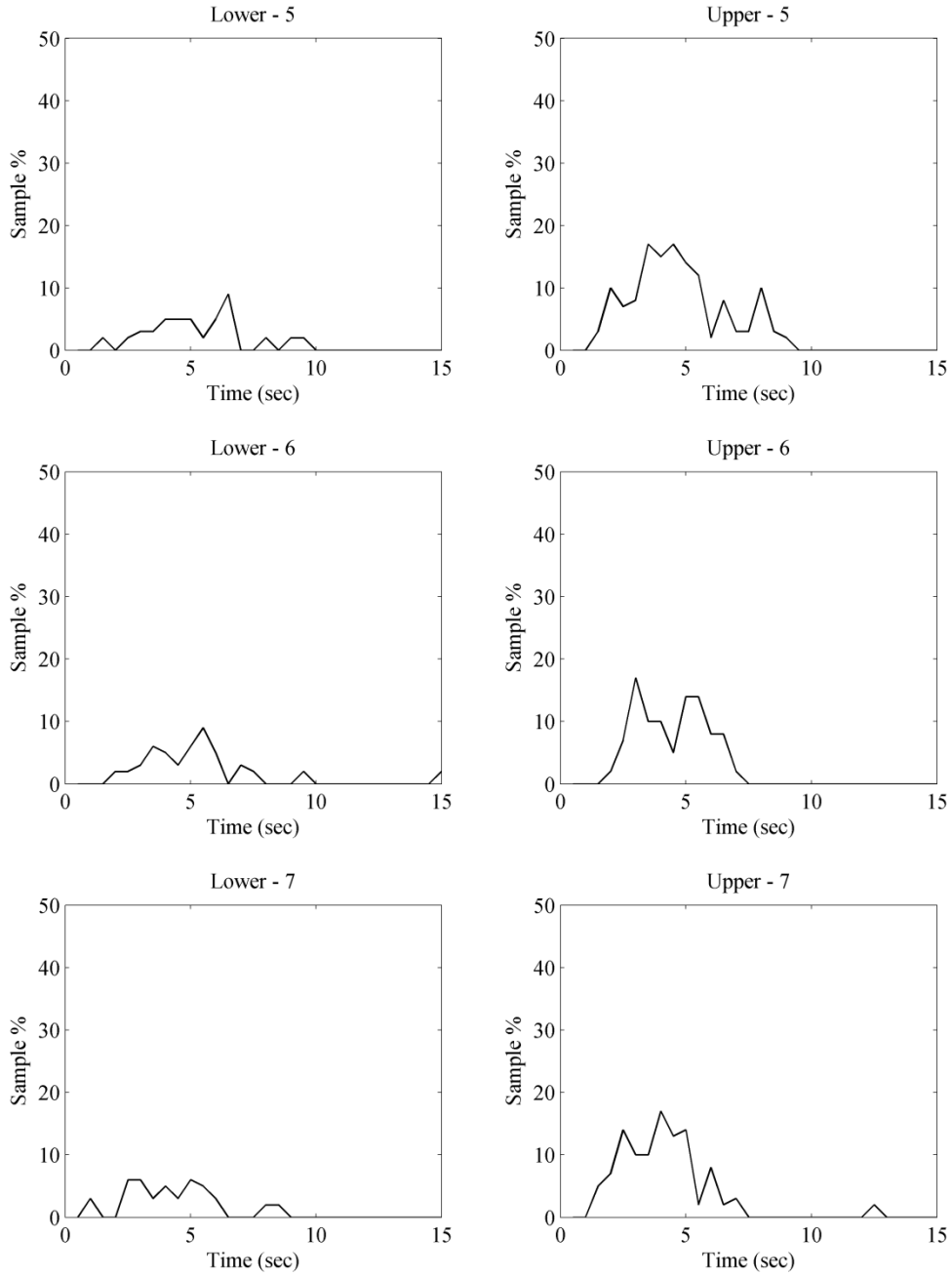

Figure III.0.2 Brake activities of drivers without front vehicle (brake level 5, 6 and 7 m/sec^2 respectively)

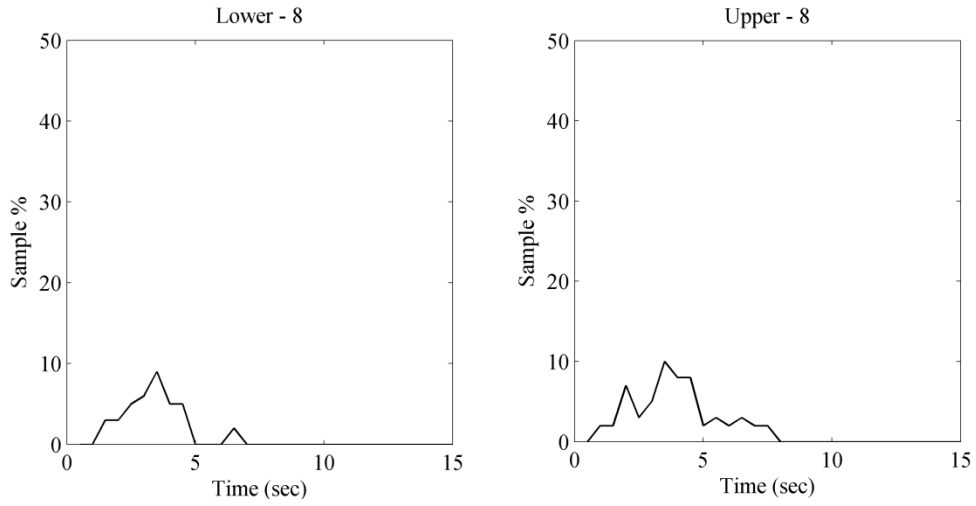

Figure III.0.3 Brake activities of drivers without front vehicle (brake level 8 m/sec^2)

Case 2: With front vehicle that stopped after earthquake

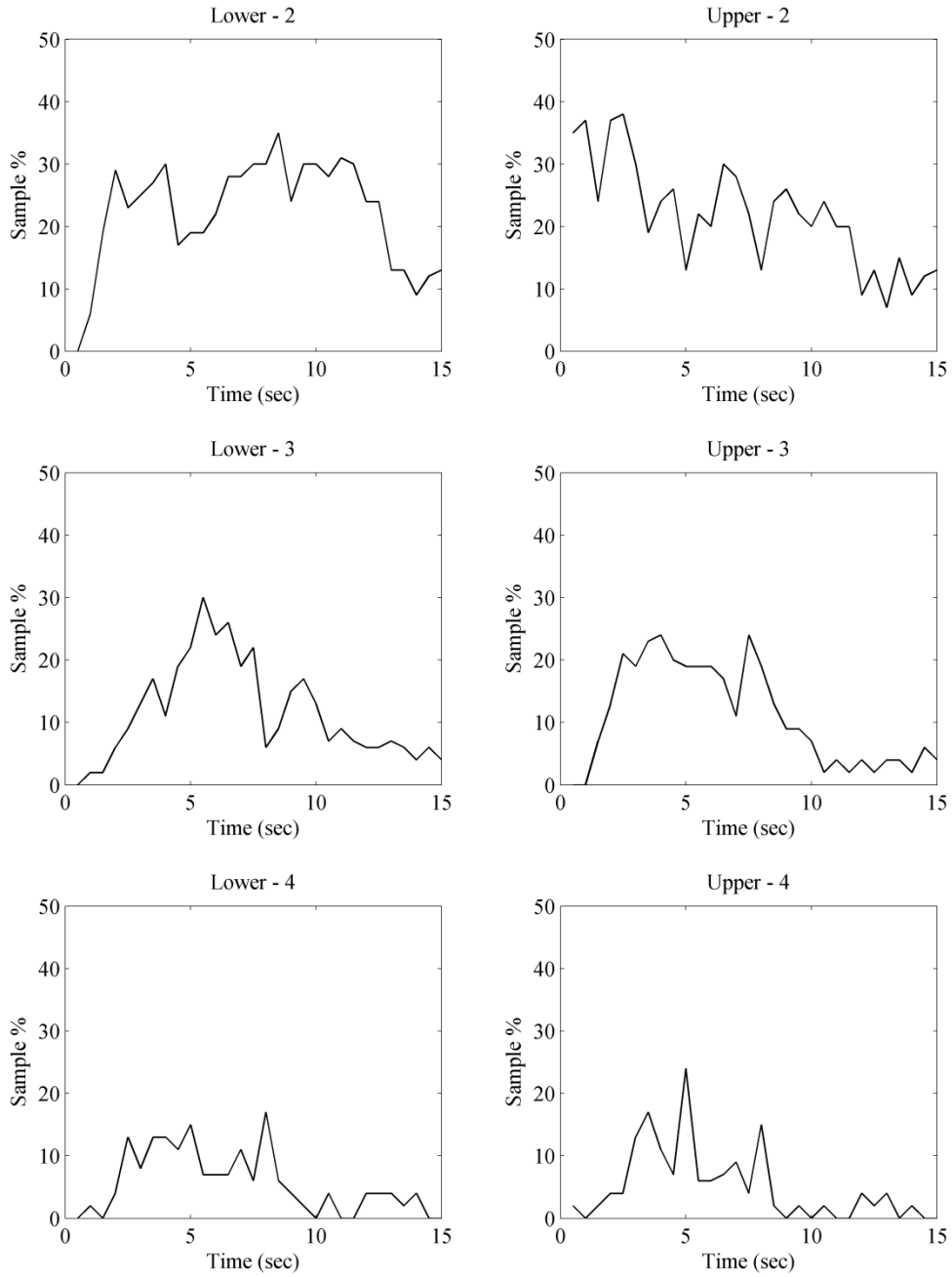

Figure III.0.4 Brake activities of drivers (brake level 2, 3 and 4 m/sec^2 respectively) in case of front vehicle STOPPED

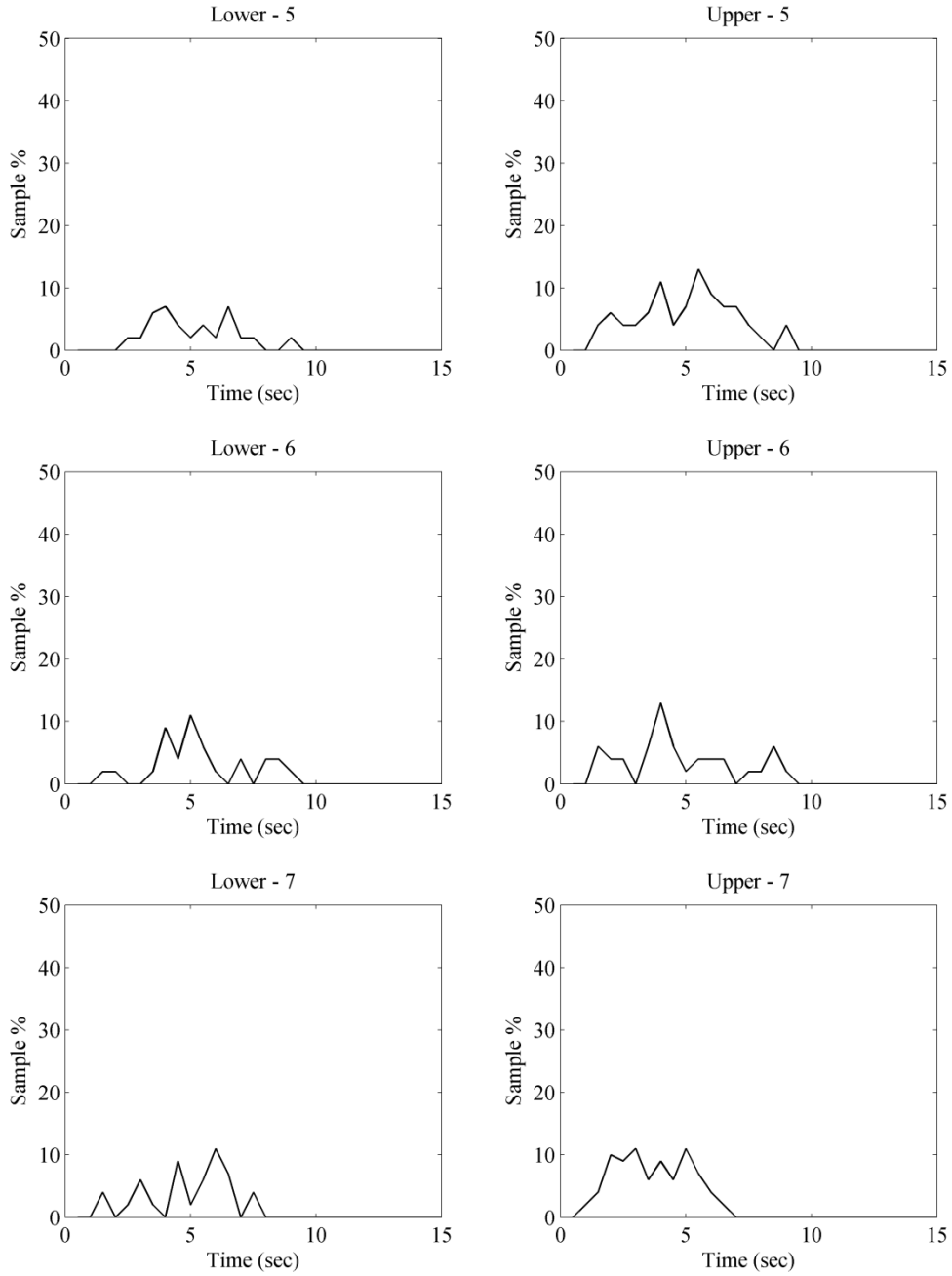

Figure III.0.5 Brake activities of drivers (brake level 5, 6 and 7 m/sec^2 respectively) in case of front vehicle STOPPED

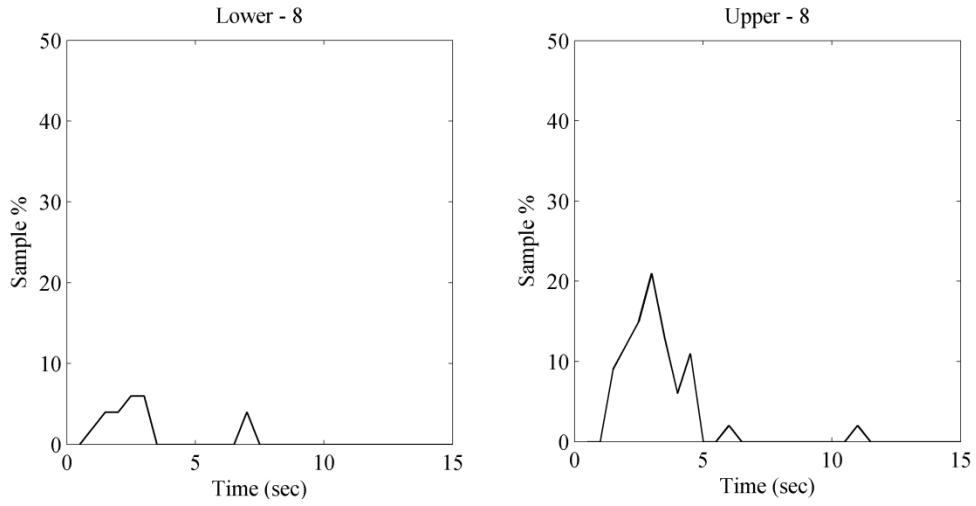

Figure III.0.6 Brake activities of drivers (brake level 8 m/sec^2) in case of front vehicle STOPPED

Case 3: With front vehicle that DO NOT STOPPED after earthquake

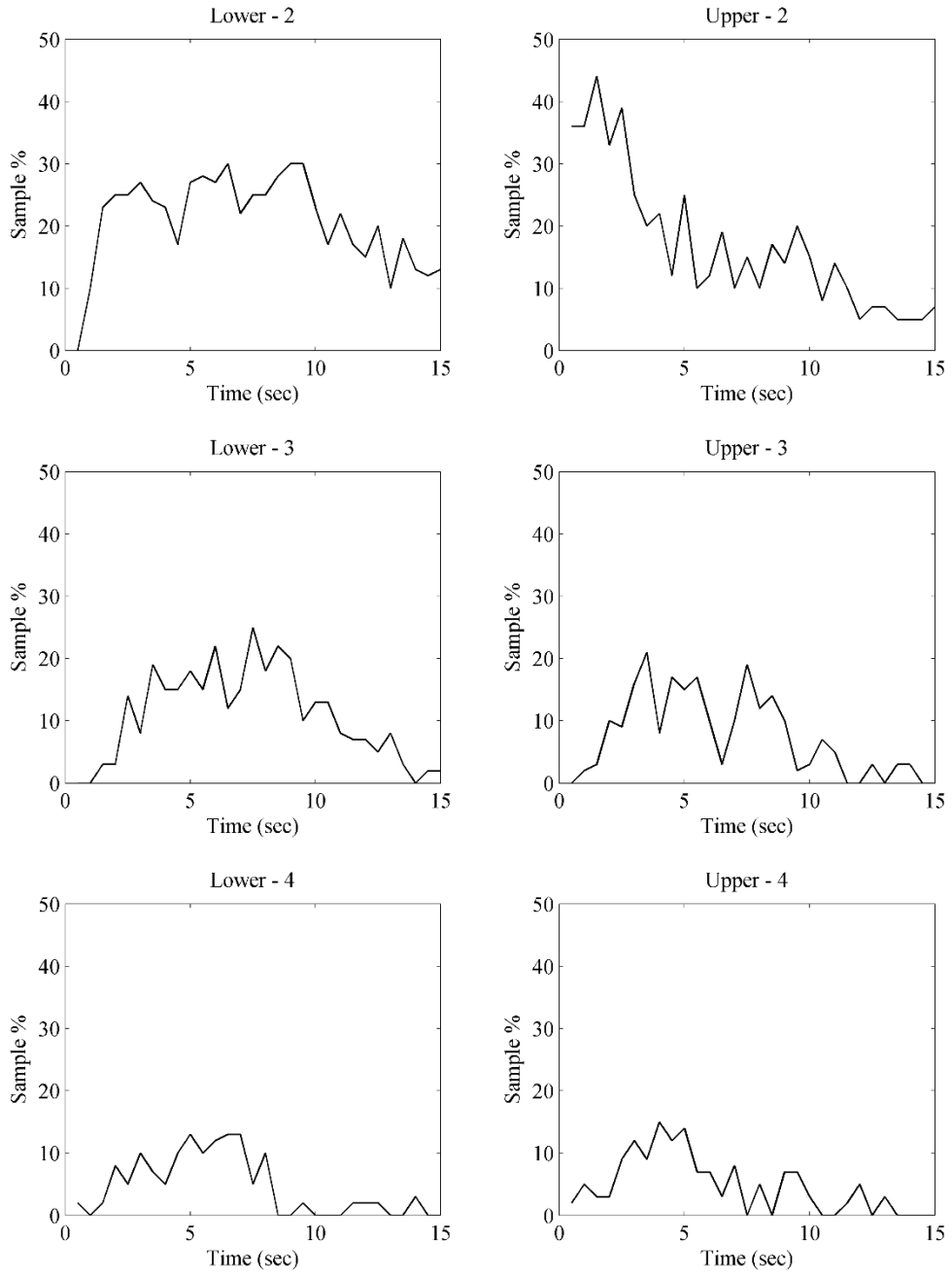

Figure III.0.7 Brake activities of drivers (brake level 2, 3 and 4 m/sec^2 respectively) in case of front vehicle NOT STOPPED

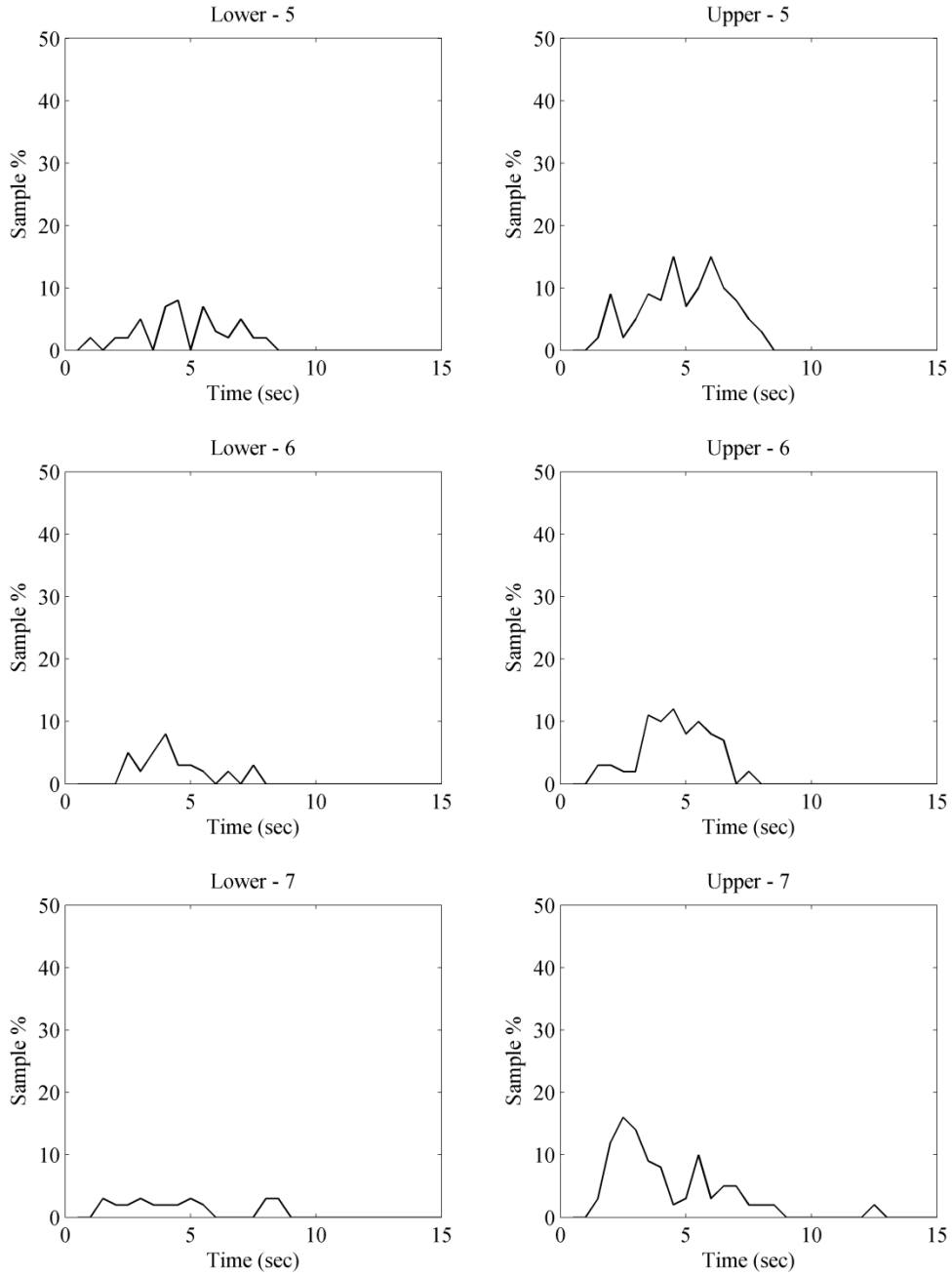

Figure III.0.8 Brake activities of drivers (brake level 5, 6 and 7 m/sec^2 respectively) in case of front vehicle NOT STOPPED

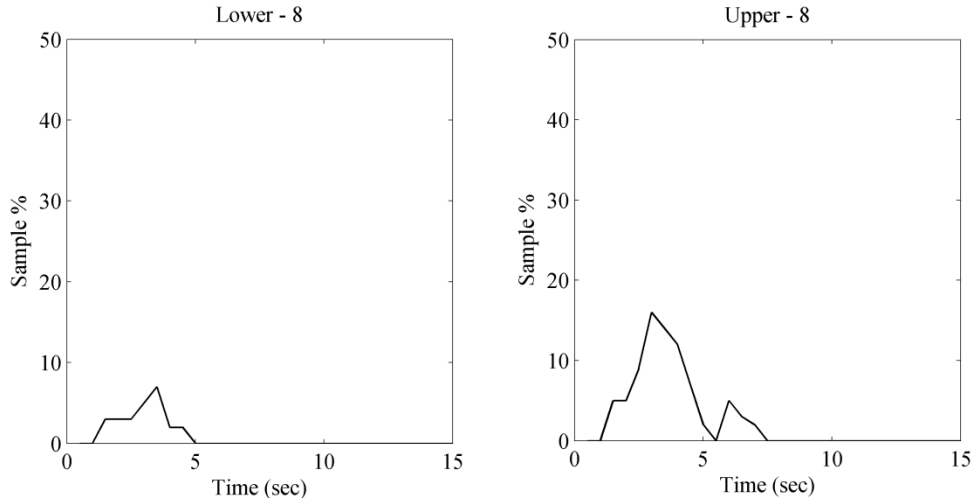

Figure III.0.9 Brake activities of drivers (brake level 8 m/sec^2) in case of front vehicle NOT STOPPED

Appendix IV: EEW: What to Do and Don'ts

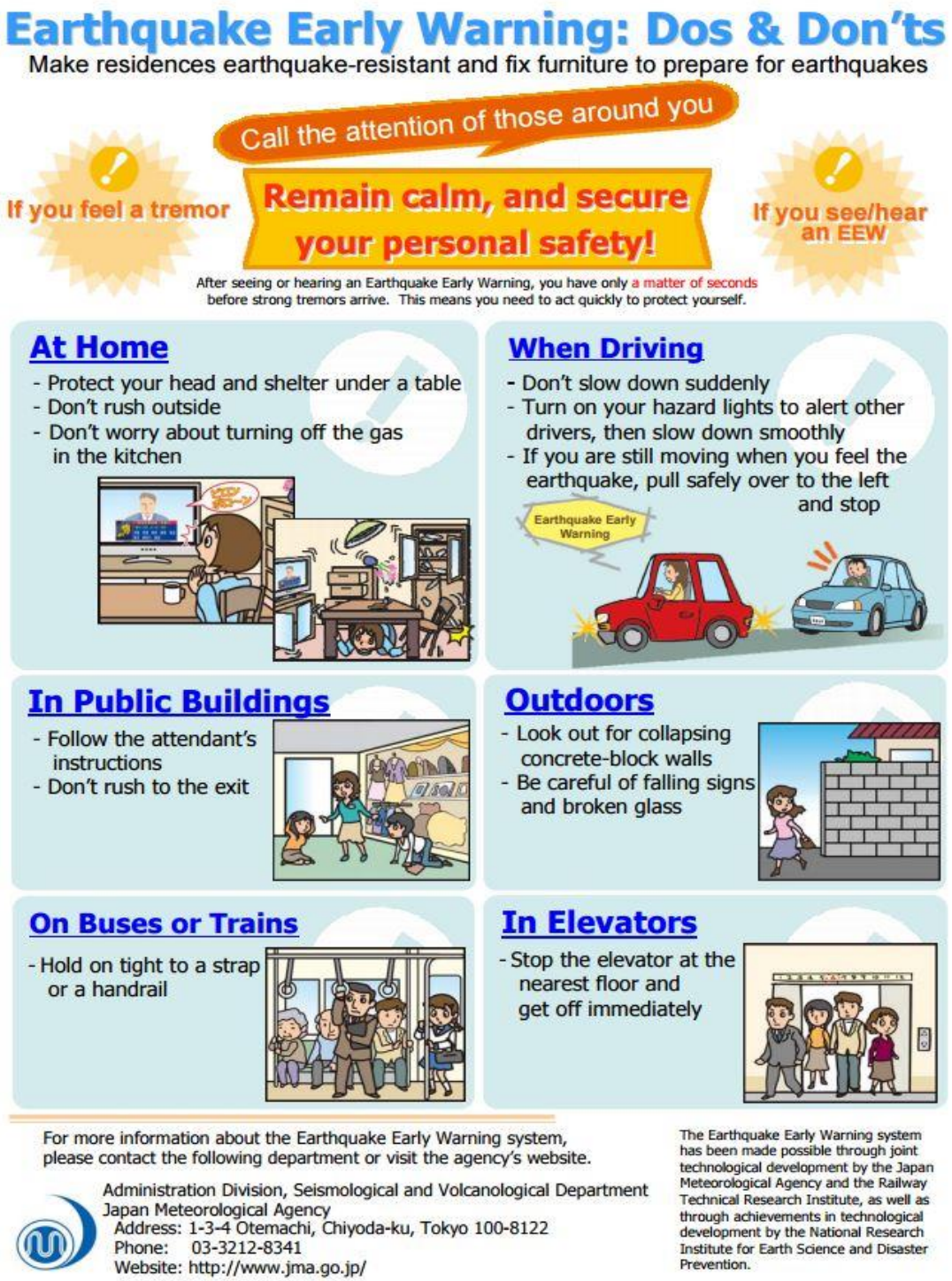

Figure IV.0.1 Information to do and not to do during earthquake shaking (Source: JMA)[7]

[7] http://www.jma.go.jp/jma/en/Activities/EEWLeaflet.pdf